

Geology, Petrology, and Geochronology of Rocks in the Our Town,  
Alabama Quadrangle

by

John Fancher Hawkins

A thesis submitted to the Graduate Faculty of  
Auburn University  
in partial fulfillment of the  
requirements for the Degree of  
Masters of Science

Auburn, Alabama  
December, 14, 2013

Copyright 2013 by John Fancher Hawkins

Approved by

Mark G. Steltenpohl, Chair, Professor of Geology and Geography  
Willis E. Hames, Professor of Geology and Geography  
Haibo Zou, Associate Professor of Geology and Geography

## Abstract

The area of the 1:24,000 Our Town Quadrangle of east central Alabama is underlain principally by generally undifferentiated metasedimentary units, the Emuckfaw and Wedowee Groups, which have been intruded by major southern Appalachian batholiths, the Elkahatchee Quartz Diorite and the Kowaliga Gneiss, and the less volumetric Zana Granite. Detailed field mapping provides lithologic detail for the Emuckfaw Group allowing for differentiation into multiple subunits. The subunits are defined based on the occurrence or absence of amphibolites and garnet-amphibole bearing quartzites of metavolcanic origin. In addition to this distinction, further differentiation is based on the occurrence of late fine-grained highly foliated metagranites that have intruded the Emuckfaw Group.

Previous reconnaissance work indicated the presence of two texturally interesting lithologic units that commonly occur within the Kowaliga Gneiss and the Emuckfaw Group. These two lithologies can be generally described as augen gneiss and megacrystic gneiss. The megacrystic potassium feldspar grains were previously thought to have been generated by metamorphic processes acting upon the Kowaliga Gneiss or on bulk compositionally appropriate metasedimentary sections of the Emuckfaw Group. Detailed petrographic and geochemical analyses indicate that the megacrysts were not generated by a metamorphic process but rather a magmatic process. The recognition of a magmatic origin reveals exposures of the Kowaliga Gneiss that preserve the initial megacrystic crystallization texture, whereas most outcrops reflect augen gneiss derived from mylonitization of the megacrysts.

Whole-rock major and trace element analyses of the megacrystic and augen varieties of the Kowaliga Gneiss indicate a strong correlation with previously reported geochemical data for the Zana Granite. U-Pb SIMS dates on zircons from the megacrystic Kowaliga Gneiss yield an age of crystallization of  $441 \pm 6.6$  Ma with no systematic or significant variations between the cores and rims. Previously reported tentative dates for the Zana Granite imply a crystallization age of 439 Ma. Strong similarities in geochemistry and crystallization ages suggest these two intrusions, previously mapped as individual suites, should be considered one intrusive suite.

In the study area, the epidote-amphibolite to amphibolite facies of the Emuckfaw Group and Kowaliga Gneiss are juxtaposed with the lower grade (greenschist to lower amphibolite facies) Jacksons Gap Group that structurally overlies them. These two terranes are separated by the Abanda fault that was previously considered a northwest-directed thrust. Detailed structural analysis of retrograde mylonites and phyllonites along the Abanda fault documents an oblique dextral-and-normal sense of movement. This oblique dextral-and-normal movement is similar to movement reported for the Alexander City fault in the northeast section of the quadrangle. In addition to constraining fault kinematics for the Abanda fault, field mapping also revealed two sets of sub-vertical brittle normal faults. Faults of the NW-SE-trending set have <2 m displacement and cut the oblique dextral-normal phyllonites of the Abanda fault. Faults of the WSW-ENE set rarely cut Abanda phyllonites and are similar to Mesozoic(?) faults known to cut the Alexander City and Towaliga mylonite zones. A  $^{40}\text{Ar}/^{39}\text{Ar}$  date of  $\sim 317\text{-}315$  Ma on cataclastically deformed muscovite from one of these faults implies either Pennsylvanian movement or failure of the crystals to record any record of this disturbance.

## **Acknowledgments**

I would like to thank the faculty of the Geology and Geography Department at Auburn University for their guidance and encouragement during my undergraduate and graduate studies. I would especially like to thank Dr. Steltenpohl who has provided me with the opportunities to map in Norway and the southern Appalachians as well as the excellent experience of assisting with field camp on multiple occasions. I would also like to express my thanks to Jonathan Prouty and Sam Wakefield who have provided much needed support over the years.

## Table of Contents

Abstract.....	ii
Acknowledgments.....	v
List of Figures .....	vii
List of Tables .....	x
List of Plates .....	xii
List of Abbreviations .....	xiii
Introduction.....	1
Methods.....	4
Lithologies .....	7
Metamorphism .....	34
Structure .....	41
Geochemistry and Petrogenetic Evolution of the Kowaliga Gneiss.....	55
<sup>40</sup> Ar/ <sup>39</sup> Ar Analysis and Interpretations.....	77
U/Pb Analysis and Interpretation .....	82
Discussion.....	88
Conclusions .....	93
Appendix 1 .....	95
Appendix 2 .....	97
Appendix 3 .....	100
References .....	102
Plate 1 .....	107

## List of Figures

1. Geologic map of Piedmont rocks in Alabama showing location of the Our Town quadrangle. Modified from Steltenpohl(2005). Our Town quadrangle outline In red .....	2
2. A. Geologic map of the Our Town quadrangle. B. Cross-section (A-A') with line of cross-section outline on map. C. Cross-section (B-B') with line of cross-section outlined on map .....	8-9
3. Photographs and photomicrographs of the quartz- biotite schists of the Emuckfaw Group. A. and B. Outcrop views of characteristic ribs. C. Thin section with a 5 mm field of view (in ordinary light). D. Same view as in C., but with crossed polars.....	12
4. Amphibolite Photomicrographs A. Amphibole defining the primary foliation occurring with monocrystalline quartz (2.5 mm field of view). B. Crossed polar view of photomicrograph A. C. Subidioblastic to xenoblastic garnets (1mm field of view). D. Monocrystalline quartz and clinozoisite inclusions with amphibole (1 mm field of view).....	14
5. Photomicrographs of garnet amphibole-bearing quartzite. A. Amphibole with an epidote/clinozoisite inclusion (2.5 mm field of view). B. Crossed polar view of photograph A. C. Garnet, amphibole, and fibrous amphibole (5mm field of view). D. Kink bands in quartz and sericitized potassium feldspar (1 mm field of view).....	17
6. Photomicrographs of the biotite-rich quartzite. A. Interlobate quartz grain boundaries (1 mm field of view). B. Plagioclase deformation twinning (1 mm field of view). C. Deformation induced tartan twinning (Vernon, 2004) in potassium feldspar (2.5 mm field of view).....	19
7. Photomicrographs of protomylonitic granite A. Muscovite defining the primary foliation with minor ductile deformation (2.5 mm field of view). B. Quartz ribbon between two feldspar grains (2.5 mm field of view). C. Kinked and bent Albite twins in plagioclase feldspar with margins indicating grain boundary migration (2.5 mm field of view). D. Muscovite showing kink bands and undulose zones (5 mm field of view) .....	22
8. Photomicrographs of Kowaliga augen gneiss A. Sheared potassium feldspar grains that are mantled by myrmekitic to granophyric colonies replacing the larger phenocrysts of potassium feldspar (10 mm field of view). B. Quartz ribbons drape larger more competent grains of potassium feldspar (10 mm field of view).....	25

9. Photomicrographs meta-gabbro A. tartan twinning of a microcline adjacent to a calc-clino amphibole (2 mm field of view). B. Pleochroic green colors of the calc-clino amphibole with the dusty appearance of the plagioclase grains reflecting sericite alteration (2 mm field of view).....	29
10. Photographs of late-stage aplite dikes. A. Aplite dike cross cutting layering and foliation of the Emuckfaw Group foliation. Note brittle stockwork made by injection. B. Aplite dike within the Emuckfaw Group. (N32 51.180 W85 56.220).....	31
11. Photograph of the Abanda Fault. Base of the Jacksons Gap Group is marked by the red line. Quartz veins in the Jacksons Gap Group and the Abanda Fault are noted by black arrows .....	33
12. Metamorphic conditions suggested for the peak Neocadian metamorphic event with eastern Blue Ridge in purple and Jacksons Gap Group in green. Grid univariant reaction curves and facies boundaries are from Holdaway (1971) and Ernst (1973) .....	35
13. Photomicrograph of both varieties of amphibole found within the Emuckfaw Group amphibolites. Amphibole in the center (yellow brown in color) is corroded or embayed indicating disequilibrium textures. Field of view is 2.5 mm.....	37
14. Photomicrograph of subhedral garnets with $S_1$ defining calcic-amphiboles. Photograph is in plane light with a 10 mm field of view .....	38
15. Lower hemisphere stereographic projections of foliation and lineation data for rocks of the Our Town quadrangle. A. Poles to metamorphic foliation $S_1$ and $S_2$ , where $N=334$ . B. Lineation data, $L_1$ and $L_2$ where $N=77$ . C. Hinge line measurements from outcrop-scale post-metamorphic folds where $N=14$ . Contours were generated using percent concentrations below .....	43
16. Form line map generated from structural data from the Our Town quadrangle. See Figure 2 for Legend .....	44
17. Photograph of post-metamorphic folds in a muscovite schist from the Emuckfaw Group .....	46
18. Shear zone map generated from S-C fabric locations within the Our Town quadrangle. Fields marked as "Z" indicate shear zones and dashed lines represent approximate margins. See Figure 2 for Legend.....	47
19. Lower hemisphere equal-area stereoplot of S and C slip line data from the shear zones in the Our Town quadrangle, slip lines were geometrically determined.....	48
20. Lower hemisphere equal-area stereoplot of S and C plane data from the Alexander City fault zone. Poles to S (blue circles; $n = 36$ ) and C (blue dots; $n = 36$ ) planes and slip lines (red triangles; $n = 36$ ). Black arcs connect S-C pairs, slip lines were geometrically determined (Steltenpohl et al., 2013) .....	50

21. Lower hemisphere stereographic projections of fault rocks associated with the Brevard zone. A. Contoured plot of slip lines geometrically determined, and poles to C planes are the unoriented end of the arrow while the S planes are the tip of the arrow. B. Contoured plot of poles to brittle normal fault planes in the Emuckfaw Group and Jacksons Gap Group N=77. Contours were generated using percent concentrations below .....	52
22. Photographs of phyllonite fabrics of the Abanda fault. A. S-C fabrics within an Emuckfaw Group schist, looking northeast. B. Small-scale dextral (Z) folds of a quartz vein within Abanda fault phyllonites, looking southeast. C. Mesoscopic dextral (Z) folds indicating dextral movement of the Abanda. Upper Emuckfaw Group lithology is a metasiltstone that is intruded by a fine to medium grained potassium-feldspar-rich granite.....	53
23. North/northwest-striking brittle normal faults. A. Normal faults in upper Emuckfaw Group units; view looking southeast with pencil for scale. B. Same view as A where brittle faults are outlined in black, horsts and grabens are outlined in red, and two quartzite layers marking offset are colored green and blue. C. Close up view of normal fault in index rectangle in B. D. Typical displacement observed in individual outcrops is about 0.7 meters as shown in the photograph. Lithology is Emuckfaw Group. (N32 45.240 W85 53.220).....	54
24. CIPW normative classification (Barker, 1979) of the Kowaliga Gneiss and Zana Granite based on chemical analyses reported by Stoddard (1983) and Kowaliga analysis from the current report .....	61
25. Harker plots of six major oxides (Fe <sub>2</sub> O <sub>3</sub> , CaO, MgO, K <sub>2</sub> O, Na <sub>2</sub> O, and Al <sub>2</sub> O <sub>3</sub> ) for the Kowaliga Gneiss compared to earlier Zana Granite and Kowaliga Gneiss geochemical data presented by Stoddard (1983). Shaded area defines area for recent data populations.....	63
26. Discrimination plots for the Kowaliga Gneiss A. Data from the Kowaliga Gneiss plotted on Rb-(Yb + Ta) and Rb-(Yb +Ta) discrimination plots (Pearce et al., 1984) with fields of syn- collisional granites (syn-COLG), within-plate granites (WPG), volcanic-arc granites (VAG) and ocean-ridge granites (ORG). B. Data from the Kowaliga Gneiss plotted on Hf-Rb/30-Ta x 3 discrimination plot (Harris et al., 1986).....	64
27. Photographs of megacrystic feldspar grains A. A weak preferred orientation of megacrysts within the Kowaliga gneiss. B. Strongly preferred-length orientation of megacrysts (left side of photograph) within the Tarnvika pluton in northern Norway .....	68
28. Collage of photomicrographs stitched together to provide one complete view of a euhedral potassium feldspar gain. Photographs were taken in crossed polars with a 4 cm field of view; total length of the crystal is 3.2 cm. A. Unobstructed view. B. Orientations of inclusions are outlined in red.....	70
29. Photographs of a ~5 cm diameter phenocryst from the Kowaliga gneiss. A. Crystal was cut and hand sample was photographed to examine oscillatory zoning within	



the crystal. B. Digitized outlined portions of the zoning .....	71
30. Weight percent of Ca, Na, and K plotted for ten whole-rock analyses of samples of the Kowaliga Gneiss.....	73
31. Weight percent of Mg, Ca, Mn, and Sr plotted for five whole-rock analyses of samples of the Kowaliga Gneiss. JHKGa is megacrystic; JHKG5, JHKG20, and JHK32 are sheared varieties; and JHK43 is slightly sheared .....	74
32. Parts per million of Rubidium plotted for five whole-rock analyses of samples of the Kowaliga Gneiss. JHKGa is megacrystic; JHKG5, JHKG20, and JHK32 are sheared varieties; and JHK43 is slightly sheared .....	75
33. Cataclastic fault rock sample number CV1 used for $^{40}\text{Ar}/^{39}\text{Ar}$ muscovite dating (N32°51.840 W85°55.200). A. Full thin section slide view of the cataclastically deformed granite sample CV-1. B.to D. Enlarged view of the cataclastically deformed granite (2 mm field of view) E. Muscovites that were extracted and used for analysis .....	78
34. Muscovite age data. A. Plateau age for a single crystal indicating $317.4 \pm 0.7$ Ma. B. Probability density diagram for the ten muscovite grains from cataclastically deformed granite sample CV-1 analyzed in ANIMAL indicating $315.8 \pm 0.7$ Ma with a MSWD of 2.11.....	80
35. Optical photographs of zircons from the Kowaliga Gneiss. A. Ten numbered zircons that were used for SIMS analysis (6 mm field of view). B. Location of core/rim analysis locations for the ten selected zircons (2 mm field of view) .....	83
36. U/Pb isochron plot for zircons from Kowaliga Gneiss sample 2012_12_10Dec\AI. Chart was constructed and ages were determined using Isoplot (Ludwig, 2003) .....	86
37. Tectonic models for the Cambrian to Middle Ordovician. A. Tectonic model showing the rifting of the Argentine Precordillera and region of induced subduction. B. Tectonic model of the developing volcanic arc and the depositional center for the Emuckfaw Group. Modified from Hatcher (2010).....	89
38. Tectonic setting illustrating the depositional environment and possible source terranes for the Emuckfaw Group during Late Ordovician intrusion of the Kowaliga and Zana granites .....	91

## List of Tables

1. Major and trace element concentration data from ten samples of Kowaliga Gneiss. Data is reported in weight percent and parts per million (ppm).....56-60
2. Raw data for Kowaliga Gneiss zircon rims and cores collected from SIMS analyses. 1 s.e. is the standard error, which represents measurement uncertainty.....84-85

**List of Plates**

Plate 1. Geologic Map of the Our Town, Alabama Quadrangle.....107

## List of Abbreviations

An	Percent Anorthite
CIPW	Cross, Iddings, Pirsson and Washington
em	Emuckfaw Group sub-grouping
EBR	eastern Blue Ridge
EQD	Elkahatchee Quartz Diorite Gneiss
GIS	Geographic Information System
GPS	Global Positioning System
JGG	Jacksons Gap Group
LOI	Loss of Ignition
Ma	Million Years
MSWD	Mean Square of Weighted Deviates
NE	North East
ppm	parts per million
S-C	schisosity and cisaillement
SE	South East
s.e	standard error
REE	Rare Earth Elements
U.S.G.S.	United States Geological Survey

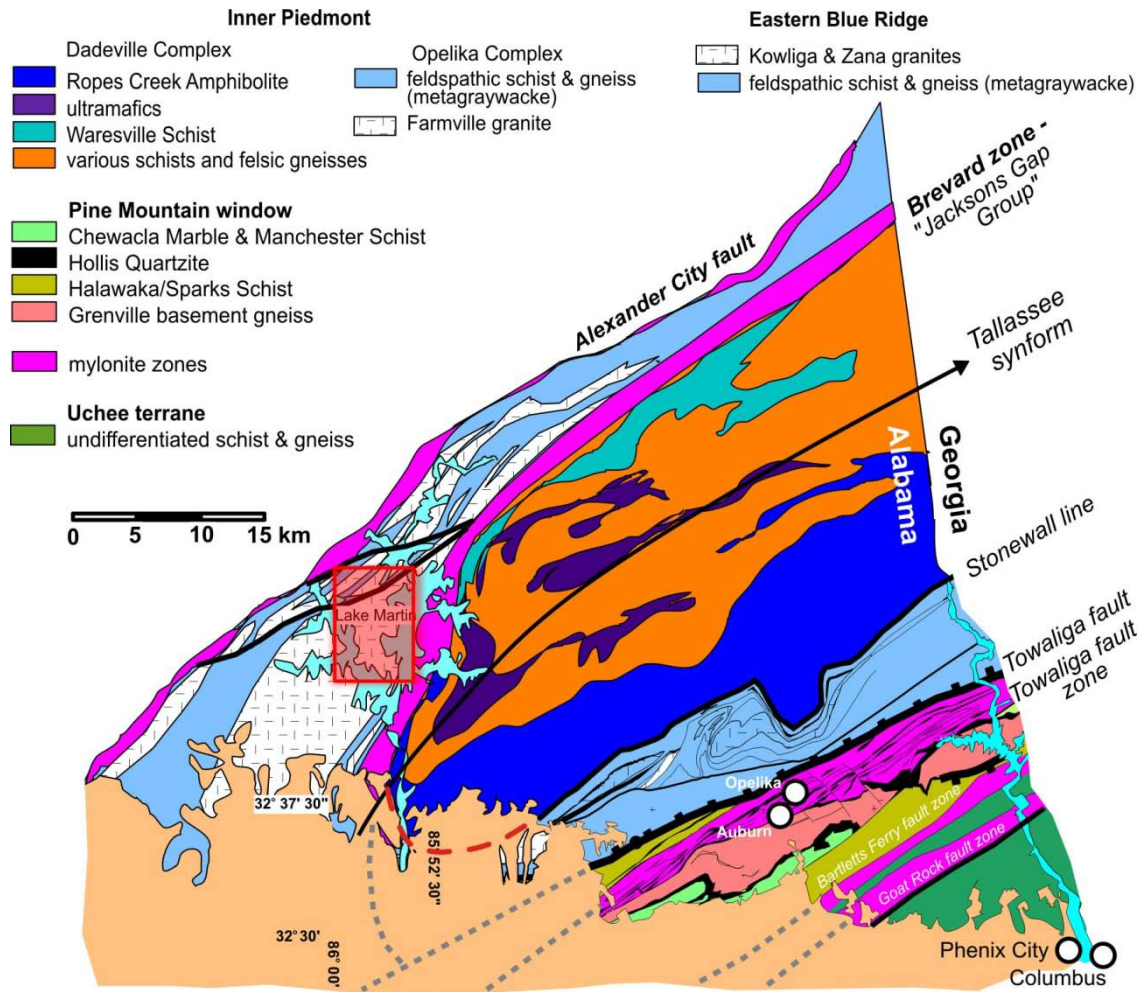
### Mineral Abbreviations

amp	amphibole
bio	biotite
czo	clinozoisite
kspar	potassium feldspar
gar	garnet
mus	muscovite
pla	plagioclase
qtz	quartz

## **Introduction**

The area of the 1:24,000 Our Town quadrangle is underlain by rocks of the eastern Blue Ridge and the Brevard zone/Jacksons Gap Group. Eastern Blue Ridge rocks in the map area comprise undifferentiated metasedimentary units of the Emuckfaw and Wedowee Groups that are intruded by major southern Appalachian batholiths, Kowaliga Gneiss, Zana Granite, and the Elkahatchee Quartz Diorite, respectively (Bentley and Neathery, 1970)(Fig. 1). Major southern Appalachian faults separate the Emuckfaw and Wedowee Groups to the northwest and the Jacksons Gap Group to the southeast (Alexander City and Abanda faults, respectively), but no modern shear-sense analyses are reported for fault rocks in the study area.

In an attempt to gain a better understanding of the eastern Blue Ridge rocks within the study area, the tectonic setting for deposition, timing of intrusions, and fault kinematics were investigated. The following objectives were followed: (1) to map lithologies and structures in the Our Town quadrangle with emphasis on subdividing and providing a detailed lithologic description of the subunits within the Emuckfaw Group, and to create a vector-GIS geologic map; (2) to geochemically characterize the magma source for the Kowaliga Gneiss and to compare it with geochemical data previously published for the Zana Granite; (3) to petrographically and geochemically characterize the feldspar megacrysts found in the augen varieties of the Kowaliga Gneiss in order to determine if the megacrysts have a magmatic or metamorphic origin, and to determine possible effects of potassium metasomatism on the Kowaliga Gneiss; (4) to analyze U-Pb isotopes in zircons from the Kowaliga Gneiss to determine



**Figure 1.** Geologic map of Piedmont rocks in Alabama showing location of the Our Town quadrangle. Modified from Steltenpohl (2005). Our Town quadrangle outlined in red.

the age of crystallization to better understand its significance for middle Paleozoic evolution of the southern Appalachians; and (5) to obtain an  $^{40}\text{Ar}/^{39}\text{Ar}$  muscovite cooling age for an uncharacterized brittle fault transecting the Our Town quadrangle.

## Methods

Geologic mapping at a scale of 1:24,000 was conducted over an area of approximately 56 square miles. All primary and secondary roads with open access were mapped, including logging roads, hunting lands, and private properties where permission was obtained. Mapping of the Lake Martin shoreline was accomplished by the use of kayak, canoe, and foot. The majority of mapping was conducted along the shoreline due to the abundant outcrops and ease of access. Four-hundred-and-fifteen stations were established at which lithologic, structural, and fabric observations were recorded. The Our Town 7½-minute U.S.G.S. topographical quadrangle was used as a primary base map. Data collected at the different stations were plotted on this base map and a structural form-line map was constructed. The form-line map, combined with the lithologic information, was used to generate the geologic map, which was digitized using ARCmap version 10®. The ARCmap geologic map (Hawkins and Steltenpohl, 2011) is available at the Geological Survey of Alabama digital online data repository, and a hard copy is provided as Plate 1.

A Garmin *GPSmap 60CSx* handheld GPS unit was used to record the latitude and longitude of the data collection sites. Data collected by the GPS unit were imported into ARCMAPS® to display precise locations for each station and to assist in the planning of future traverses. This allowed for an accurate projection of field stations on the digitized geologic map.

Laboratory work included petrographic analysis of approximately 30 thin sections. Thin sections were examined to determine lithologic characteristics, metamorphic mineral



assemblages, and textural relationships. Plagioclase An numbers were established using the Michel Levy method. Thin sections were cut perpendicular to the dominant metamorphic or mylonitic foliation and parallel to the mineral or elongation lineation. Thin sections were analyzed using a Motic BA300Pol. microscope with a camera attachment, and photomicrographs were taken using a Canon Rebel xti. The software PTGui was used when it was necessary to stitch photographs together for a larger field of view.

Ten samples of igneous rocks from the Our Town quadrangle were selected for geochemical study. Samples weighing approximately 20 grams were submitted to Acme Analytical Laboratories (Vancouver) Ltd. for commercial analysis. Samples were analyzed by whole rock XRF (X-ray fluorescence) and ICP-MS (inductively coupled plasma mass spectrometry) for major-oxide, LOI, and REE-element content. The geochemical results were compared to published geochemical data of other regional meta-igneous bodies to explore for possible petrogenetic relationships.

Muscovites were extracted from a meta-granite sample in the study area for  $^{40}\text{Ar}/^{39}\text{Ar}$  isotopic analysis. The grains were extracted at the rock preparation facilities at Auburn University using a mortar and pestle and various sized sieves. The mortar and pestle and sieves were cleaned using a wire brush and compressed air to prevent cross contamination. Grains of appropriate size were separated by hand using a binocular microscope. Grains were analyzed, under the supervision of Dr. W. Hames, in the ANIMAL lab at Auburn University for  $\text{Ar}^{40}/\text{Ar}^{39}$  to determine cooling ages. The obtained date was compared to other published cooling age data for the region to determine possible tectonic relationships.

Zircons were extracted from samples of unweathered Kowaliga megacrystic gneiss for U-Pb isotopic analysis. Rock preparation was conducted at Auburn University and samples were crushed using a disc mill to approximately 25-50 microns. The disc mill was cleaned with a wire brush, ethanol, and compressed air before use to prevent contamination. After crushing, the sample was sieved and separated using heavy liquid methods (methylene iodide) and zircons were picked by hand from the separated portion. Zircons were analyzed using Secondary Ion Mass Spectrometry (SIMS) at the University of California at Los Angeles by Dr. Haibo Zou. The obtained crystallization age can be used to determine the timing of intrusion of the Kowaliga Gneiss. Materials resulting from this study, including computer data, hand samples, thin sections, and maps will be archived in the facilities of the Department of Geology and Geography, Auburn University.

## **Lithologies**

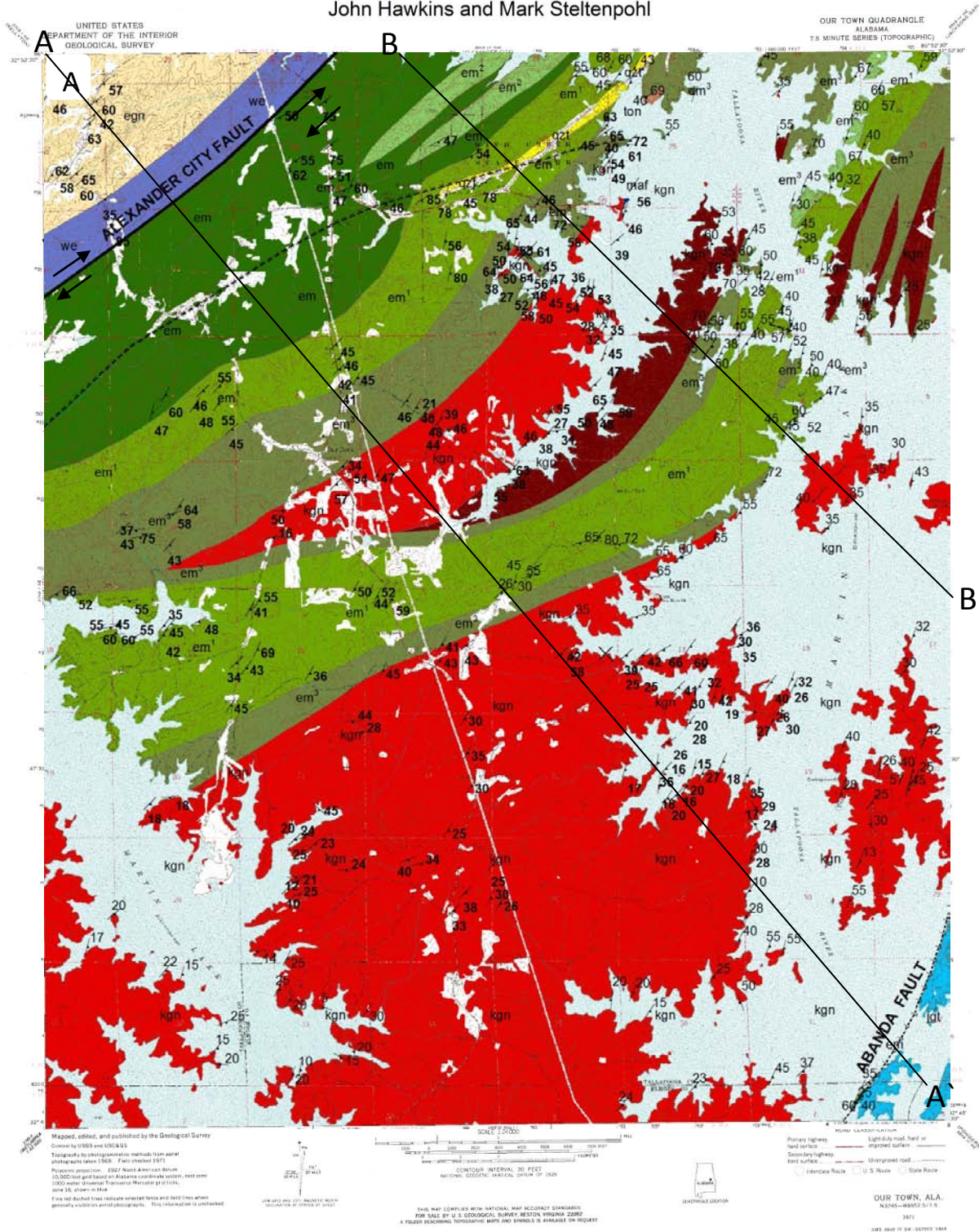
Rocks of the eastern Blue Ridge comprise the majority of units mapped in the Our Town quadrangle and include metamorphosed sedimentary, volcanic, and plutonic types. These rocks have been regionally metamorphosed up to middle-amphibolite facies conditions (Bentley and Neathery, 1970). The eastern Blue Ridge is structurally below the Brevard zone/Jacksons Gap Group in the southeast portion of the Our Town quadrangle, and is separated by the Abanda fault. The units of the eastern Blue Ridge, starting with the structurally lowest unit are, the Wedowee Group and its intrusion the Elkahatchee Quartz Diorite, the Emuckfaw Group and its associated subunits, and the Kowaliga Gneiss. They are discussed in the same order. Minerals are listed in order with abundances increasing from left to right. Units described are those depicted on the geologic map and cross-sections of the Our Town quadrangle (Figs. 2A to 2C).

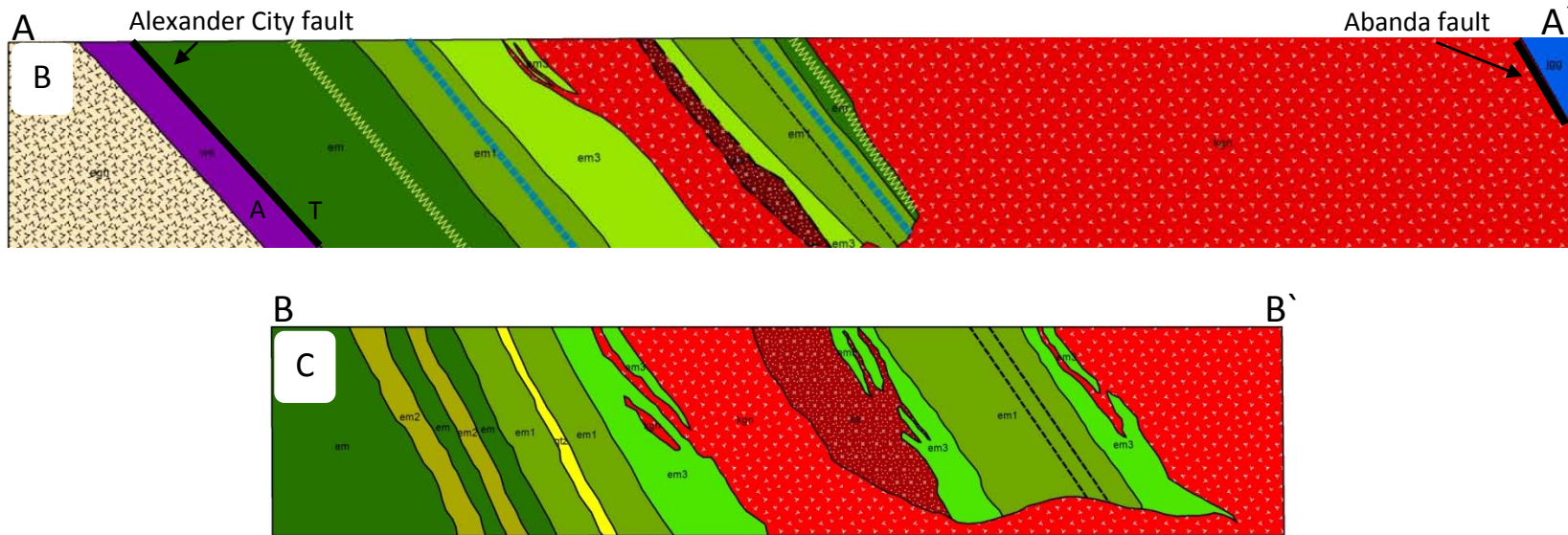
### ***Wedowee Group***

The Wedowee group is described as a dark-green to black, fine-grained biotite chlorite sericite phyllite, graphite sericite phyllite, and tan fine-grained quartzite and meta-siltstone (Raymond et al., 1988; Guthrie and Dean, 1989). The phyllite is locally garnetiferous on the 1:24K quadrangle and directly to the west it has been interpreted to have a gradational contact with the Emuckfaw Group above it and an intrusional contact with the Elkahatchee Quartz Diorite below it (Pazel, 2012). Within the phyllites are light- to dark gray fine-to medium-grained biotite-rich quartzites. The Wedowee Group has very limited exposure within the Our Town quadrangle and is difficult to distinguish from the Emuckfaw Group. Mylonites and

# Geologic Map of the Our Town Quadrangle Alabama













John Hawkins and Mark Steltenpohl






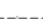
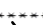







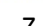


**Figure 2.** A. Geologic map of the Our Town quadrangle. B. Cross-section (A-A') with line of cross-section outline on map. C. Cross-section (B-B') with line of cross-section outlined on map

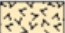







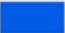
### Lithologies

	<b>egn</b> Elkahatchee Quartz Diorite Gneiss Mesocratic to melanocratic, fine- to coarse-grained, massive to strongly foliated, locally sheared quartz diorite gneiss.
	<b>we</b> Wedowee Group Schist and phyllonite with alternating, centimeter and finer scale, dark and light colored banding (garnet and biotite-rich vs. quartz-rich). Minor quartzite and amphibolite layers occur in this package of rocks.
	<b>em</b> Emuckfaw Group Tan to buff muscovite schist containing 2-5 cm layers of quartzite. Schist weathers to a deep red and the quartzite has a reddish stain.
	<b>em<sup>1</sup></b> Emuckfaw Group 1 Tan to buff muscovite schist interbedded with more silty, biotite-rich layers, thin (2-5 cm) rare amphibolites, and thin (10-15 cm) quartzites that locally contain amphiboles and garnets. Schist weathers to a dark red, biotite-rich layers are light to dark brown, and quartzites have a reddish stain.
	<b>em<sup>2</sup></b> Emuckfaw Group 2 Tan to buff muscovite schist with interbedded layers of highly competent fine grained biotite-rich quartzites. Schist weathers to a dark red and biotite-rich layers are light to dark brown.
	<b>em<sup>3</sup></b> Emuckfaw Group 3 Layers up to 1.5 m of tan to buff muscovite schist with tabular bodies of interbedded muscovite rich, biotite poor, highly foliated granites, ranging up to 2 m thick. Schist weathers to a dark red and the granites are light tan.
	<b>qzt</b> Emuckfaw Quartzite Layers up to 15 cm containing amphiboles and garnets up to 3 mm in diameter. Color ranges from light gray to black. Quartzite weathers a white and rust color oxidation surface.
	<b>ptm</b> Protomylonite Coarse to fine-grained metagranite with angular quartz exposed on weathered surfaces. Weathers to pale pink in color.
	<b>kgn</b> Kowaliga Gneiss Biotite rich granite to granodiorite with sheared potassium feldspar grains up to 2 cm in diameter, highly foliated, and sheared by discrete shear zones. Brown to bronze in color and weathers to a deep red.
	<b>kgn</b> Kowaliga Augen Gneiss Intermediate granite varying to alkali feldspar granite containing euhedral potassium feldspar megacrysts up to 10 cm long, with biotite defining foliation, anastomosing shearing of potassium feldspar grains seen locally in this lithology. Surface exterior is stained black, augen are pink in a white and black matrix, augen weather to white with matrix weathering to a light gray.
	<b>maf</b> Meta-gabbro Fibrous to bladed calc-clinoamphiboles with an interstitial matrix of potassium feldspars, massive to highly foliated with asbestos form amphiboles occurring along small scale shears, locally epidote rich. Color ranges from pale to dark green.
	<b>jgt</b> Jacksons Gap Group Medium to fine-grained, tan to buff colored, massive to thinly layered quartzite and metaconglomerates and layers of graphitic quartz schist, locally containing small garnets (5 mm).

### Legend

	Aplite and pegmatite dikes
	Strike and Dip
	Biotite lineation
	Normal fault
	Brittle fault
	Right slip fault
	Oblique dextral-normal fault
	Metagranite
	Amphibolites
	Quartz/Amphiboles/Garnets
	Thin quartzites
	Shear zones
	Contacts

### units

	egn
	we
	em
	em1
	em2
	qzt
	ka
	kgn
	jgg

phyllonites of the right-slip Alexander City fault (Steltenpohl et al., 2013) separate the Wedowee Group from the Emuckfaw Group in the Our Town Quadrangle.

### ***Elkahatchee Quartz Diorite Gneiss***

The Elkahatchee Quartz Diorite Gneiss is a medium-to coarse-grained biotite tonalite gneiss that intruded the Wedowee Group. It is a dark-gray, foliated granitoid consisting of plagioclase, quartz, biotite, muscovite, epidote, and traces of alkali feldspar, sphene, allanite, and secondary calcite (Gault, 1945). The Elkahatchee Quartz Diorite has a medium-grained, hypidiomorphic texture with the majority of mineral grains aligned to the predominant gneissic fabric. Within the Our Town quadrangle the Elkahatchee Quartz Diorite presents limited exposure.

### ***Emuckfaw Group***

The Emuckfaw Group is described as a metasedimentary unit ranging from schist and phyllonite to high-grade paragneiss of various compositions (Neathery and Reynolds, 1973). No detailed lithologic information was reported for the Emuckfaw Group, however, and its stratigraphic makeup and, consequently, its significance is largely conjectural. Lithologic variations identified during field mapping allows for a subdivision of the Emuckfaw Group within the Our Town quadrangle. These subdivisions include the following: muscovite schist containing 2-5 cm thick layers of quartzite (*em* on Fig. 2 and Plate 1); muscovite schist with interbedded silty biotite layers, rare centimeter thick amphibolite, and garnetiferous amphibole-bearing quartzite (*em*<sup>1</sup> on Fig. 2 and Plate 1); muscovite schist with interbedded layers of biotite-rich quartzite (*em*<sup>2</sup> on Fig. 2 and Plate 1); muscovite schist with interbedded, muscovite-rich, biotite-poor, highly foliated granite ranging up to 2 meters in thickness (*em*<sup>3</sup> on

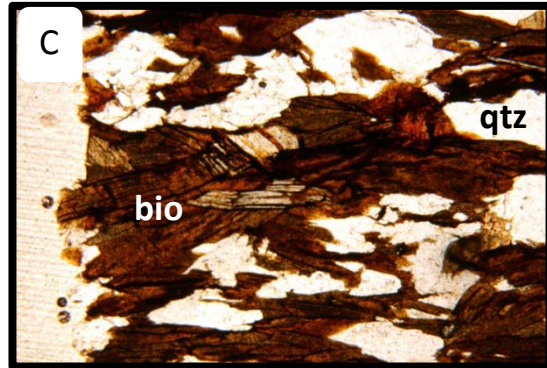
Fig. 2 and Plate 1 ). In addition to highly foliated biotite-poor metagranite, there are 1 to 2 m thick layers of Kowaliga Gneiss interbedded within the muscovite schist. These Kowaliga Gneiss layers are generally proximal to pluton contact margins, and this is in contrast to the biotite-poor metagranites found throughout the  $em^3$  lithotype. Analysis of these lithotypes will be discussed individually instead of in tectono-stratigraphic order to avoid repetition in the discussion.

#### *Muscovite Schist*

Muscovite schist found in Emuckfaw Group subdivisions:  $em$ ,  $em^1$ ,  $em^2$ , and  $em^3$  is a coarse grained (up to 2.5 cm long muscovite grains) schist that primarily consists of muscovite. Where composition allows, garnets up to 1 cm in diameter occur locally throughout the muscovite schist. Garnets are porphyroblastic, euhedral, and commonly leave divots in the schist where they were plucked out. It is highly foliated and where cross cut by shear zones has a well developed S-C fabric causing a “button-like” appearance. Muscovite grains are tan to bronze colored with various sections occurring within the schist being more graphitic. Exposures weather to a deep red-maroon color with garnets oxidizing to a dark brown. This unit commonly occurs with inter-layers of quartzite, amphibolite, and meta-granite.

#### *Quartz-Biotite Schist*

Quartz-biotite schist (found in  $em^1$  and  $em^3$ ) in outcrop is easily distinguished from the surrounding muscovite schist. Quartz-biotite rich layers are tabular, up to 5 cm in thickness, and stand in high relief when compared to the muscovite schist (Figs. 3A and 3B). The color ranges from light brown to a reddish-brown with minor amounts of sheet silicates (muscovite) causing a reflective quality visible in the outcrop. It has thin, well developed cleavage that is



**Figure 3.** Photographs and photomicrographs of the quartz-biotite schists of the Emuckfaw Group. A. and B. Outcrop views of characteristic ribs. C. Thin section with a 5 mm field of view (in ordinary light). D. Same view as in C., but with crossed polars.

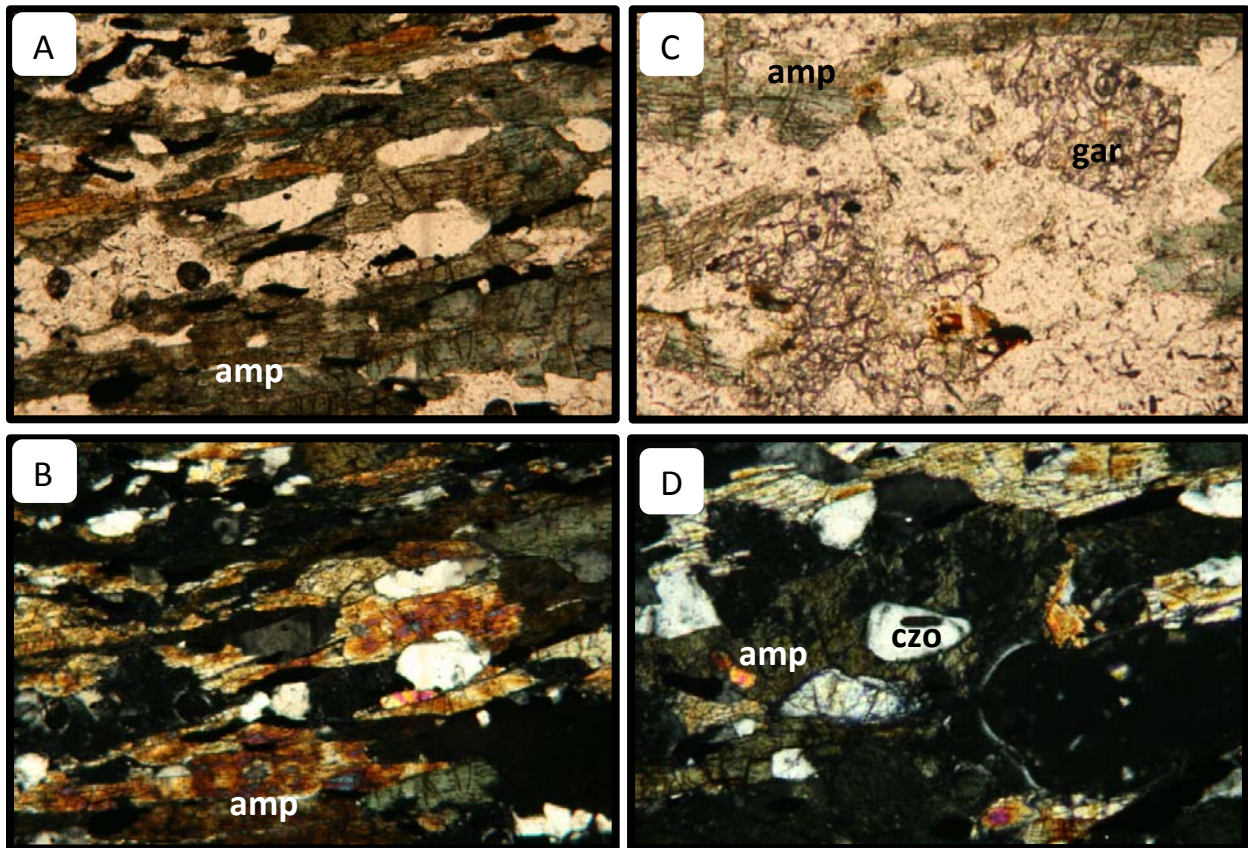


consistently even in deeply saprolitized exposures. Mineralogy consists of biotite, quartz, muscovite, and minor amounts of opaque minerals. The foliation is defined by the biotite and muscovite, with a majority of the sheet silicates observed length parallel to the foliation (Figs. 3C and 3D). Individual biotite grains range up to 5 mm in length. The biotite is dark brown and is slightly pleochroic in thin section. Quartz ranges up to 2 mm in length, and is monocrystalline to polycrystalline with straight to interlobate grain boundaries. Quartz generally displays strong undulose extinction. Muscovite ranges up to 3 mm in length and is clear in ordinary light.

### *Amphibolite*

Amphibolite layers are found inter-layered with unit *em*<sup>1</sup>. Amphibolite units are rare but they are easily spotted in outcrop due to the resistivity to weathering relative to the muscovite schist. The amphibolites are thin, 2 cm to 3 cm thick, tabular, and fine to medium grained. The rock is dark green to black and has a reddish-brown oxidized rim on exposed surfaces. Idioblastic to subidioblastic amphiboles, 1 -2 mm in length can easily be observed with a hand lens in the fine grained quartz matrix.

Mineralogy of the amphibolite consists of amphibole (hornblende), quartz, biotite, garnet, and trace amounts of clinozoisite/epidote, chlorite (associated with biotite), and opaques. The amphiboles range up to 2 mm in length along the c axis and are arranged nematoblastically, length-parallel, within the foliation (Figs. 4A and 4B). Pleochroism ranges from a light pale green to a light green-blue, and grains have inclined extinction at ~12-15 degrees from parallel to the c-axis. Birefringence is first-order orange and yellow, ranging up to minor first-order blue and pink. Amphibole makes up the majority of the thin section, with biotite only occurring as alteration minerals after amphibole. There are also minor <1 mm



**Figure 4.** Amphibolite Photomicrographs A. Amphibole defining the primary foliation occurring with monocrystalline quartz (2.5 mm field of view). B. Crossed polar view of photomicrograph A. C. Subidioblastic to xenoblastic garnets (1mm field of view). D. Monocrystalline quartz and clinozoisite inclusions with amphibole (1 mm field of view).

inclusions of non-undulose single-grain quartz within the amphiboles. Other than these inclusions, quartz grains range in size from 1 mm and below with grains ranging from flat-field extinction to highly undulose. Quartz grain boundaries are polygonal to slightly interlobate and large amounts of inclusions are common. Inclusion minerals include green amphibole, clinozoisite, zircon, and rutile (Fig. 4D). Garnets range from idioblastic to xenoblastic with an average grain size of 1 mm (Fig. 4B). Grains are isotropic under crossed nicols and they have a pale yellow color in plane light. Garnet grains are highly fractured with minor inclusions of quartz. Clinozoisite and epidote are rare in thin section, and grains are less than 1 millimeter with a subidioblastic habit. Clinozoisite and epidote grains are clear in plane light and show a bluish to pistachio green colored birefringence.

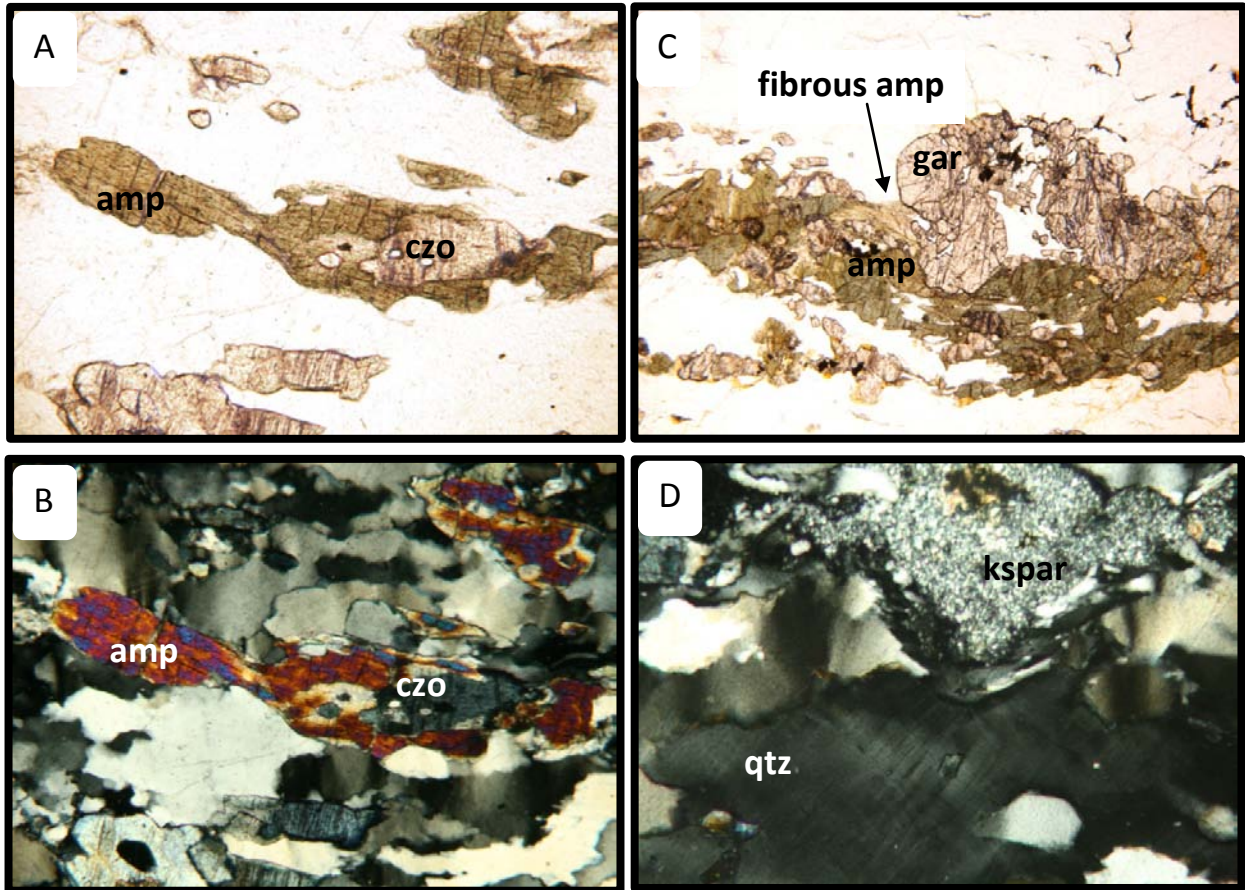
#### *Garnetiferous Amphibole-bearing Quartzite*

Garnetiferous amphibole-bearing quartzite (found in Emuckfaw Group subdivision *em*<sup>1</sup>) is more resistant to weathering than the adjacent muscovite schist and, thus, stands out from saprolite with a higher relief. Layers vary in thickness from 3 cm to 15 cm and weather to a dark red-brown color with oxidized and corroded garnets. In fresh exposures the rock is dark blue with pink garnets. In out crop, the foliation is marked by fine dark layers (1 mm to 2 mm thick) of amphibole in the quartzite with garnets only occurring along planes of foliation accompanied by amphiboles. Garnetiferous amphibole-bearing quartzite differs from the amphibolite in color and mineralogy. The garnetiferous amphibole-bearing quartzite (dark blue) is predominantly quartz with garnet and amphibole defining foliation, and the amphibolite (dark green to black) is predominantly amphibole with only minor quartz.

The mineralogy consists of quartz, amphibole, garnet, clinozoisite (disilicate), sericitized potassium feldspar, minor amounts of cordierite, zircon and sphene, and alteration minerals of chlorite and an unidentified carbonate. Quartz grains vary from 0.05 mm up to 4mm and are inequigranular and polycrystalline. Grain boundary migration is inferred based on irregular and interlobate grain contacts (Passchier and Trouw, 2005). The larger (up to 4 mm) relict grains contain deformation lamellae (Fig. 5D) and all quartz grains have strong undulose extinction. Inclusions of clinozoisite are rare and are observed in less than 5% of the quartz in the thin section. Amphiboles are xenoblastic and vary from 0.05 mm to 3 mm in length (Figs. 5A and 5C). They are biaxial negative with inclined extinction with light-green to pale-green pleochroism. Amphiboles occur along foliation planes and are associated with clinozoisite and garnets. Rarely, fibrous amphibole is present, but only in conjunction with garnet (Fig. 5C). Amphiboles have been retrograded to two alteration minerals, chlorite and an unidentified carbonate. Garnets are subidioblastic to xenoblastic, isotropic, and vary in size from 0.025 mm to 2 mm in diameter. Cores of the garnets have inclusions of clinozoisite and quartz while the rims are inclusion free. Garnets principally occur along the dominant foliation. Cordierite is subidioblastic and is ~1 mm in diameter with well defined cyclic twins. They occur along the foliation with garnet and clinozoisite. Clinozoisite is subhedral, ranging from 1 mm to 3 mm in length, with parallel extinction and anomalous birefringence ranging from steel blue to pistachio (Fig. 5C).

#### *Biotite-rich Quartzite*

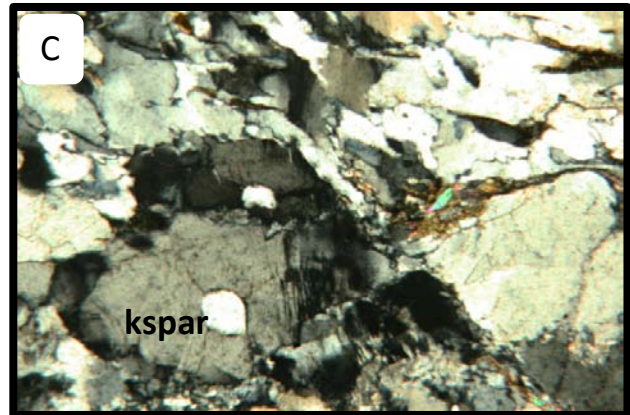
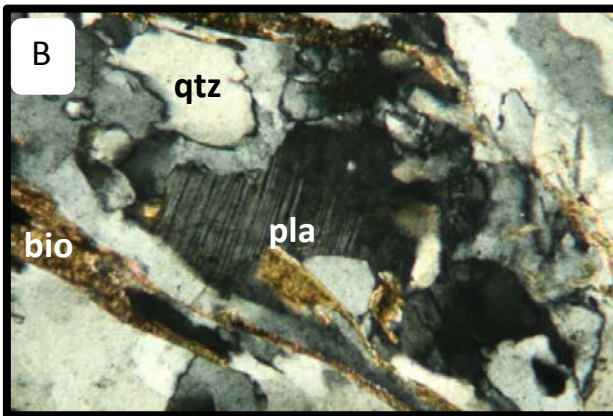
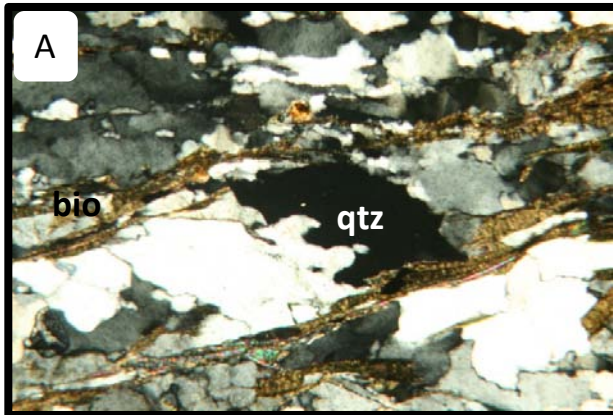
Biotite-rich quartzite is denoted as  $em^2$  in plate 1 and is mapped as discontinuous layers within the Emuckfaw Group. In outcrop the biotite-rich quartzite layers are more resistant to



**Figure 5.** Photomicrographs of garnet amphibole-bearing quartzite. A. Amphibole with an epidote/clinozoisite inclusion (2.5 mm field of view). B. Crossed polar view of photograph A. C. Garnet, amphibole, and fibrous amphibole (5mm field of view). D. Kink bands in quartz and sericitized potassium feldspar (1 mm field of view).

weathering and stand out in contrast to the more easily weathered muscovite schist. Fresh surfaces are coated with biotite and are black in color set in brownish-tan colored matrix. Biotite grains also define the principal foliation along with muscovite. The biotite-rich quartzite differs from the garnetiferous amphibole-bearing quartzite in color and in mineralogy. The biotite-rich quartzite is a dark gray compared to the blue gray of the amphibole bearing quartzite. The biotite-rich quartzite also lacks amphibole.

The mineralogy of the biotite-rich quartzite is quartz, potassium feldspar, plagioclase, biotite, clinozoisite/epidote, and trace amounts of apatite and muscovite. Quartz grains range in size from 0.025 mm to 3 mm and are predominantly polycrystalline. Interlobate and irregular grain boundaries predominate and indicate grain boundary migration (Passchier and Trouw, 2005) (Fig. 6A). The degree of undulose extinction varies throughout the thin section. Potassium feldspar ranges from 0.5 mm to 3 mm and is concentrated primarily into bands that are parallel to foliation. Grains show tartan twins along the grain boundaries most likely generated by solid-state deformation (Vernon, 2004) (Fig. 6C). In addition to tartan texture, flame perthite and granophyric intergrowths are observed. Flame perthite is interpreted to be a replacement of potassium feldspar by albite in high-strain sites during deformation (Vernon, 2004). The granophyric texture suggests rounding and deformation of older myrmekitic intergrowths (Vernon, 2004). Inclusions in potassium feldspar consist of sub-millimeter, rounded monocrystalline quartz, polycrystalline quartz, and clinozoisite/epidote. Plagioclase grains are anhedral and approximately 1 mm in diameter. Albite twins, pericline twins, and untwinned varieties are present. Albite-twin geometry suggests growth by deformation with only minor amounts of albite twinning resulting from lamellar growth (Fig. 6B). Plagioclase An



**Figure 6.** Photomicrographs of the biotite-rich quartzite. A. Interlobate quartz grain boundaries (1 mm field of view). B. Plagioclase deformation twinning (1 mm field of view). C. Deformation induced tartan twinning (Vernon, 2004) in potassium feldspar (2.5 mm field of view).

numbers are not reliable due to nature of albite twinning. Biotite grains are up to 3 mm in length and grains are length parallel to define the lepidoblastic foliation. Pleochroic colors range from clear to light brown and transition to dark brown. Minor amounts of 2 mm long muscovite grains occur within the biotite layers. Biotite is also observed draping around potassium feldspar grains. Clinozoisite and epidote are sub-millimeter to 3 mm in length and range from subidioblastic to xenoblastic in habit and are observed along foliation together with the biotite.

### *Metagranite*

Metagranite occurs in lithotype  $em^3$  and is more resistant than the surrounding muscovite schist. The metagranite bodies are tabular (1-2 m thick), commonly strongly foliated, muscovite-rich and biotite poor, this latter feature being a defining characteristic that separates it from the Kowaliga Gneiss. In outcrop the metagranite is finer grained than the Kowaliga Gneiss with no observed augen and light pink to whitish-gray in color. More massive (non-foliated) varieties of this lithotype occur along the margins of the Kowaliga megacrystic gneiss.

The mineralogy of the metagranite consists of potassium feldspar, plagioclase (An<sub>40-45</sub>), quartz, biotite, muscovite, garnet, and opaques. Potassium feldspar constitutes ~70% of the feldspars present. Potassium feldspar grains are up to 2 mm in diameter with minor inclusions of sub-millimeter monocrystalline quartz. Potassium feldspar has patchy areas of tartan twinning emanating from points of high strain (Vernon, 2004). Plagioclase grains are up to 1.5 mm with the larger grains showing a more rounded appearance. Albite twins are deformed and some twin geometries indicate twinning by deformation. Quartz grains are up to 1 mm in diameter and are polycrystalline with interlobate to polygonal grain boundaries.

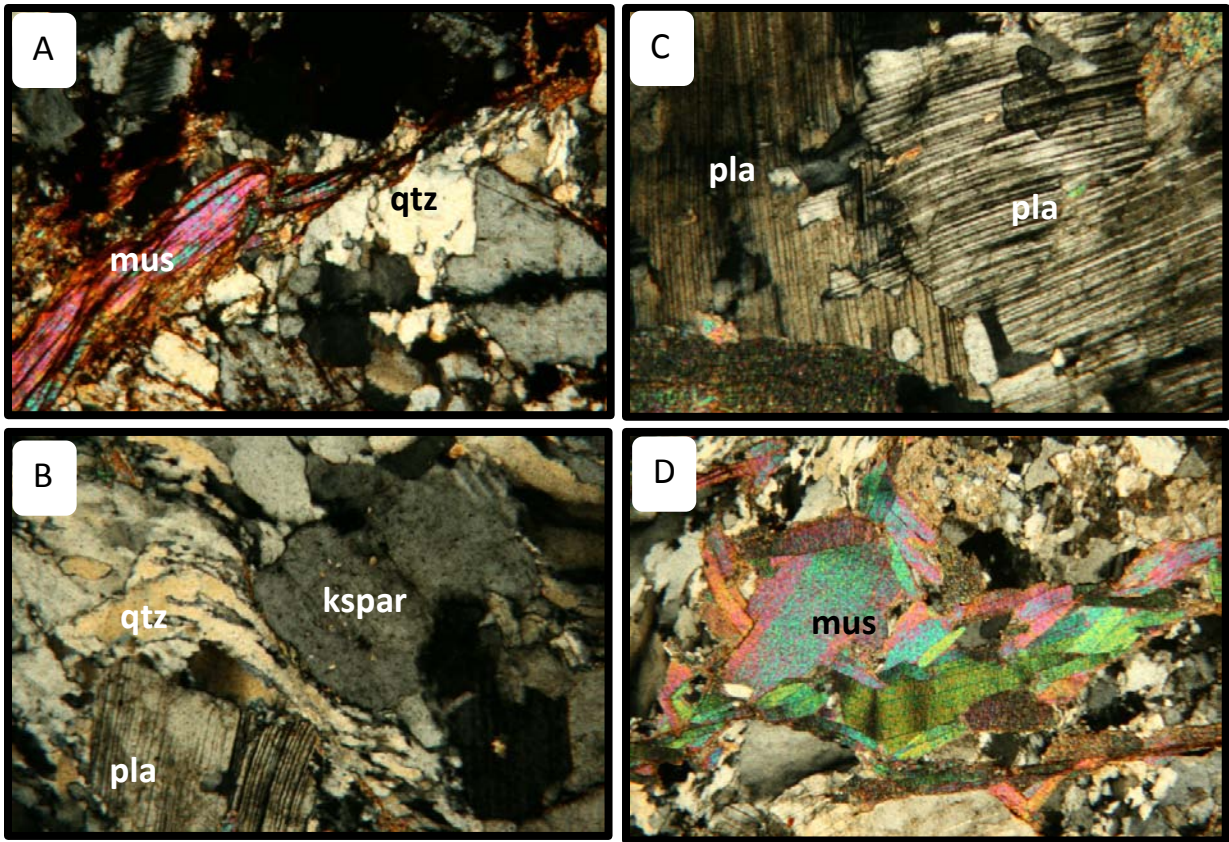


Microstructures representing grain boundary migration and minor recrystallization textures in quartz are present, as are isolated quartz ribbons indicating a proto-mylonite in some areas (Passchier and Trouw, 2005). Biotite occurs primarily along the dominant foliation and grains are up to 2 mm in length. Pleochroic colors range from light brown to dark brown. Garnets are up to 1.5 mm in diameter and are strongly fractured. Smaller, 0.5 millimeter garnets have a subidioblastic habit. Garnets have alteration oxides within the fractures.

### *Protomylonite*

Within the Emuckfaw Group proximal to the contact with the Kowaliga Gneiss, are pods of protomylonitic metagranite. It is unclear if it is a separate phase from the Kowaliga Gneiss due to limited exposure. Maximum thickness of the protomylonite bodies are at least 20 meters and their extent along strike is undetermined due to spotty exposure. Color ranges from pale gray to light pink, and quartz grains up to 5 mm extend out giving the outcrop a jagged texture. Deep-red stains are observed in hand sample likely due to the oxidation of iron.

Mineralogy of the protomylonitic metagranite consists of quartz, plagioclase ( $An_{55-60}$ ), potassium feldspar (microcline and orthoclase), muscovite, trace garnets, and minor amounts of opaques. Plagioclase constitutes ~80% of the feldspar present. Quartz grains are polycrystalline with irregular grain boundaries formed in response to grain boundary migration (Passchier and Trouw, 2005). Dynamically recrystallized quartz formed by sub-grain rotation are evident with grains having weak shape-preferred orientation in direction of flow is seen in quartz ribbons concentrated between more competent grains (Passchier and Trouw, 2005) (Fig. 7A). Quartz grains are up to 3 mm in diameter with 0.01 mm to 0.5 mm diameter grains occurring as inclusions in other minerals. Plagioclase ( $An_{55-60}$ ) grains are subhedral to anhedral



**Figure 7.** Photomicrographs of protomylonitic granite A. Muscovite defining the primary foliation with minor ductile deformation (2.5 mm field of view). B. Quartz ribbon between two feldspar grains (2.5 mm field of view). C. Kinked and bent Albite twins in plagioclase feldspar with margins indicating grain boundary migration (2.5 mm field of view). D. Muscovite showing kink bands and undulose zones (5 mm field of view).

and are up to 3 mm in diameter. Grains have well defined albite and pericline twinning with plastic deformation of the albite twins (Figs. 7B and 7C). Some grains have a faux microcline appearance due to the combination of albite and pericline twinning, creating a tartan-like pattern. Along grain margins, twins are observed extending from one plagioclase grain into another, indicating grain boundary migration (Fig. 7C.). Plagioclase grains are weathered or otherwise altered to sericite. Within the plagioclase grains, inclusions of quartz, smaller plagioclase, microcline and muscovite are common. Muscovite grains are idioblastic to subidioblastic, up to 3 mm in length, and exhibit kink folds on undulatory extinction (Fig. 7D). Muscovite grains appear to be porphyroblastic and have 0.1 mm to 0.75 mm inclusions of quartz and plagioclase. Principal foliation is defined by muscovite (Fig. 7A). Subidioblastic garnet, ~0.5mm in size, is present in thin section, but only in trace amounts.

### ***Kowaliga Gneiss***

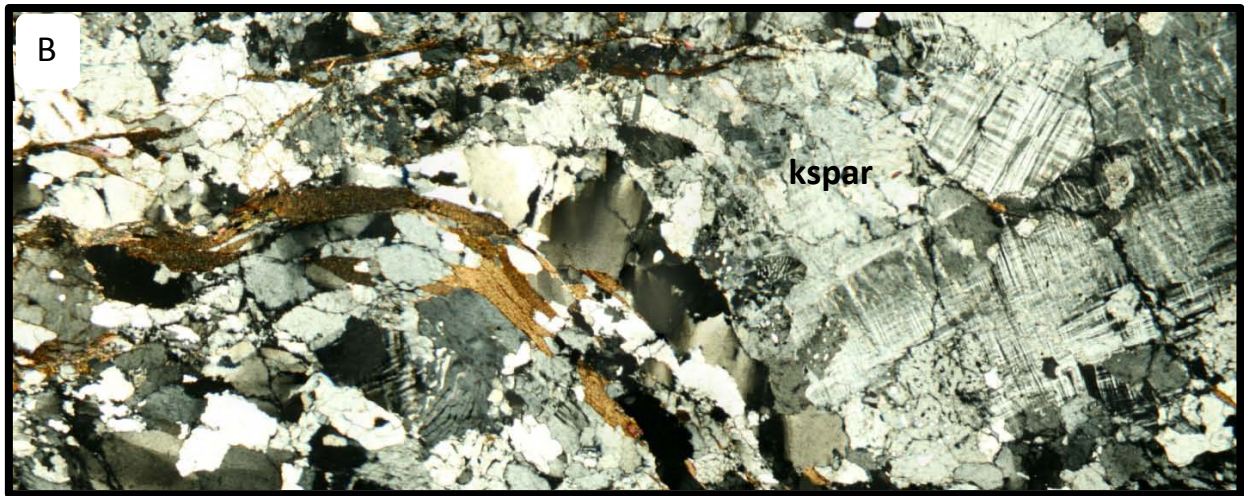
The Kowaliga Gneiss intrudes the Emuckfaw Group and is described as a batholith of granite to granodioritic gneiss that extends nearly 65 km along strike (Bentley and Neathery, 1970; Stoddard, 1983; Bieler and Deininger, 1987). These gneisses are interpreted to have an I-type magmatic source with possible metasedimentary contamination (Drummond et al., 1997). Field relations in the Our Town quadrangle are that the Kowaliga Gneiss become interleaved as sill-like layers of granitic gneiss within the Emuckfaw Group as the contact is approached. Based on the results of field mapping, petrology, and geochemistry, rocks previously lumped into the Kowaliga Gneiss are here subdivided into Kowaliga augen gneiss and Kowaliga megacrystic gneiss, the latter being distinguished by the occurrence of euhedral potassium feldspar megacrysts. For this reason the current author uses the informal term

Kowaliga gneiss (i.e., lower case “gneiss”) where no distinction is made between the textural varieties.

*Kowaliga augen gneiss*

In out crop, the Kowaliga augen gneiss is medium-to-coarse grained, and well-foliated and lineated. Plastic shear zones, with well defined S-C fabrics, commonly cut the Kowaliga augen gneiss. Rotated potassium feldspar augen, 2-3 cm in diameter, are set in a matrix of finer-grained quartz, potassium feldspar, biotite, with minor amounts of muscovite. Stretched biotite and quartz grains are commonly observed within the plane of foliation, defining an elongation lineation. The gneiss weathers from pale pink to light gray-brown, with white augen clearly visible. Saprolitized outcrops are light orange in color with spots of white.

Mineralogy of the Kowaliga augen gneiss is quartz, potassium feldspar (orthoclase and microcline), andesine plagioclase (An<sub>35-45</sub>), biotite, and minor amounts of muscovite, clinozoisite, epidote, and amphibole. Quartz grains, up to 3 mm in length, are subhedral to anhedral with polygonal to interlobate grain boundaries ranging in size. Quartz ribbons drape larger more competent potassium feldspar phenocrysts. Potassium feldspar grains are subhedral and are primarily microcline with tartan twinning and flame-like perthitic texture. The perthitic texture is not consistent throughout the potassium feldspar but appears to have been formed in sites of high-strain. The margins of the augen grains are mantled by myrmekitic to granophyric colonies replacing the larger phenocrysts of potassium feldspar (Figs. 8A and 8B). The granophyric texture is inferred to be mymerkite texture that was modified during deformation. Inclusions of smaller (0.25 mm to 2.5 mm) rounded to irregular grains of granophyric potassium feldspar, highly sericitized potassium feldspar, mymerkitic plagioclase,



**Figure 8.** Photomicrographs of Kowaliga augen gneiss A. Sheared potassium feldspar grains that are mantled by myrmekitic to granophyric colonies replacing the larger phenocrysts of potassium feldspar (10 mm field of view). B. Quartz ribbons drape larger more competent grains of potassium feldspar (10 mm field of view).

biotite, and singular quartz grains are common. Plagioclase ( $An_{35-45}$ ) grains are subhedral to anhedral, range in diameter from 0.25 mm to 2 mm, and have inclusions of clinozoisite.

Twinned and untwinned varieties are common along with alteration to sausserite. Biotite helps define the principal foliation. Grains range up to 2.5 mm in length and pleochroism varies from dark to light brown to dark green in color.

### *Kowaliga megacrystic gneiss*

The Kowaliga megacrystic gneiss is traditionally mapped to be included into the Kowaliga Gneiss (Bentley and Neathery, 1970; Stoddard, 1983; Bieler and Deiningner, 1987). The author interprets the Kowaliga megacrystic gneiss as having the same magmatic source as the Kowaliga augen gneiss, but it is texturally expressed differently due to varying degrees of shear strain. The Kowaliga megacrystic gneiss is mapped based on the occurrence of mesoscopically euhedral potassium feldspar megacrysts (up to 15 cm) in contrast to the Kowaliga augen gneiss that has lenticular (augen) shapes formed sympathetically with increasing degrees of mylonitization. This textural transition carries a decrease in size of the potassium feldspars from up to 15 cm in the megacrystic variety to an average of 1.5 to 2 cm. A distinct change in color follows the same transition. In outcrop, the megacrystic gneiss has a dark gray-to-black matrix with potassium feldspar megacrysts that are light gray to white in color. Potassium feldspar megacrysts are zoned and are simple-twinned euhedral crystals with near 90 degree cleavages. The color of the matrix changes from a grey-to-black to a light pale gray where it has been saprolitized.

The matrix to the megacrystic gneiss is a porphyroblastic rock with weak foliation defined by biotite and quartz ribbons. The mineralogy consists of quartz, potassium feldspar (orthoclase and microcline), plagioclase ( $An_{55-60}$ ), biotite, muscovite, and minor amounts of apatite, garnet,

clinozoisite, and opaques. Quartz grains are monocrystalline to polycrystalline, up to 3 mm in diameter, with polygonal to interlobate grain boundaries. Samples have minor quartz ribbons, indicating grain boundary migration recrystallization and sub-grain rotation recrystallization with grains having weak shape-preferred orientation, in surrounding more competent potassium feldspar megacrysts (Passchier and Trouw, 2005). Potassium feldspar grains range up to 15 cm in diameter, and display perthitic, tartan, and untwinned textures with megacrysts commonly displaying transitions from one texture to another within the same grain. Megacrysts have a variety of inclusions including plagioclase (similar An number to primary plagioclase), potassium feldspar (twinned and untwinned), muscovite, and monocrystalline quartz. Inclusions of plagioclase and potassium feldspar show high levels of alteration to sericite and sausserite with some plagioclase grains completely replaced. Inclusions along the margins of the megacrysts have a linear orientation parallel to the edges of the megacryst. Plagioclase grains are subhedral and are up to ~2 mm in diameter with varying degrees of alteration to sericite and/or sausserite. Grains do not have well defined albite twins, but albite and pericline twins are locally present. Biotite grains are euhedral to subhedral, up to 2 mm in length, show a pleochroism ranging from light brown to dark green, and define the predominant gneissic banding. Occurring with the biotite are minor amounts of muscovite, idioblastic garnet, idioblastic apatite, clinozoisite, and opaques. The garnets are ~ 1 mm in diameter with the apatite grains up to 2 mm in diameter, and both are porphyroblastic within the predominant foliation.

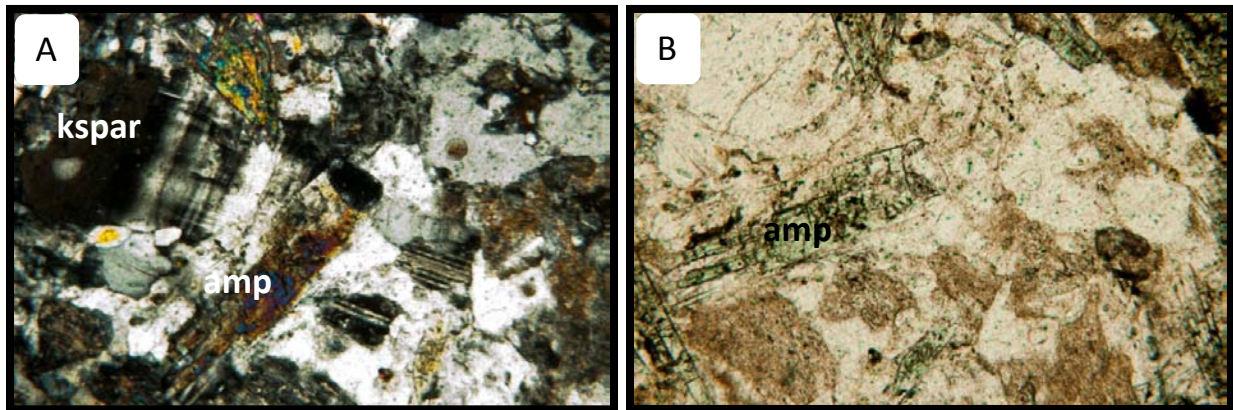
### ***Meta-gabbro***

Exposures of the meta-gabbro were found only within the boundaries of Wind Creek State Park along the shore of Lake Martin during periods of low-water levels (November to February).

This unit is more resistant to weathering than the Kowaliga Gneiss, and it has up to 0.5 m of relief along the shore. It is light-to-dark green colored with 0.5 to 1 cm bands of white rock composed of potassium feldspar, plagioclase, and quartz. Pale-green stringers (up to 2 cm thick) of fibrous asbestos-form amphibole cut the dominant foliation at high angles (nearly 90 degrees).

The meta-gabbro comprises calc-clinoamphibole, alkali feldspar (interpreted as a result of potassium metasomatism), plagioclase (An<sub>30</sub>), low-Ca pyroxene, quartz, epidote and apatite. The calc-clinoamphiboles are bladed crystals that are elongated parallel to the c-axis. The crystals are idioblastic to subidioblastic ranging in length up to 6 mm. Crystal growth is restricted to within foliation with random orientations (sprays) within this plane. The calc-clinoamphiboles are a pale-bluish-green colored in thin section with a pleochroism that ranges from transparent to a pale greenish-yellow color (Figs. 9A and 9B). Grains have an extinction angle of ~13 degrees from parallel, and are biaxial negative. Being biaxial negative eliminates the possibility of tremolite-ferroactinolite, and other optical properties (extinction angle and pleochroic behavior) suggest a chemical composition similar to pargasite-ferropargasite  $(K,Na)Ca_2(Mg,Fe)_4Al[Si_6Al_2O_{22}](OH)_2$ . Quartz grains range in length from 0.25 mm to 1 mm and are interstitial. Quartz has undulose extinction and contains small (0.01 mm-0.25 mm) inclusions of calc-clinoamphiboles. Plagioclase crystals range from less than 1 mm to 2 mm, are anhedral, and are highly altered to sericite (Fig. 9B). Albite twinning is common in thin section with planar twin boundaries suggesting they did not result from deformation. The plagioclase crystals do not have the inclusions of calc-clinoamphibole as seen in the quartz and alkali feldspar. Alkali feldspar ranges in size from less than 1 mm to 2 mm in diameter, occurs as anhedral as well as interstitial grains, and displays tartan twinning with minor





**Figure 9.** Photomicrographs of the meta-gabbro. A. tartan twinning of a microcline adjacent to a calc-clino amphibole (2 mm field of view). B. Pleochroic green colors of the calc-clino amphibole with the dusty appearance of the plagioclase grains reflecting sericite alteration (2 mm field of view).

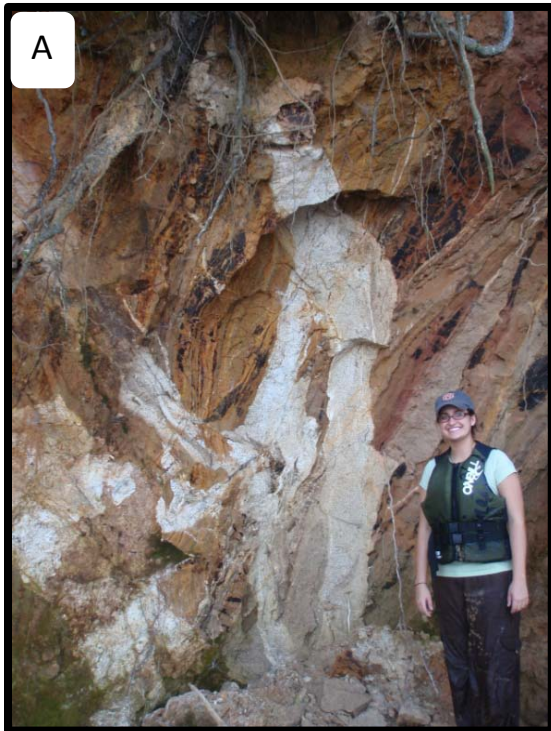
patchy perthitic exsolution (Fig. 9A). Tartan twinning is poorly developed and only is visible in parts of the crystals.

### ***Aplite Dikes***

Aplite dikes are light-colored hypabyssal igneous rock characterized by a fine-grained texture (Neuendorf et al., 2005), and have been mapped in multiple locations within the Emuckfaw Group. The aplite dikes are highly weathered and in most cases are completely saprolitized. The dikes are light gray to bright pink in color (Fig. 10). Principal mineralogy consists of potassium feldspar, quartz, muscovite, and an undetermined amount of plagioclase. The aplite dikes lack foliation and cut the  $S_1$  foliation of the host rock. This indicates a late stage (late-to-post Alleghanian) period of injection.

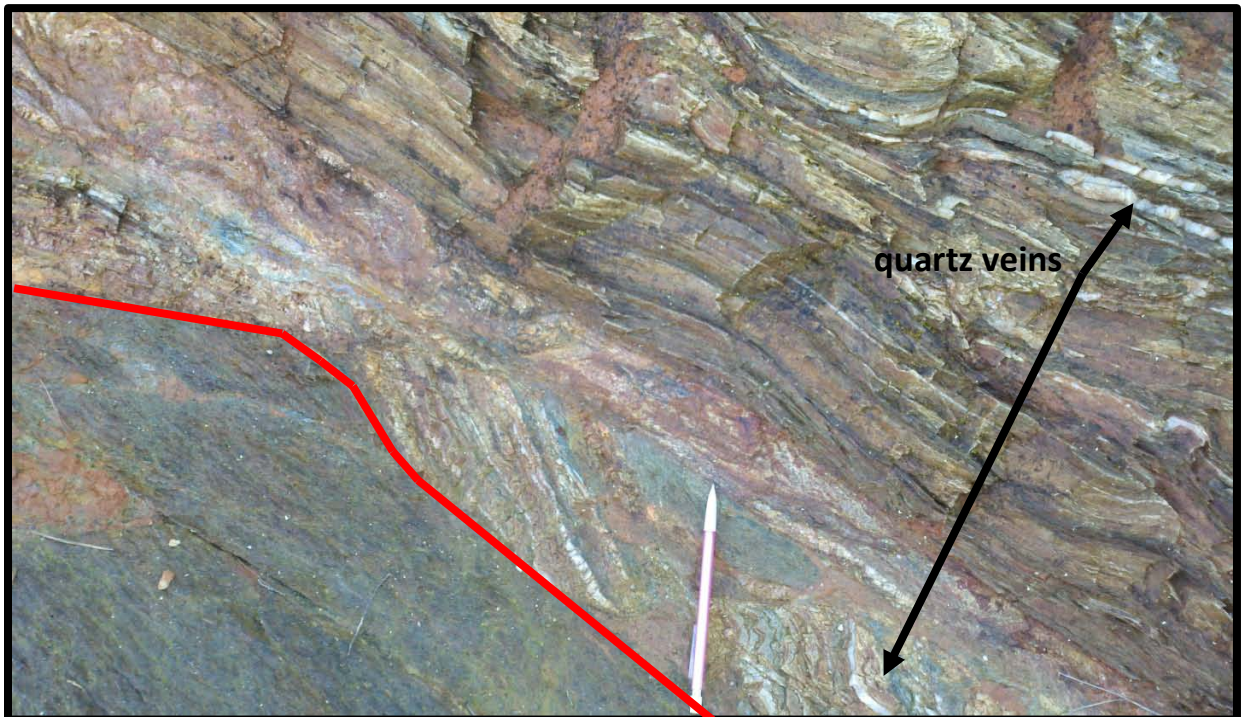
### ***Brevard zone/Jacksons Gap Group***

In the Our Town quadrangle rocks of the Brevard zone/Jacksons Gap Group account for a very minor percentage of the lithologies and they only outcrop in the southeastern corner of the map with exposure that is chiefly limited to water access. The structurally lower fault contact of the Brevard zone, the Abanda fault, juxtaposes the Jacksons Gap Group on top of the Emuckfaw Group and the Kowaliga Gneiss, and the upper fault contact, the Katy Creek Fault, emplaces the Inner Piedmont terrane but does not occur within the confines of the Our Town quadrangle. The lowest and only unit of the Brevard zone/Jacksons Gap Group exposed in the Our Town quadrangle is garnetiferous graphitic schist with interbedded thin (3-5 cm) layers of phyllitic quartzite. The base of the Jacksons Gap Group, cut by the Abanda fault, is predominantly phyllitic quartzite with a distinct absence of the garnetiferous schist. The unit is fine-to-coarse grained with a phyllitic cleavage defined by fine-grained micas and sericite. The



**Figure 10.** Photographs of late-stage aplite dikes. A. Aplite dike cross cutting layering and foliation of the Emuckfaw Group foliation. Note brittle stockwork made by injection. B. Aplite dike within the Emuckfaw Group. (N32 51.180 W85 56.220)

phyllitic quartzite is interbedded with thin (1-3 cm) layers of quartz and both layers are locally folded (Fig. 11). The Jacksons Gap Group weathers to a light-tan to dark-brown in color. Within the area of the Our Town quadrangle, the Jacksons Gap Group was not observed to contain magmatic injections. Quartz veins are present in the Jacksons Gap Group and are concentrated along the Abanda fault and are not observed within the Emuckfaw Group (Fig. 11). These observations are arbitrarily used to separate the lithologies of the Jacksons Gap Group from the Emuckfaw Group where the Abanda fault places the two in contact with each other. Emuckfaw Group units have magmatic injections observed to within one meter of the Abanda fault.



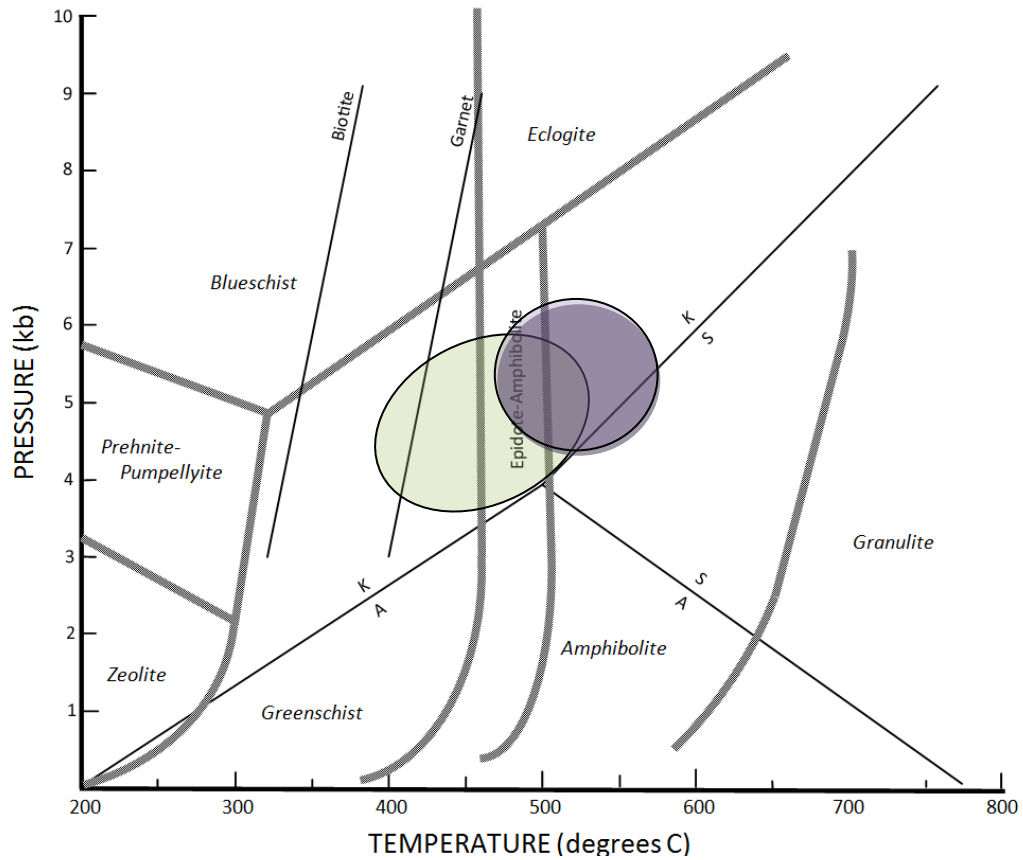
**Figure 11.** Photograph of the Abanda Fault. Base of the Jacksons Gap Group is marked by the red line. Quartz veins in the Jacksons Gap Group and the Abanda Fault are noted by black arrows.

## Metamorphism

Field and petrographic analysis of rocks in the Our Town quadrangle indicate dynamothermal Barrovian-type metamorphism with a peak garnet/ epidote-amphibolite to middle-amphibolite facies assemblage that defines the regional principal metamorphic  $S_1$  foliation (gneissosity, schistosity, and phyllitic cleavage). The epidote-amphibolite facies is a narrow band in pressure-temperature space overlapping with the garnet stability field that limits temperatures to 450-550°C, with higher temperatures possible where pressures exceed 8 kbars (Fig. 12) (Blatt et al., 1996). Sample locations with peak metamorphic mineral assemblages have been plotted (Appendix 1). Metamorphic grade is interpreted to remain relatively consistent across the quadrangle even though index minerals are rare to nonexistent even in the more pelitic lithologies of the Emuckfaw Group.

Within the Emuckfaw Group pelitic lithologies, the dominant mineral assemblages observed are biotite + muscovite + quartz with garnet occurring sporadically at all levels. The lack of consistent index minerals (garnet and disilicates) is most likely due to insufficient amounts of the aluminum necessary to generate them. Within the Emuckfaw Group quartzites, the dominant mineral assemblage observed is quartz + amphibole + epidote/clinozoisite/zoisite + garnet, and the biotite-rich quartzites have a dominant assemblage of quartz + biotite + epidote/clinozoisite + garnet.

Amphibolites within the Emuckfaw Group have a dominant mineral assemblage of amphibole + quartz + garnet + minor amounts of epidote/clinozoisite/zoisite. The amphibolites



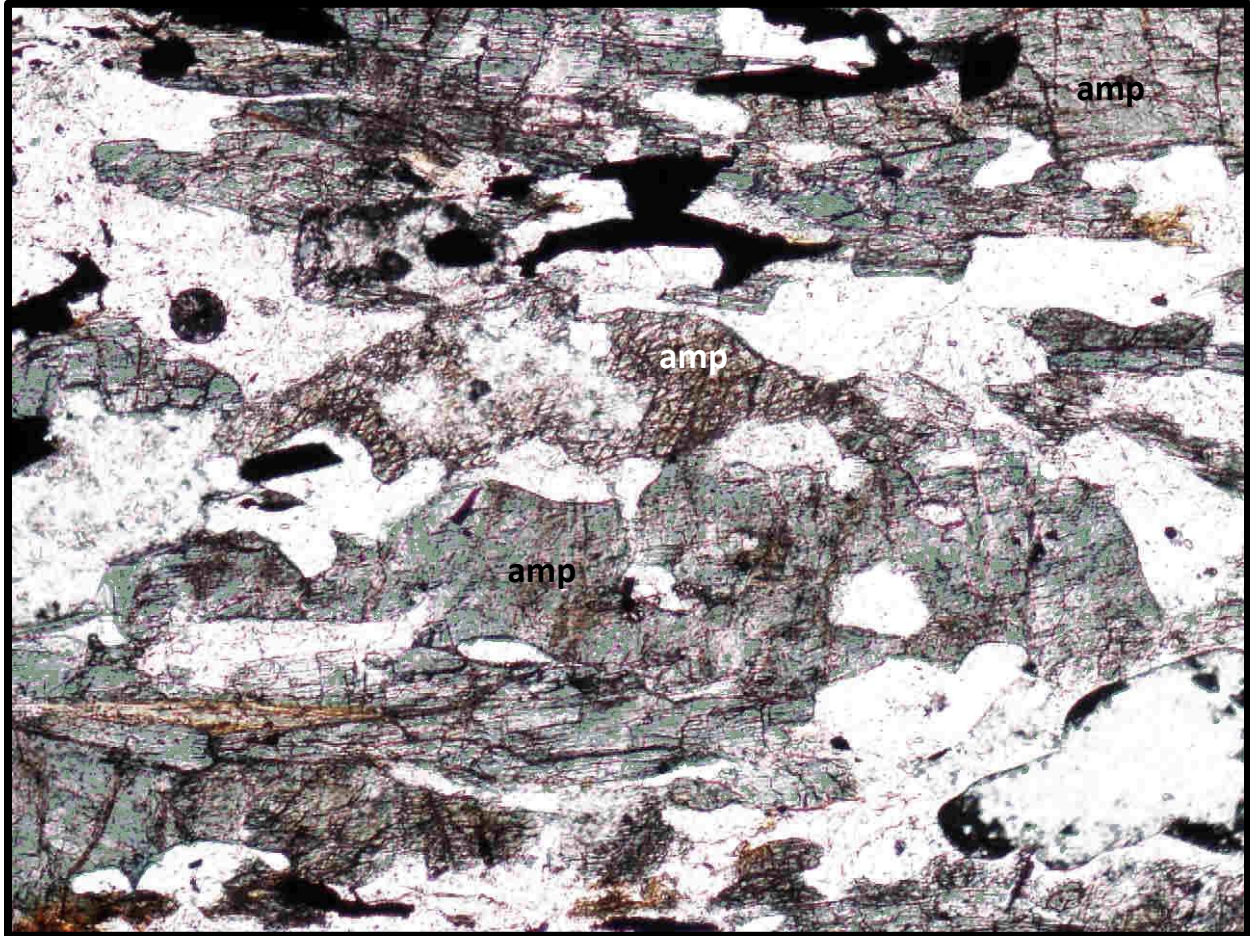
**Figure 12.** Metamorphic conditions suggested for the peak Neoacadian metamorphic event with eastern Blue Ridge in purple and Jacksons Gap Group in green. Grid univariant reaction curves and facies boundaries are from Holdaway (1971) and Ernst (1973).

contain two types of amphiboles. One type, interpreted as an earlier expression, shows signs of corrosion as evident by embayment textures. The second, interpreted as later growth (Alleghanian?), is free of corrosion /embayment (Fig. 13). Garnet growth indicates prograde and retrograde phases, and the earlier amphibole (Neoacadian?) is embayed or corroded and commonly fractured demonstrating disequilibrium throughout the Emuckfaw Group. The prograde garnets are xenoblastic and are commonly fractured in contrast to the retrograde garnets that are subidioblastic to rarely idioblastic (Fig. 14).

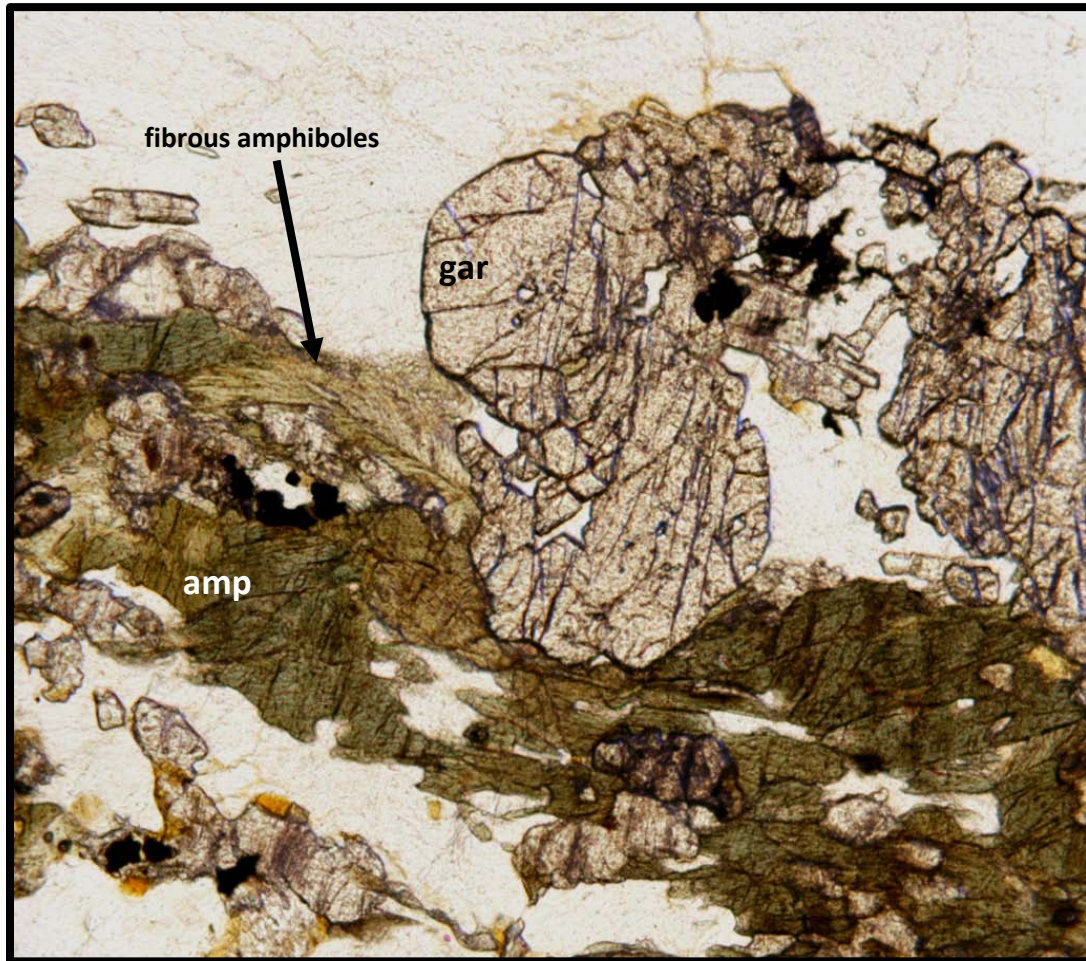
The meta-gabbros have a mineral assemblage of amphibole + epidote/clinozoisite + quartz + alkali feldspar. The amphiboles, as in the amphibolites, are of two varieties: an earlier formed amphibole with disequilibrium textures (Neoacadian), and a later euhedral amphibole lacking any evidence for disequilibrium (Alleghanian). Epidote within the meta-gabbro occurs with the later-formed more euhedral amphiboles, interpreted as growth under epidote-amphibolite facies conditions. Amphibole displays disequilibrium textures observed in the amphibolites and the meta-gabbro suggest an earlier higher-grade metamorphic event followed by a later, more pervasive epidote-amphibolite facies event in rocks throughout the quadrangle.

Both varieties of Kowaliga Gneiss were analyzed for metamorphic grade. Granites, which are very voluminous in the Our Town quadrangle, do not generate assemblages that are very helpful in constraining metamorphic conditions based on petrogenetic grid treatments. Some general temperature constraints can be supplied by deformational microstructures present in quartz and feldspar. Samples demonstrate subgrain rotation, bulging recrystallization, and grain boundary migration indicating lower amphibolite





**Figure 13.** Photomicrograph of both varieties of amphibole found within the Emuckfaw Group amphibolites. Amphibole in the center (yellow brown in color) is corroded or embayed indicating disequilibrium textures. Field of view is 2.5 mm.



**Figure 14.** Photomicrograph of subhedral garnets with  $S_1$  defining calcic-amphiboles. Photograph is in plane light with a 10 mm field of view.

temperatures (Passchier and Trouw, 2005). However, with dynamothermal metamorphism the temperature ranges traditionally reported for quartz deformation do not apply. Temperature is an important controlling factor for quartz deformation, but with increasing differential stress the slip systems in the quartz lattice can become active at lower temperatures. Feldspar grains have flame perthite, undulose extinction, tapering twin lamellae, and minor bulges indicating a temperature range of 400-500 degrees Celsius (Passchier and Trouw, 2005). Samples of the Kowaliga Gneiss do not have core-and-mantle structures that are common in mylonites formed in the range between 450 and 600 degrees Celsius (Passchier and Trouw, 2005). This limits the metamorphic range to lower amphibolite/epidote amphibolite facies. However, the possibility of lowering the deformation activation temperature makes determining the peak metamorphism based on the quartz and feldspar deformational microstructures impossible (Passchier and Trouw, 2005).

The Jacksons Gap Group constitutes a very minor volume of rocks of the Our Town quadrangle and thus only a few thin sections were made. The Jacksons Gap Group is reported to contain siliciclastics and carbonate-bearing pelites with metamorphic assemblages that suggest predominantly greenschist facies to lower-amphibolite facies in some areas (Steltenpohl, 2005; Sterling, 2006). The Jacksons Gap Group has well-preserved primary sedimentological structures such as cross stratification and conglomerate pebbles, cobbles, and boulders (Steltenpohl, 2005). The preserved sedimentological components and its predominant greenschist metamorphic assemblages are characteristics that set the Jacksons Gap Group apart from the Emuckfaw Group. This requires either a post-metamorphic fault or an upright unconformity marking the base of the Jacksons Gap Group. The present author favors the

interpretation that the post-metamorphic Abanda fault resulted in this metamorphic break. The apparent lower-metamorphic grade on the hanging wall block is consistent with oblique right-slip and normal motion observed for the Abanda fault (see below).

## Structure

Structural analysis of rocks of the Our Town quadrangle involves measurements of metamorphic foliation ( $S_1$ ), mineral elongation lineations, S-C fabrics, small-scale folds (hinge line, hinge surfaces, long limb and short limb), brittle fault planes, and sense-of-shear of brittle and ductile faults associated with the Alexander City and Abanda faults as well as internal shears. Structural data are divided into three subareas, the eastern Blue Ridge north and south of the Alexander City fault and the Brevard zone. The northern section of the eastern Blue Ridge includes structural measurements taken in the Elkahatchee Quartz Diorite and the Wedowee Group. The southern section includes the Emuckfaw Group and its igneous intrusive suites. The Brevard zone subarea contains Jacksons Gap Group units but structural data is limited by the small area expressed in the Our Town quadrangle. Statistical structural analysis includes contoured lower-hemisphere stereographic projections of metamorphic foliation, mineral elongations, and fold data. A form line map of the entire quadrangle area is also included. Analysis of the Alexander City and Brevard fault zones consists of fault kinematics, fault geometries, and fault rheologies.

### ***Northern Eastern Blue Ridge subarea***

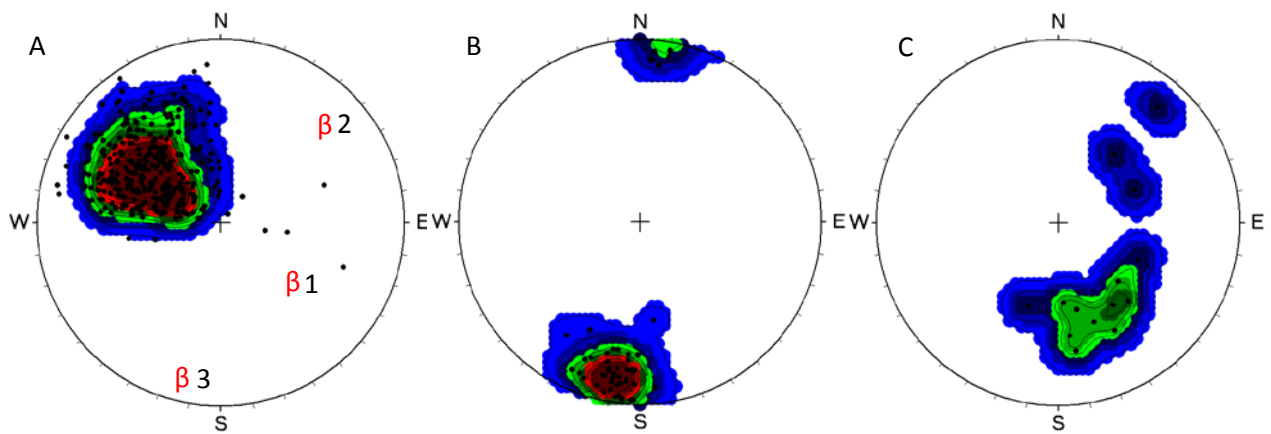
The northern eastern Blue Ridge subarea only accounts for a minor northwestern portion of the Our Town quadrangle.  $S_1$  has an average strike and dip of N44°E, 55°SE that is similar to the regional average of N40°E, 45°SE (see below). Due to the limited exposure there are not enough  $S_1$  measurements to make any statistically valid analysis.

### ***Southern Eastern Blue Ridge subarea***

The southern subarea contains the vast majority of structural measurements. A contoured stereonet of 334  $S_1$  foliation measurements (Fig. 15A) documents an average orientation of approximately N40°E, 45°SE. Although no obvious partial girdle spreads are observed, three very weak  $\pi$  girdles are numbered  $\beta_1$  to  $\beta_3$  in Figure 15A.  $\beta_1$  has a weak  $\pi$  girdle that ranges between 15 degrees of strike and 10 degrees in dip defining a weak beta axis that predominately trends to the southeast with a plunge ranging from 30 to 40 degrees.  $\beta_2$  has a more confined beta axis compared to  $\beta_1$  with a trend of N40E and a plunge of 15-20 degrees, and  $\beta_3$  trends to the south-southwest plunging 10-20 degrees.

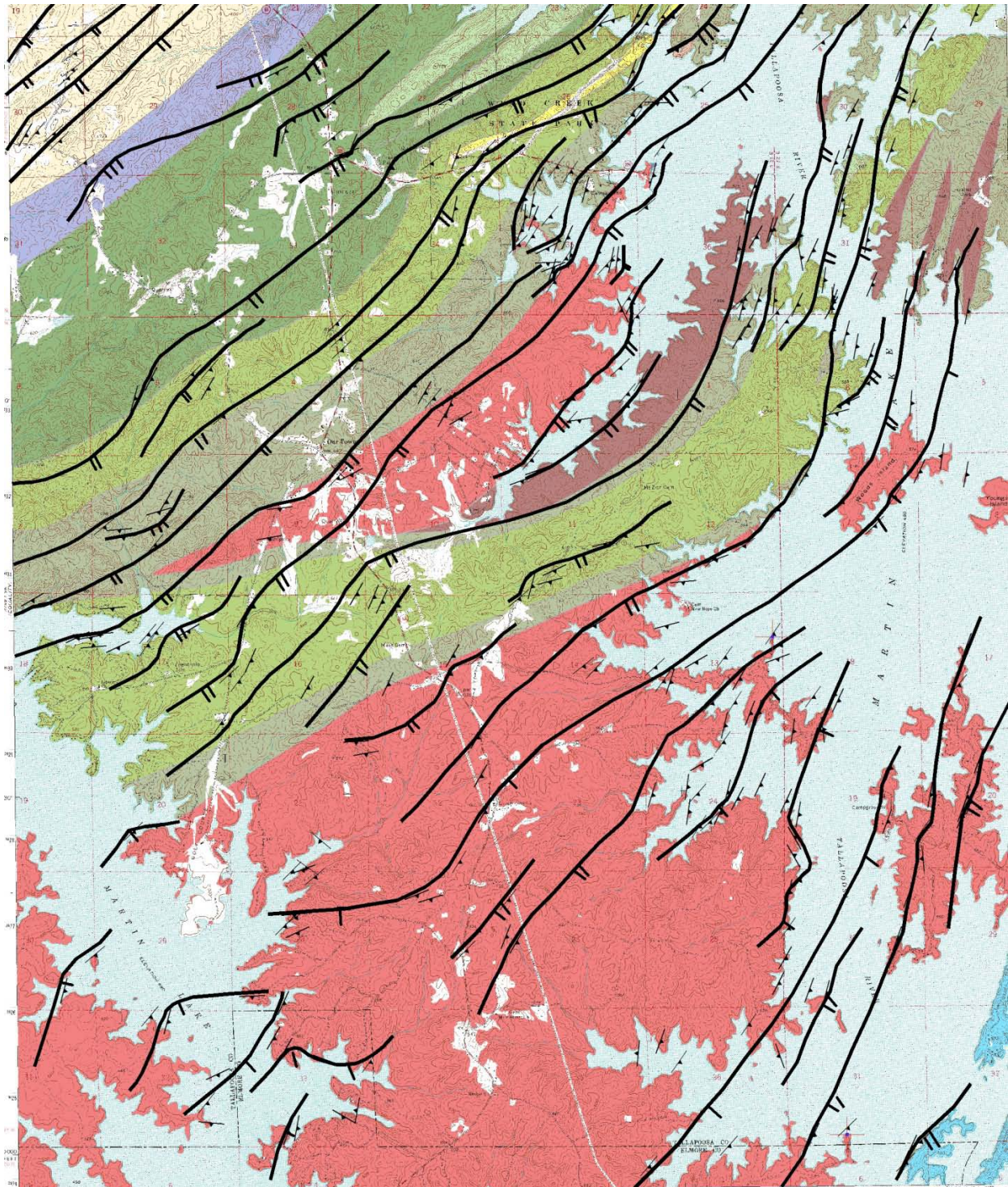
A form line map generated from  $S_1$  measurements of rocks across the entire Our Town quadrangle is presented in Figure 16. The form lines were constructed by visually contouring lines parallel to strike and dip (Marshak and Mitra, 1988). The form line map documents the regional northeast strike and southeast dip of  $S_1$  and a weak undulatory pattern reflecting synclinal and anticlinal fold pairs. Hinge line measurements of post-metamorphic folds (see below) parallel these south-southeast plunging macro folds and relate to the beta axis  $\beta_1$  in Figure 15A.

A contoured stereonet of 77 lineation ( $L_2$ , mylonitic) measurements of both mineral (quartz, biotite, and feldspar) and elongation lineations (Fig. 15B) indicates a point maximum with a south-southwest trend plunging from near horizontal to 30 degrees. The stereoplot also has a minor population to the north-northeast with a shallow plunge. This population could indicate warping that post dated the formation of the lineations. The lineation point maximum corresponds to the  $\beta_3$  direction indicating correspondence of  $\beta_3$  folding with the formation

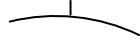
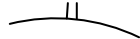



**Figure 15.** Lower hemisphere stereographic projections of foliation and lineation data for rocks of the Our Town quadrangle. A. Poles to metamorphic foliation,  $S_1$  and  $S_2$ , where  $N=334$ . B. Lineation data,  $L_1$  and  $L_2$  where  $N=77$ . C. Hinge line measurements from outcrop-scale post-metamorphic folds where  $N=14$ . Contours were generated using percent concentrations below.





**Figure 16.** Form line map generated from structural data from the Our Town quadrangle. See Figure 2 for Legend.

-  0° to 30° dip
-  31° to 60° dip
-  61° to 90° dip



of the lineations. In addition, a weak partial girdle of the lineations is approximately perpendicular to the  $\beta_2$  direction which parallels small-scale fold hinge lines, implying that warping of the lineations resulted from folding by the southeast-plunging undulatory folds observed on the form line map (Fig. 16).

Outcrop-scale fold hinge measurements from 14 gentle post-metamorphic folds (folding  $S_1$ ) (Fig. 17) indicate a broad primary grouping that plunges toward the south-southeast and a weaker grouping to the east-northeast (Fig. 15C). Regional foliation data (Fig. 15A) combined with hinge line data (Fig. 15C) indicates a strong correlation between the beta-axis  $\beta_1$  and the south-southeast cluster of fold hinge lines.  $\beta_2$  is similar to the region defined by the north-northeast population of hinge line data although the small number of hinge measurements does not lend itself to any robust statistical correlation.

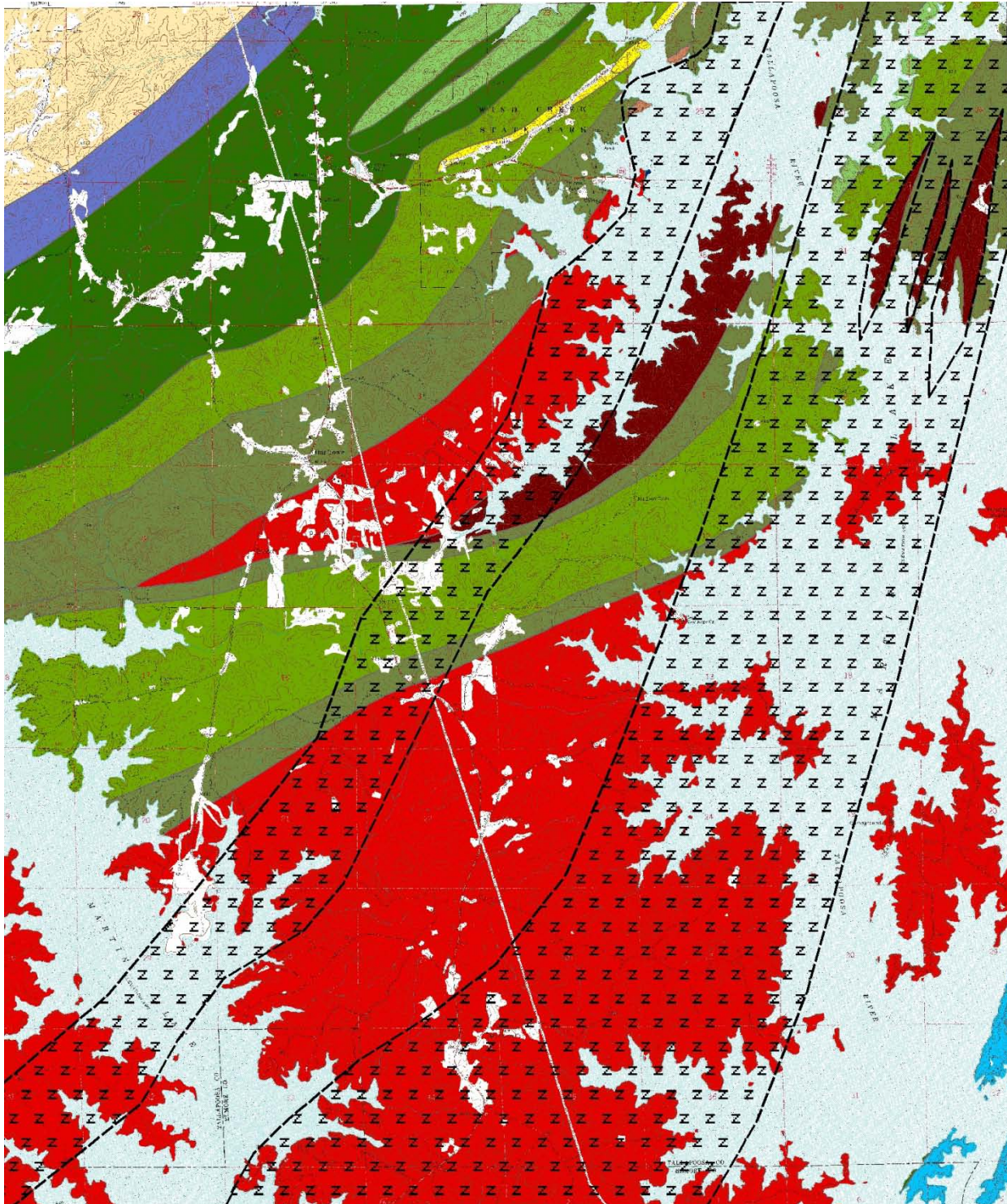
S-C fabrics measured within the southern eastern Blue Ridge subarea indicate two broad shear zones striking northeast/southwest (Fig. 18). The retrogressive shear zones cut the regional metamorphic foliation at a slight angle, but are cut by the northeast/southwest striking cataclasites (see below). Slip-line density is greatest between  $N50^\circ E$  and  $N70^\circ E$  with a plunge of  $\sim 15$  degrees (Fig. 19).

#### *Alexander City Fault*

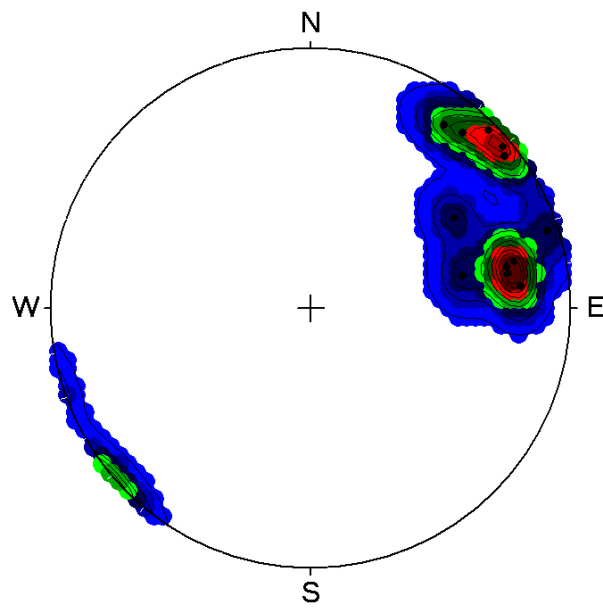
Retrogressive mylonites or phyllonites of the Alexander City fault zone are observed within rocks of the Wedowee and Emuckfaw groups, as well as the Elkahatchee Quartz Diorite and Kowaliga Gneiss. The main ductile shear zone lies within Wedowee metapelitic rocks and thins and thickens along strike from less than a few meters to as much as  $\sim 75$  meters. Sigma clasts of feldspar, meso- and microscopic asymmetric folds and well-developed S-C fabrics



**Figure 17.** Photograph of post-metamorphic folds in a muscovite schist from the Emuckfaw Group.



**Figure 18.** Shear zone map generated from S-C fabric locations within the Our Town quadrangle. Fields marked as “Z” indicate shear zones and dashed lines represent approximate margins. See Figure 2 for Legend



**Figure 19.** Lower hemisphere equal-area stereoplot of S and C slip line data from the shear zones in the Our Town quadrangle, slip lines were geometrically determined. N=13

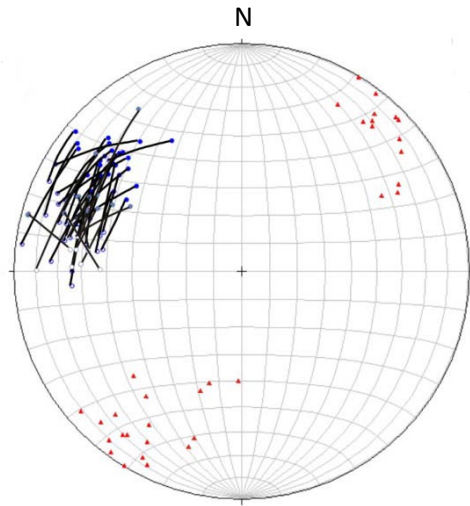


consistently record tops-to-the-west dextral movement along the entire trace of the fault zone (Steltenpohl et al., 2013). The rheologies of the retrogressive mylonites are discussed in more detail in Steltenpohl et al. (2013).

Lower hemisphere, equal-area stereographic analysis of measured C- and S planes (Fig. 20) further document predominantly right-slip movement recorded in mylonites and phyllonites of the Alexander City fault zone. An oblique normal-slip (more down-dip) component recognized in some outcrops is also indicated in Figure 20. C- and S-plane point maxima are oriented N44° E, 64° SE and N16° E, 64° SE, respectively. Slip lines were geometrically determined (rotating the intersection of the C-and S-plane within the C plane) with maxima at N46° E, 4° and S31°W, 22°, documenting mainly strike parallel movement (Steltenpohl et al., 2013).

#### *Cataclasites*

Within the southern eastern Blue Ridge subarea are tabular zones of cataclasite striking northeast/southwest across the quadrangle (Plate 1). After detailed field investigations, no consistent sense of shear was documented in out crops within the Our Town quadrangle. The cataclasites are generally 1 to 2 m in thickness and appear to be near vertical in orientation. The cataclasites cut the regional S<sub>1</sub> foliation and crosscut the various lithologies found in the Our Town quad. In some areas the cataclasite is a ridge former presenting higher relief particularly along shoreline exposures. These cataclastic zones are described in more detail in Steltenpohl et al. (2013).



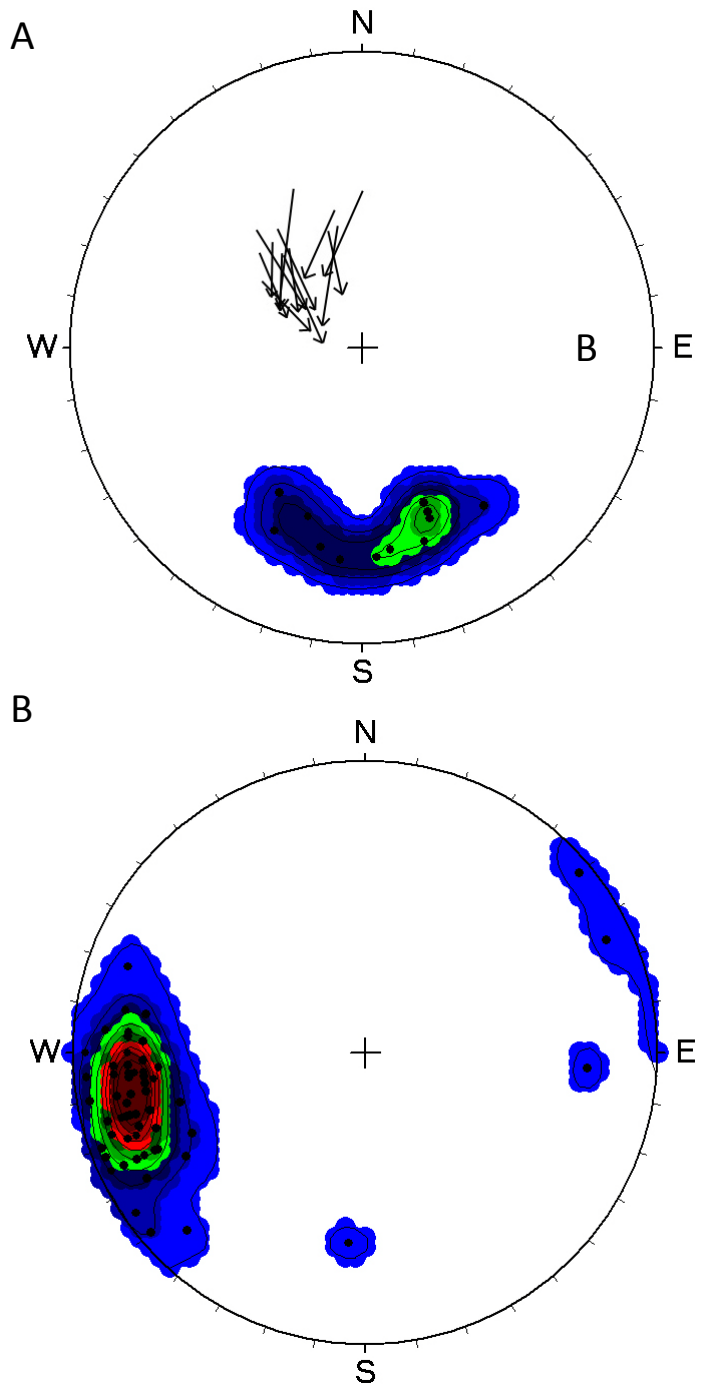
**Figure 20.** Lower hemisphere equal-area stereonet of S and C plane data from the Alexander City fault zone. Poles to S (blue circles; N = 36) and C (blue dots; N = 36) planes and slip lines (red triangles; N = 36). Black arcs connect S-C pairs, slip lines were geometrically determined (Steltenpohl et al., 2013)

### ***Brevard zone subarea***

Outcrops of the Emuckfaw Group adjacent to the Abanda fault contain well defined phyllonitic (S-C) fabrics indicating oblique-dextral and tops-down to the east normal-slip movement (Figs. 21A and 22A). Small-scale Z folds (hinge lines N85°E to N70°E plunging ~15 degrees) also corroborate oblique-dextral-normal fault movement (Figs. 22B and 22C). A contoured stereoplot with geometrically constrained slip-lines from 14 S-C pairs indicates a tight grouping ranging in plunge from 30-40 degrees in the down-dip direction (south). Slip-line density is greatest near the maximum dip of the C plane (~N50°E, 35°S) indicating predominantly normal-slip movement but the southwest “tail” documents transitions toward dextral oblique movement components (Fig. 21A).  $S_1$  data collected in foliations within the Emuckfaw Group as well as  $S_0/S_1$  ( $S_0$ , compositional layering) foliations collected in the Jacksons Gap Group yielded an average strike and dip of N36°E, 39°S

### ***Brittle Faults***

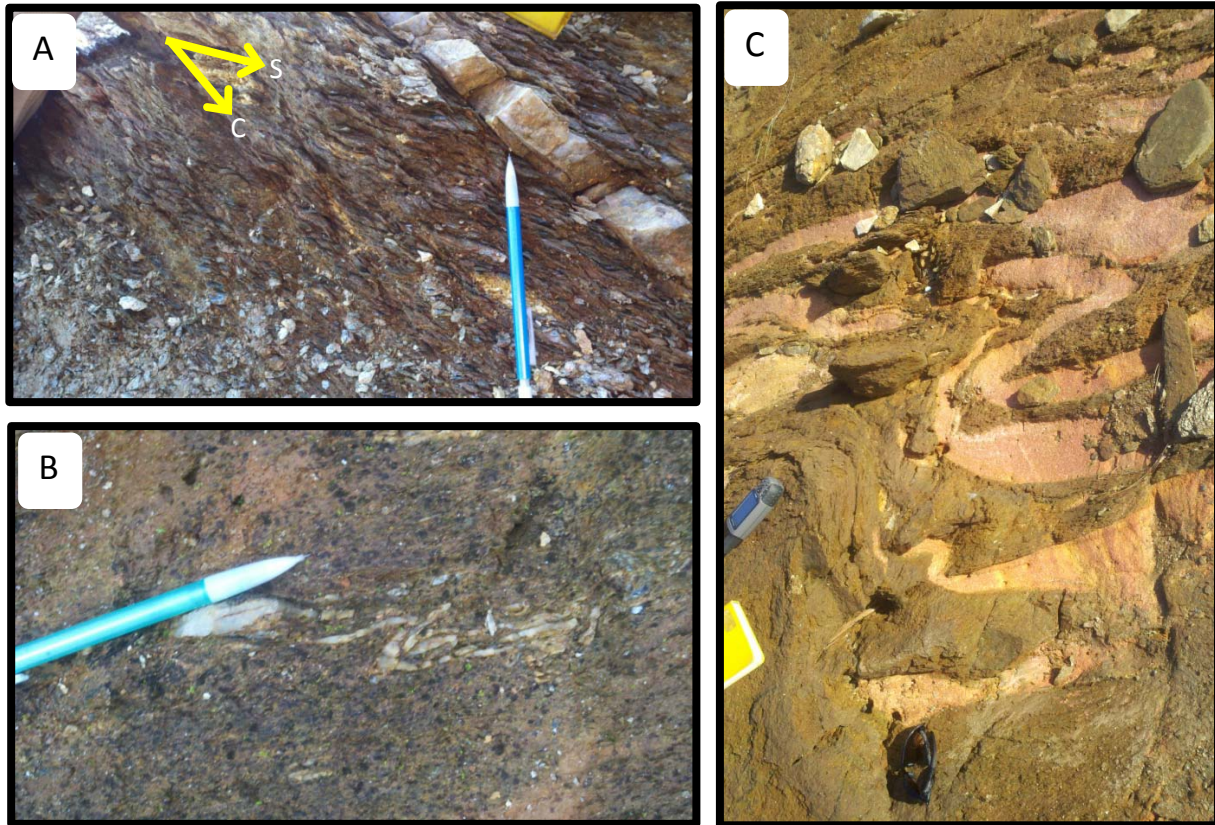
Brittle normal faults are commonly found to cut the Abanda fault phyllonites in both the Jacksons Gap and Emuckfaw groups (Fig. 23). Brittle faults strike west-northwest and dip ranges from 65 to 85 degrees northeast (Fig. 21B). Mesoscopic horst and graben structures are concordant with the larger-scale brittle normal faults (Fig. 23B). Displacement along the brittle normal faults is generally on a scale from a few centimeters to nearly a meter (Figs. 23C and 23D).



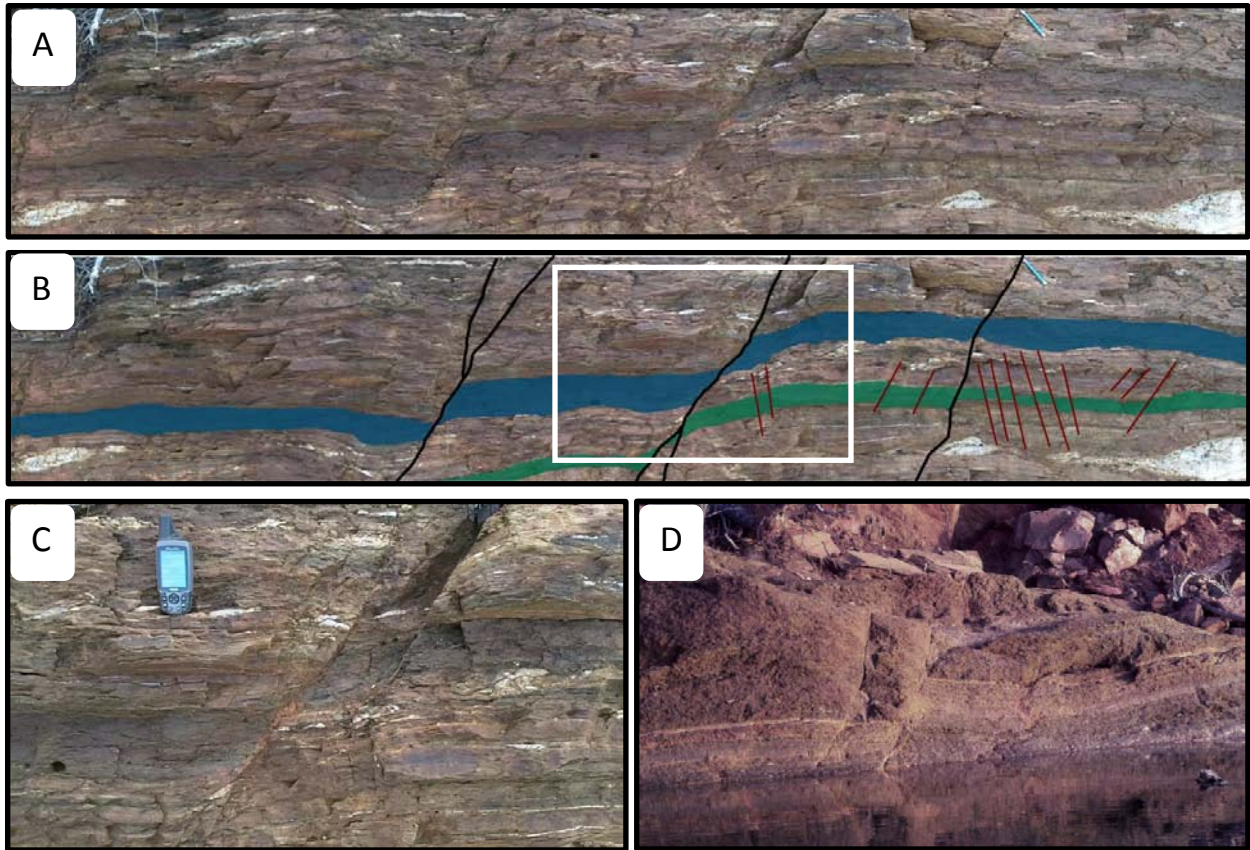
**Figure 21.** Lower hemisphere stereographic projections of fault rocks associated with the Brevard zone. A. Contoured plot of slip lines geometrically determined, and poles to C planes are the unornamented end of the arrow while the S planes are the tip of the arrow. B. Contoured plot of poles to brittle normal fault planes in the Emuckfaw Group and Jacksons Gap Group N=77. Contours were generated using percent concentrations below.







**Figure 22.** Photographs of phyllonite fabrics of the Abanda fault. A. S-C fabrics within an Emuckfaw Group schist, looking northeast. B. Small-scale dextral (Z) folds of a quartz vein within Abanda fault phyllonites, looking southeast. C. Mesoscopic dextral (Z) folds indicating dextral movement of the Abanda. Upper Emuckfaw Group lithology is a metasiltstone that is intruded by a fine to medium grained potassium-feldspar-rich granite.



**Figure 23.** North/northwest-striking brittle normal faults. A. Normal faults in upper Emuckfaw Group units; view looking southeast with pencil for scale. B. Same view as A where brittle faults are outlined in black, horsts and grabens are outlined in red, and two quartzite layers marking offset are colored green and blue. C. Close up view of normal fault in index rectangle in B. D. Typical displacement observed in individual outcrops is about 0.7 meters as shown in the photograph. Lithology is Emuckfaw Group. (N32 45.240 W85 53.220)

## **Geochemical and Petrogenetic Evolution of the Kowaliga Gneiss**

Ten samples of the Kowaliga Gneiss from the Our Town quadrangle were selected for geochemical study. The purpose of the study is twofold: (1) to explore the hypothesis (Bieler and Deininger, 1987) that the Zana and Kowaliga Gneiss are varieties of the same intrusive granite suite; and (2) to explore the origin of the potassium feldspar megacrysts. Samples approximately 20 grams in size were submitted to Acme Analytical Laboratories (Vancouver) Ltd. for commercial analysis. The samples were analyzed by whole-rock XRF (X-ray fluorescence) and ICP-MS (inductively coupled plasma mass spectrometry) for major-oxide, LOI, and REE-element content. Data tables and results are in Table 1. Samples in the analysis include Kowaliga megacrystic gneiss (samples JHKG1 1 and 2), samples of heavily sheared Kowaliga augen gneiss (samples JHKG5 1 and 2, JHKG20 1 and 2, JHKG32 1 and 2), and samples of slightly sheared Kowaliga augen gneiss (samples JHKG43 1 and 2) with sample locations and hand sample descriptions in Appendix 2. To examine similarities and differences of the Kowaliga and Zana meta-granites, geochemical data is plotted together with previously reported geochemical data (Stoddard, 1983).

### *Kowaliga Gneiss Magma Genesis*

CIPW normative mineral percentages from the ten Kowaliga gneiss samples were plotted on an An-Ab-Or granite classification diagram documenting them to lie within the granite composition field (Fig. 24). The two samples from the Kowaliga megacrystic gneiss (JHKG1 1 and 2) plot near the boundary of the granodiorite and the quartz monzonite fields; this

Sample	Wgt kg	SiO <sub>2</sub> %	Al <sub>2</sub> O <sub>3</sub> %	Fe <sub>2</sub> O <sub>3</sub> %	CaO %	MgO %	Na <sub>2</sub> O %	K <sub>2</sub> O %	MnO %	TiO <sub>2</sub> %	P <sub>2</sub> O <sub>5</sub> %	Cr <sub>2</sub> O <sub>3</sub> %	Ba %	LOI %	SUM %
JHKG A-1	0.18	69.1	15.12	2.84	2.11	0.82	3.54	4.53	0.06	0.26	0.32	0.011	0.11	1	99.79
JHKG A-2	0.17	68.8	14.99	3.16	2.41	0.94	3.78	3.84	0.07	0.28	0.4	0.003	0.09	1.03	99.8
JHKG 5-1	0.14	74.3	13.84	1.39	0.68	0.22	2.93	5.12	0.03	0.15	0.05	0.001	0.04	1.6	100.3
JHKG 5-2	0.16	74.2	13.81	1.31	0.65	0.23	2.8	5.37	0.03	0.14	0.04	0.002	0.04	1.62	100.3
JHKG 20-1	0.13	72.9	13.87	1.9	1.03	0.49	3.1	4.82	0.05	0.26	0.05	<0.001	0.06	1.36	99.87
JHKG 20-2	0.13	73.4	13.47	1.9	1.04	0.48	3.11	4.57	0.05	0.25	0.05	<0.001	0.05	1.21	99.6
JHKG 32-1	0.14	71.5	15.16	1.68	0.53	0.42	1.98	5.51	0.05	0.25	0.04	0.002	0.07	2.99	100.2
JHKG 32-2	0.12	70.6	15.42	1.68	0.45	0.38	1.66	5.92	0.05	0.24	0.03	<0.001	0.08	3.21	99.7
JHKG 43-1	0.12	75.7	10.72	4.78	0.51	1.34	2.18	2.71	0.05	0.72	0.05	0.005	0.08	1.19	99.99
JHKG 43-2	0.11	75.6	10.77	5.04	0.5	1.41	2.08	2.79	0.05	0.73	0.05	0.005	0.07	1.21	100.3

**Table 1.** Major and trace element concentration data from ten samples of Kowaliga Gneiss. Data is reported in weight percent and parts per million (ppm).

Sammple	Wgt kg	Cu %	Ni %	Pb %	SO <sub>3</sub> %	Sr %	V <sub>2</sub> O <sub>5</sub> %	Zn %	Zr %	TOT/C %	TOT/S %
JHKGGA-1	0.18	<0.001	0.005	<0.001	<0.002	0.103	0.007	0.002	0.017	<0.02	<0.02
JHKGGA-2	0.17	<0.001	<0.001	<0.001	<0.002	0.1	0.008	0.003	0.019	<0.02	<0.02
JHKG5-1	0.14	<0.001	0.002	<0.001	<0.002	0.006	0.004	0.001	0.004	<0.02	<0.02
JHKG5-2	0.16	<0.001	0.002	<0.001	<0.002	0.005	<0.002	<0.001	0.002	<0.02	<0.02
JHKG20-1	0.13	<0.001	<0.001	<0.001	<0.002	0.009	0.004	0.002	0.009	0.05	<0.02
JHKG20-2	0.13	<0.001	<0.001	<0.001	<0.002	0.012	0.006	0.002	0.007	0.03	<0.02
JHKG32-1	0.14	<0.001	<0.001	0.001	<0.002	0.003	0.004	0.002	0.009	<0.02	<0.02
JHKG32-2	0.12	<0.001	<0.001	<0.001	<0.002	0.002	0.006	0.002	0.01	0.05	<0.02
JHKG43-1	0.12	<0.001	<0.001	<0.001	<0.002	0.011	0.013	0.005	0.042	<0.02	<0.02
JHKG43-2	0.11	<0.001	<0.001	<0.001	<0.002	0.005	0.013	0.005	0.044	<0.02	<0.02

**Table 1 continued.** Major and trace element concentration data from ten samples of Kowaliga Gneiss. Data is reported in weight percent and parts per million (ppm).

Sample	Wgt kg	Ba ppm	Be ppm	Co ppm	Cs ppm	Ga ppm	Hf ppm	Nb ppm	Rb ppm	Sn ppm	Sr ppm	Ta ppm	Th ppm	U ppm	V ppm
JHKG A-1	0.18	1127	6	5.2	1.3	17.3	5.8	34	137.2	2	1082	1.4	9.1	2.7	38
JHKG A-2	0.17	869	3	5.6	1.4	17.9	4.3	36.5	117.9	2	1044	1.3	16.9	2.8	44
JHKG 5-1	0.14	403	2	1.8	1.4	15.1	2.9	9.5	165.3	3	76.5	0.5	12.2	3.1	9
JHKG 5-2	0.16	441	2	2.5	1.7	15.9	2.3	9.4	170	2	81.2	1.1	12.5	3.2	9
JHKG 20-1	0.13	564	<1	3.3	2	14.7	4	14.5	178.4	2	143	1.2	15.3	3.9	23
JHKG 20-2	0.13	533	3	3.7	1.8	18.3	4.6	11.3	165.5	3	133.8	1.1	15.6	3.7	20
JHKG 32-1	0.14	688	2	3.2	1.6	18	6.2	21.3	202.7	2	76.5	2.9	17.5	6.8	16
JHKG 32-2	0.12	877	1	4	1.8	16	4.3	22.4	222.8	3	83.6	2.5	20.4	7.4	17
JHKG 43-1	0.12	699	<1	9	1.4	16	11.9	16	82.1	2	121.5	1	10.8	2.4	70
JHKG 43-2	0.11	682	<1	9.3	1	17.1	12.7	18.1	87.1	2	112.1	1	10.1	2.4	73

**Table 1 continued.** Major and trace element concentration data from ten samples of Kowaliga Gneiss. Data is reported in weight percent and parts per million (ppm).

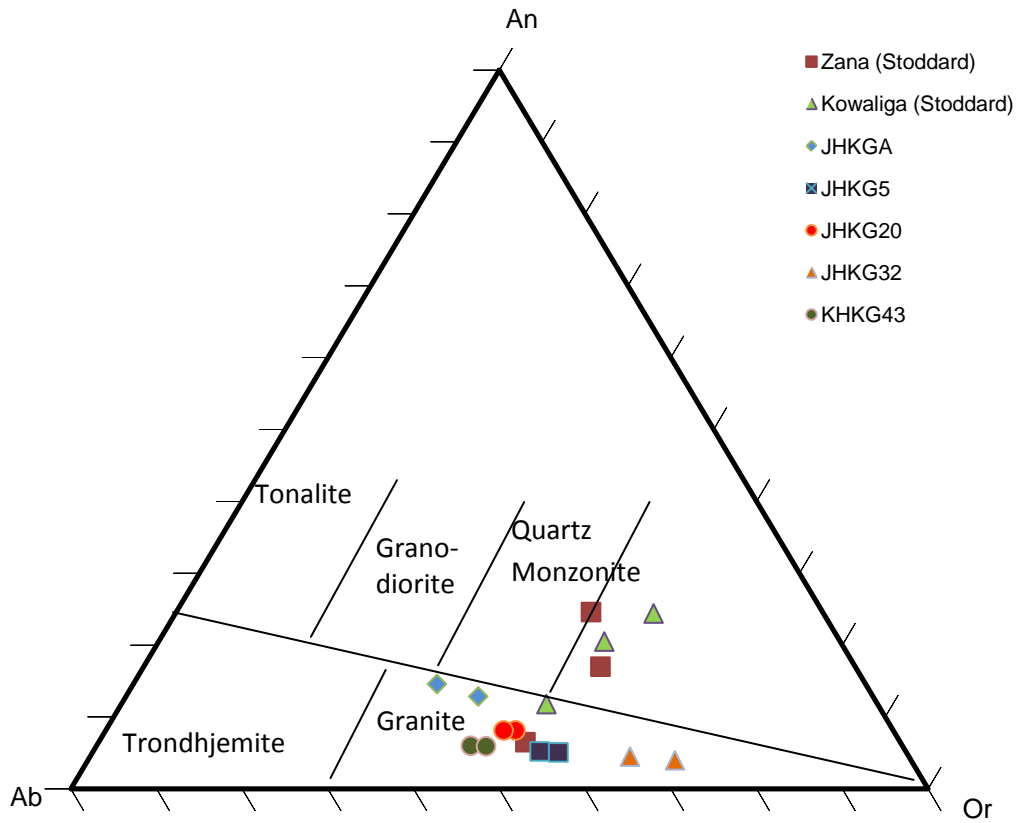
Sample	Wgt kg	W ppm	Zr ppm	Y ppm	La ppm	Ce ppm	Pr ppm	Nd ppm	Sm ppm	Eu ppm	Gd ppm	Tb ppm	Dy ppm	Ho ppm	Er ppm
JHKG A-1	0.18	<0.5	22.02	16.3	42.4	51.5	8.6	28.5	5	1.44	3.81	0.6	2.78	0.57	1.4
JHKG A-2	0.17	0.06	219.5	19.4	59	116.5	12.29	45.1	6.79	1.57	4.49	0.71	3.64	0.67	1.57
JHKG 5-1	0.14	<0.5	91.7	8.9	24.5	53.2	4.48	14.9	1.92	0.33	1.37	0.22	1.38	0.31	0.85
JHKG 5-2	0.16	<0.5	76.1	10.7	24.6	58.8	4.46	10	2.28	0.34	1.7	0.28	1.67	0.36	0.98
JHKG 20-1	0.13	<0.5	131.5	25	47.7	48.6	10.75	33.7	6.43	0.92	5.09	0.95	5.42	1.08	3.03
JHKG 20-2	0.13	<0.5	126	26.2	35.7	35.5	8.28	30.2	5.84	0.74	4.99	0.9	4.97	1.05	3.07
JHKG 32-1	0.14	<0.5	135	41.2	56.1	66.8	11.17	38.8	8.01	1	8.13	1.22	7.34	1.47	4.42
JHKG 32-2	0.12	<0.5	128	40.6	49.8	43.3	9.76	34.4	6.87	0.94	7.35	1.17	6.33	1.44	4.18
JHKG 43-1	0.12	0.5	396	34.5	31.6	63.5	8.47	32.8	6.66	1.16	5.37	0.99	6.18	1.27	3.78
JHKG 43-2	0.11	0.9	458	39.9	30.2	58.4	7.9	28.3	6.01	1.12	6.05	1.02	5.62	1.77	4.44

**Table 1 continued.** Major and trace element concentration data from ten samples of Kowaliga Gneiss. Data is reported in weight percent and parts per million (ppm).

Sample	Wgt kg	Tm ppm	Yb ppm	Lu ppm	Mo ppm	Cu ppm	Pb ppm	Zn ppm	Ni ppm	As ppm	Cd ppm	Sb ppm	Bl ppm	Ag ppm	Au ppm	Hg ppm	Tl ppm	Se ppm
JHKG A-1	0.18	0.23	1.39	0.24	1.6	2.9	4.2	32	3.1	<0.5	<0.1	<0.1	<0.1	<0.1	<0.5	<0.1	0.3	<0.5
JHKG A-2	0.17	0.21	1.27	0.25	1.8	3	3.7	36	4.7	<0.5	<0.1	<0.1	<0.1	<0.1	0.6	<0.1	0.3	<0.5
JHKG 5-1	0.14	0.12	1.02	0.17	0.2	4.4	3	14	2.3	<0.5	<0.1	<0.1	<0.1	<0.1	<0.5	<0.1	0.1	<0.5
JHKG 5-2	0.16	0.17	1.28	0.2	0.3	4.5	3.1	14	3.7	<0.5	<0.1	<0.1	<0.1	<0.1	<0.5	<0.1	0.1	<0.5
JHKG 20-1	0.13	0.45	3.07	0.47	<0.1	1.7	4.7	32	3.3	<0.5	<0.1	<0.1	<0.1	<0.1	<0.5	<0.1	0.5	<0.5
JHKG 20-2	0.13	0.49	3.14	0.51	0.2	2.5	2.4	32	4.9	<0.5	<0.1	<0.1	<0.1	<0.1	<0.5	<0.1	0.5	<0.5
JHKG 32-1	0.14	0.71	4.69	0.72	<0.1	2.6	6.2	25	2.6	<0.5	<0.1	<0.1	<0.1	<0.1	<0.5	<0.1	0.3	<0.5
JHKG 32-2	0.12	0.63	4.43	0.68	0.3	3.6	5.5	23	3.5	<0.5	<0.1	<0.1	<0.1	<0.1	<0.5	<0.1	0.3	<0.5
JHKG 43-1	0.12	0.56	3.95	0.6	0.3	2	1.4	56	16.4	<0.5	<0.1	<0.1	<0.1	<0.1	<0.5	<0.1	0.4	<0.5
JHKG 43-2	0.11	0.72	4.85	0.71	0.1	1.8	3.5	55	15.2	<0.5	<0.1	<0.1	<0.1	<0.1	0.8	<0.1	0.3	<0.5

**Table 1 continued.** Major and trace element concentration data from ten samples of Kowaliga Gneiss. Data is reported in weight percent and parts per million (ppm).



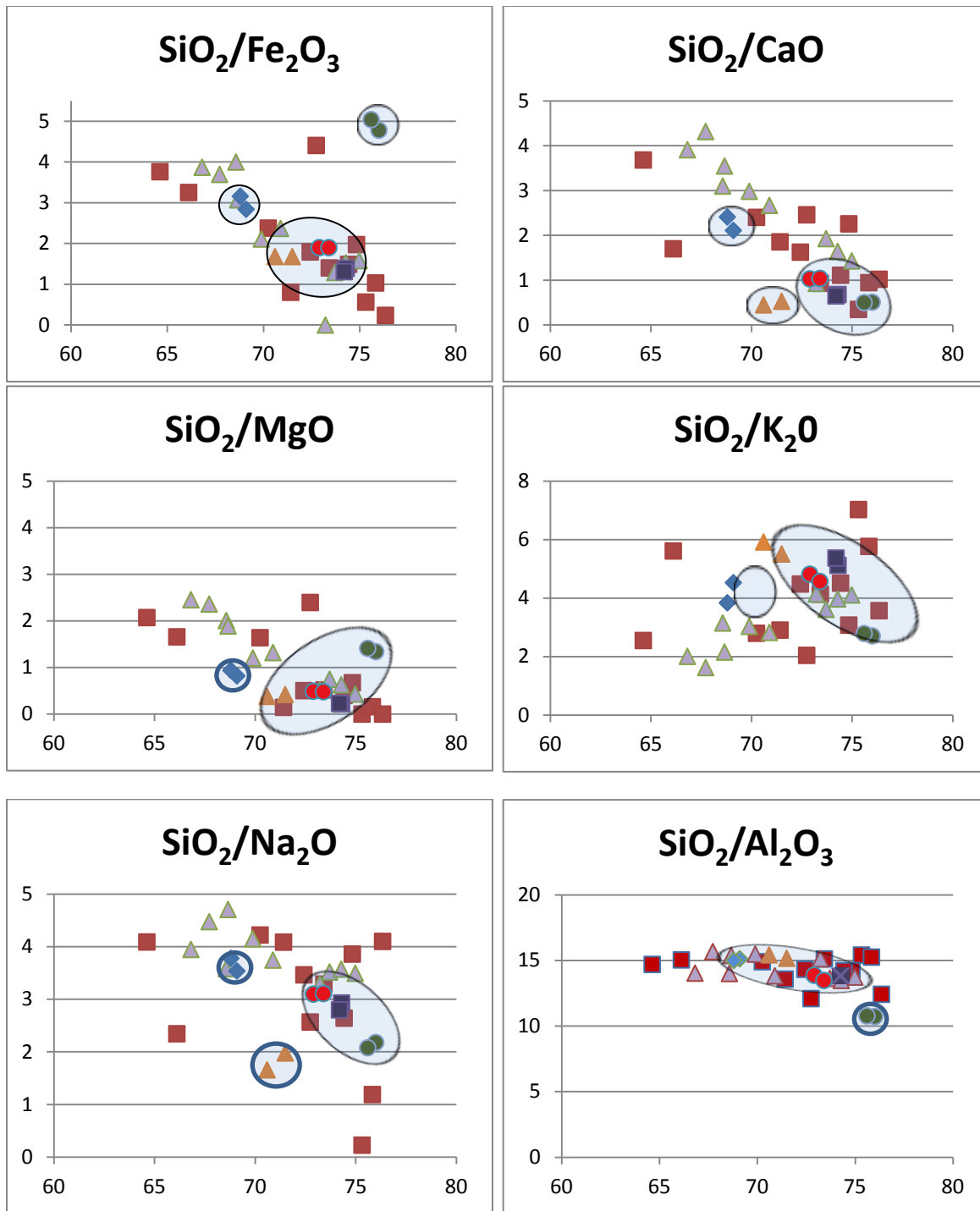


**Figure 24.** CIPW normative classification (Barker, 1979) of the Kowaliga Gneiss and Zana Granite based on chemical analyses reported by Stoddard (1983) and Kowaliga analysis from the current report.

indicates a less evolved magma than the other samples. The two samples JHKA32 1 and 2 have increased potassium content suggesting a more highly evolved melt.

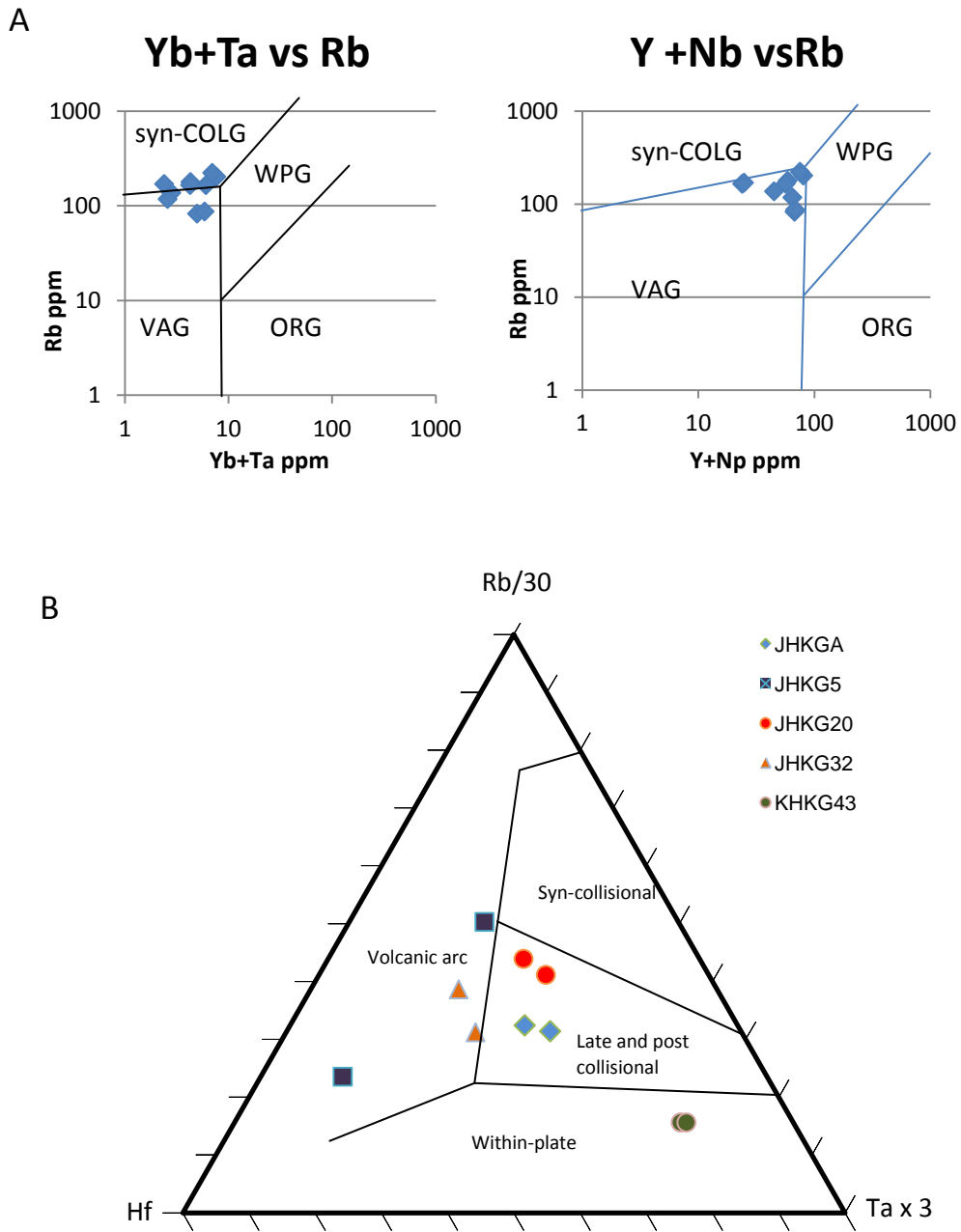
Figure 25 plots selected major oxide analyses of the Kowaliga Gneiss from the Our Town quadrangle with those published on the Zana and Kowaliga meta-granites (Stoddard, 1983) to compare and explore for petrogenetic relationships. Harker plots of six major oxides ( $\text{Fe}_2\text{O}_3$ , CaO, MgO,  $\text{K}_2\text{O}$ ,  $\text{Na}_2\text{O}$ , and  $\text{Al}_2\text{O}_3$ ) were generated, and the Kowaliga Gneiss and the Zana Granite follow similar trends (Fig. 25). One exception is that samples JHKG43-1 and JHKG43-2 have a high  $\text{Fe}_2\text{O}_3$  content that sets them apart from the generalized trend. This sample also has a higher MgO and lower  $\text{Al}_2\text{O}_3$  and  $\text{K}_2\text{O}$  amounts compared to the other Kowaliga samples analyzed. Higher biotite content combined with lower potassium feldspar content, determined by petrography, resulted in these outliers. Data indicates that the megacrystic gneiss (JHKGGA) is the least evolved, most primitive of the melts, which supports the U-Pb dates retrieved from samples collected near JHKGGA. Major oxide data from the majority of the samples supports a similar geochemical and, therefore, petrogenetic/magmatic trends.

Rare-Earth Element data for the Kowaliga Gneiss from the Our Town quadrangle are plotted on discrimination diagrams for granites (Fig. 26) using Rb-Y-Nb, Rb-Yb-Ta, and Rb-Hf-Ta variations to explore the tectonic setting for the Kowaliga Gneiss (Pearce et al., 1984). Plots of Y+Nb vs. Rb indicate clusters in the volcanic-arc granite field (VAG) and along the boundary between VAG and the within-plate granite field (WPG). The Yb+Ta vs. Rb discrimination plots the data along the boundary between VAG and collisional granite (syn-COLG) (Fig. 26A). These plots indicate that the Kowaliga Gneiss is indistinguishable from a VAG or a syn-COLG tectonic



**Figure 25.** Harker plots of six major oxides ( $\text{Fe}_2\text{O}_3$ ,  $\text{CaO}$ ,  $\text{MgO}$ ,  $\text{K}_2\text{O}$ ,  $\text{Na}_2\text{O}$ , and  $\text{Al}_2\text{O}_3$ ) for the Kowaliga Gneiss compared to earlier Zana Granite and Kowaliga Gneiss geochemical data presented by Stoddard (1983). Shaded areas define general data populations from the current report.

- Zana (Stoddard)
- ▲ Kowaliga(Stoddard)
- ◆ JHKG A
- JHKG 5
- JHKG 20
- ▲ JHKG 32
- JHKG 43



**Figure 26.** A. Data from the Kowaliga Gneiss plotted on Rb-(Yb + Ta) and Rb-(Yb +Ta) discrimination plots (Pearce et al., 1984) with fields of syn-collisional granites (syn-COLG), within-plate granites (WPG), volcanic-arc granites (VAG) and ocean-ridge granites (ORG). B. Data from the Kowaliga Gneiss plotted on Hf-Rb/30-Ta x 3 discrimination plot (Harris et al., 1986)

setting. According to Rollinson (1993), post-orogenic granites cannot be distinguished from volcanic-arc and syn-collisional granites using Rb-Y-Nb, Rb-Yb-Ta discrimination plots because both will plot within the same field. Combined, the discrimination plots narrow the origin of the Kowaliga Gneiss to VAG, syn-COLG, or post-orogenic. In order to subdivide into classifications of syn-collisional, late and post collisional, volcanic arc, or within-plate settings, a trivariate plot of  $Hf-Rb/30-Ta^3$  is used (Harris et al., 1986)(Fig 26B). The  $Hf-Rb/30-Ta^3$  plot indicates samples JHKGA and JHKG20 to plot within the late and post collisional fields, whereas samples JHKG5 and JHKG32 plot within volcanic arc, and sample JHKG43 plots in the within-plate field. Sample JHKGA better represents the geochemistry of the Kowaliga Gneiss due to its pristine euhedral igneous texture and the low to absent levels of potassium metasomatism (see below) compared to the other samples in the suite. This would imply that sample JHKGA likely has intruded as a late and post-collisional granite in a back-arc setting.

### **Kowaliga Gneiss Megacrystic Texture**

The Kowaliga Gneiss is an orthogneiss that is subdivided in this report into augen gneiss and megacrystic gneiss. The megacrystic gneiss is characterized by euhedral megacrysts of potassium feldspars averaging 5 cm in length but crystals as long as 15 cm are not uncommon. The megacrysts have been described in the literature as idioblastic and xenoblastic (Bentley and Neathery, 1970) as well as hypidioblastic (Sterling, 2006), which implies a metamorphic origin. For reasons described below, the current author favors a magmatic origin for these megacrysts, and hence they are discussed to be phenocrysts.

The megacrysts are mesoscopically euhedral in shape. Well-formed crystal faces are obvious in outcrop and hand specimen and euhedral whole-body crystals were found weathered-out of outcrops. Vernon (1968, 1986) argues for a phenocrystic origin for centimeter scale euhedral potassium feldspars rather than a porphyroblastic one. Very small scale (<1 mm) euhedral potassium feldspar crystals are known to grow in fine grained sedimentary rocks (Baskin, 1956). In thin section the Kowaliga Gneiss megacrysts have microscopic irregularities along the edges that are interpreted to be outgrowths that are crystallographically continuous with the potassium feldspar grains. This indicates a change from free growth in a liquid magmatic setting to a more limited space (interstitial) growth (Vernon, 1986).

The growth rate of potassium feldspar crystals reaches a maximum when the nucleation density is still low (Swanson, 1977). This can account for rapid growth early on of a relatively

small number of crystals, and this is interpreted to be associated with the free form growth in the melt. As the nucleation rate increases, smaller more abundant crystals will occur in the matrix and this will lead to the observed overgrowths that are crystallographically continuous but are considered interstitial. Traditionally speaking, in a Bowen's Reaction series fashion (Bowen, 1928), potassium feldspar is thought to be one of the last major mineral phases to crystallize from the solidification of a siliceous magma. Work with Zr in titanite inclusions, however, indicates potassium megacrysts from the Sierra Nevada batholith crystallized at temperatures of 735-760 degrees Celsius (Moore and Sisson, 2007). These temperatures indicate enough liquid volume available in the magma to allow for megacrystic growth even as the last phase to begin crystallization (Vernon and Patterson, 2008). The timing of crystal growth is still debated. Johnson et al. (2006), for example, states that the potassium feldspar megacrysts are an early-crystallization phase. Coleman et al. (2005), on the other hand, argues the growth to be a "late-stage" process of subsolidus crystallization. Whether the timing of megacryst growth is early, late, or some form of a combination of both, it is still a magmatic crystallization process rather than a metamorphic one.

Additional mesoscopic evidence for phenocrystic growth is in the arrangement of the megacrysts in outcrops. Megacrysts commonly have somewhat random orientations, as seen in some localities of the Kowaliga Gneiss (Fig. 27). Random orientations of non-fractured or plastically deformed megacrysts imply that there was enough liquid to suspend the megacrysts and to allow for euhedral mechanical rotation (Vernon and Patterson, 2008). The length-parallel orientation is common in granitoids and is repeatedly described as flow patterns aligning to xenoliths as well as the margins of the intrusions (Quinn, 1944). Within the Kowaliga

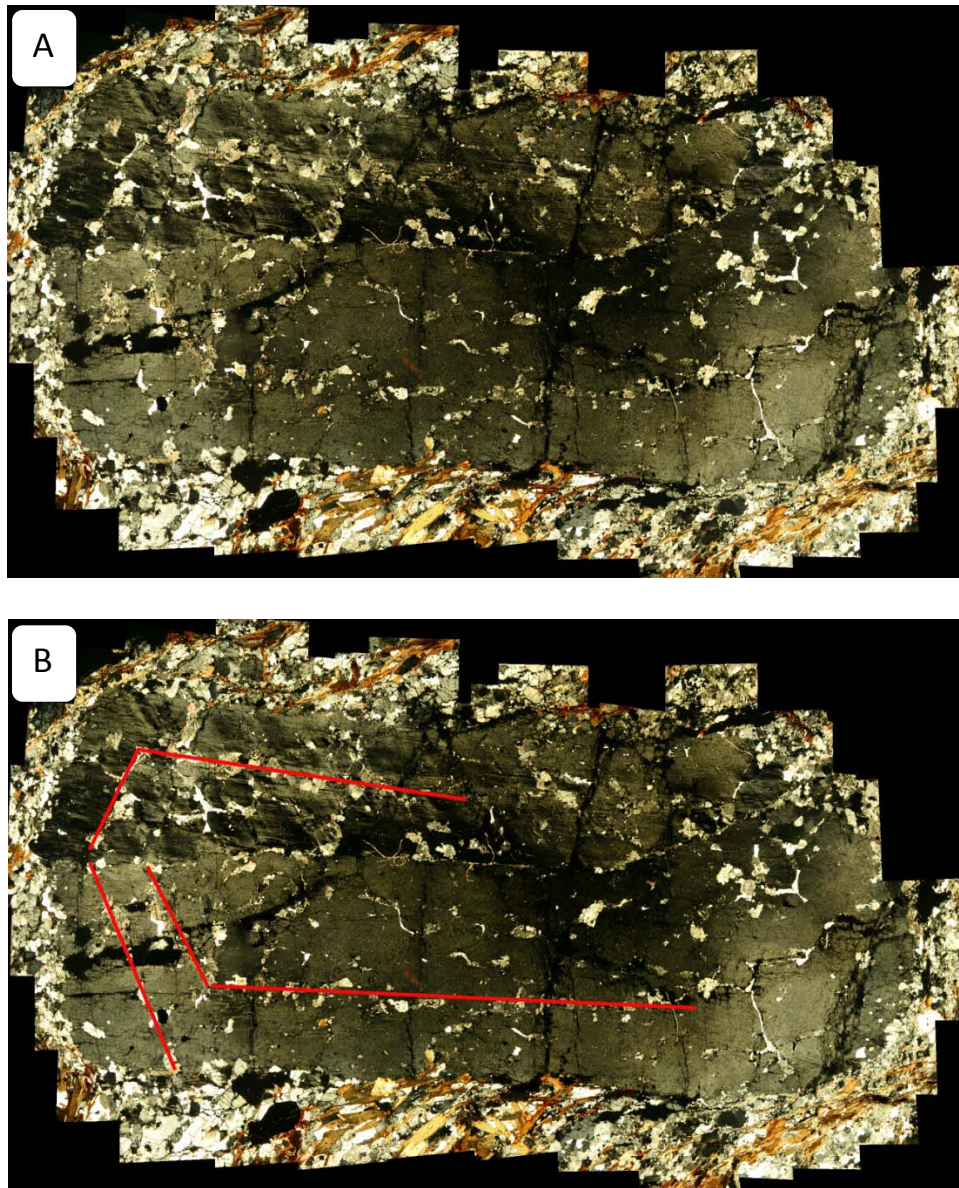


**Figure 27.** Photographs of megacrystic feldspar grains. A. A weak preferred orientation of megacrysts within the Kowaliga gneiss. Note that the weak alignment parallels the metamorphic foliation clearly indicating post-magmatic rigid-body rotation of the euhedral megacrysts. B. Strongly preferred-length orientation of megacrysts (left side of photograph) within the Tarnvika pluton in northern Norway.

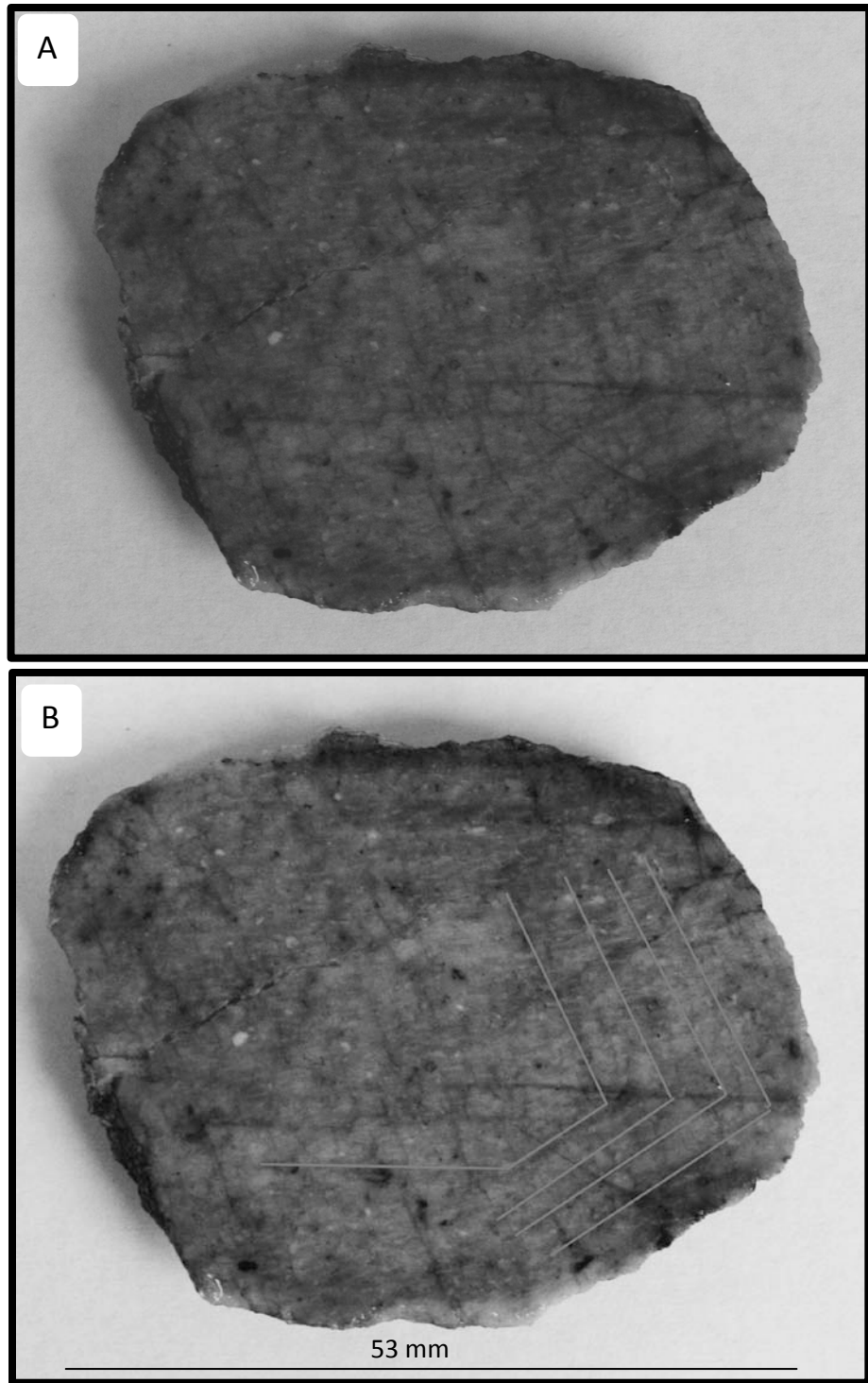


Gneiss, the margins of the batholith are so highly sheared that original megacrystic alignment, or non-alignment, is indeterminate.

Microscopic or microstructural evidence for phenocrystic growth comes in the form of four characteristics commonly observed in granites (Vernon, 1986, 1999, 2004). These include: (1) simple twinning, which is almost ubiquitous in magmatic potassium feldspar phenocrysts but is very rare in porphyroblasts (Vernon and Patterson, 2008); (2) concentric, crystallographically controlled arrangements of inclusions, as opposed to random inclusions as seen in metamorphic potassium feldspars (Vernon, 1986, 1999, 2004); (3) oscillatory zoning; and (4) euhedral inclusions of plagioclase. Within the Kowaliga megacrysts, simple twinning is observed in outcrop scale and in thin sections. In many samples, the simple twins have been damaged due to deformation that post-dated megacryst formation. Samples also have concentric inclusions aligned parallel to the oscillatory zoning (Fig. 28). Figure 28 shows a thin section of a megacryst from the Kowaliga Gneiss with inclusions that clearly occur along crystallographic controlled planes. Differences in degrees of extinction within potassium feldspar observed in this thin section reflect relict oscillatory zones and they correspond to those defined by the concentric inclusions. Later metamorphism and associated fluid infiltration has damaged the euhedral crystal causing the fractures and infilling areas with mineral precipitates. This metamorphism is responsible for the microscopic irregular edges observed in thin section. Figure 29 is also a phenocryst from the Kowaliga gneiss, and shows oscillatory zoning further reinforcing the interpretations made from Figure 28. Plagioclase inclusions found along the crystallographic planes are subhedral to anhedral. The absence of



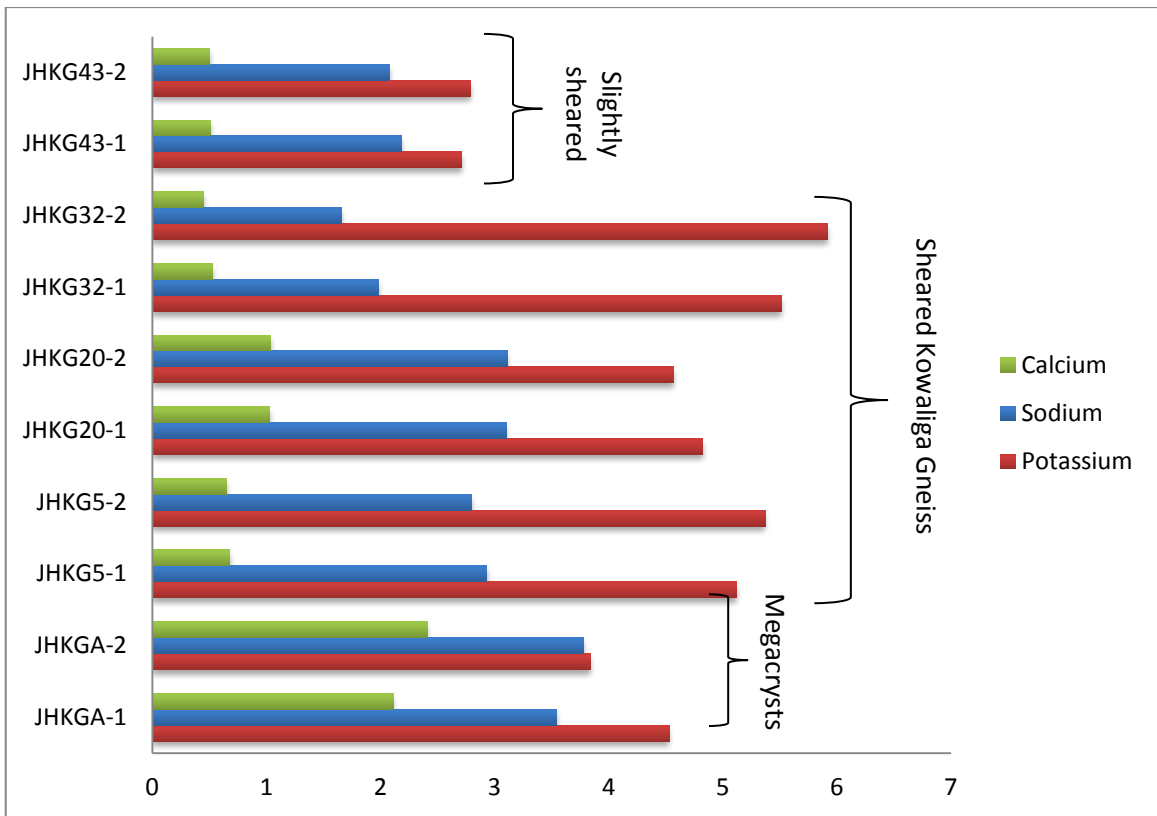
**Figure 28.** Collage of photomicrographs stitched together to provide one complete view of a euheedral potassium feldspar grain. Photographs were taken in crossed polars with a 4 cm field of view; total length of the crystal is 3.2 cm. A. Unobstructed view. B. Orientations of inclusions are outlined in red.



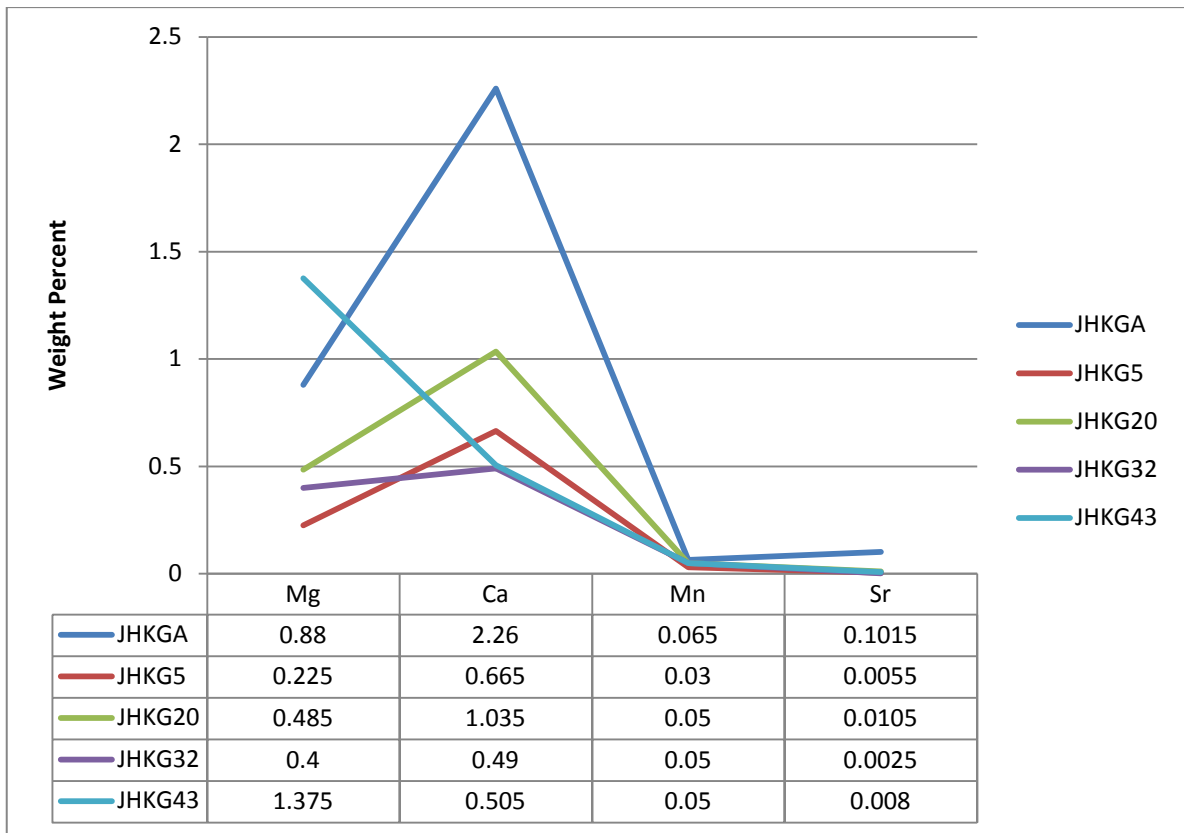
**Figure 29.** Photographs of a ~5 cm diameter phenocryst from the Kowaliga gneiss. A. Crystal was cut and hand sample was photographed to examine oscillatory zoning within the crystal. B. Digitized outlined portions of the zoning.

euohedral plagioclase inclusions is attributed to the amount of alteration and mineral precipitation commonly observed within the samples available.

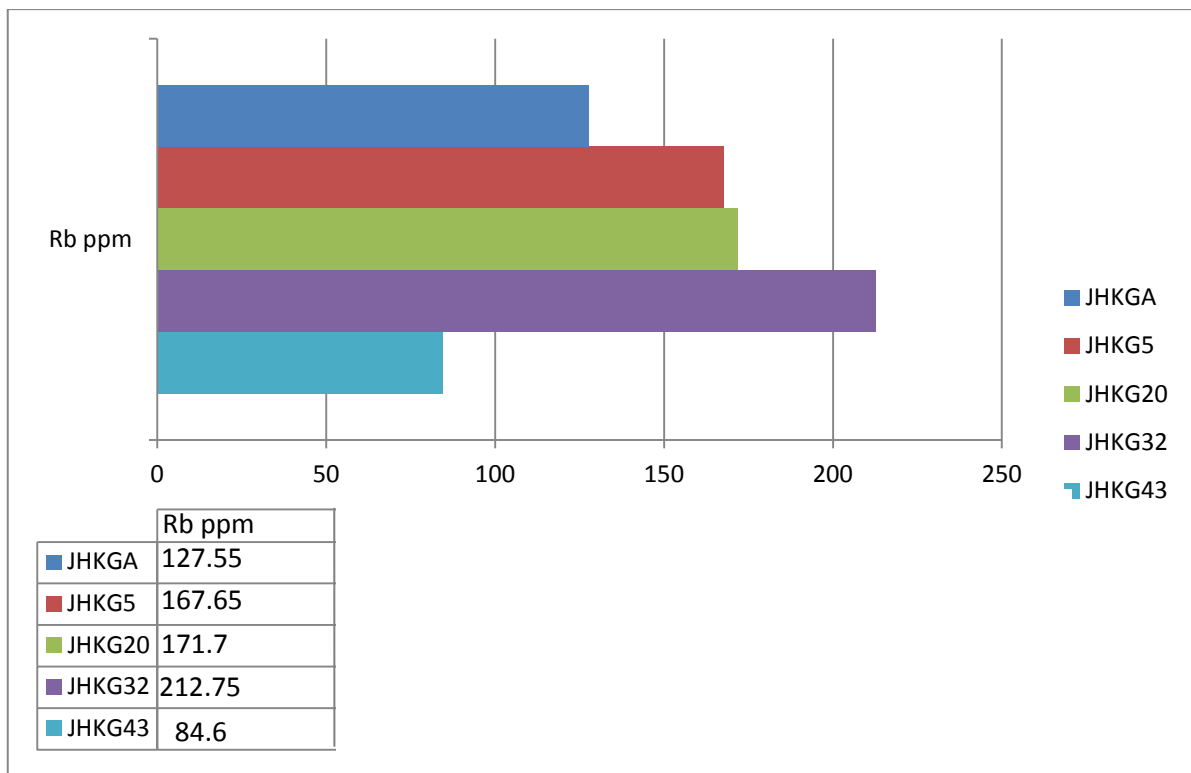
One possible theory for the presence of megacrysts observed in the Kowaliga gneiss is that they formed due to potassium metasomatism. Potassium metasomatism is the exchange of K for Na and Ca and causes the replacement of plagioclase with potassium feldspar. This alteration is known to increase within shear zones due to microcracking (Brantley et al., 1990; Tobisch et al., 1991; Oliver, 2001). To explore the possibility that potassium metasomatism was responsible for generating the Kowaliga megacryst, elemental abundances of Ca, Na, K (Fig. 30), Mg, Ca, Mn, Sr (Fig. 31), and Rb (Fig. 32) were measured by whole rock XRF (X-ray fluorescence) and plotted for all ten samples. Rocks that have been affected by potassium metasomatism will have a higher  $K_2O:Na_2O$  ratio ( $>2$ ), will be enriched in Rb, and will be depleted in Mg, Ca, Mn, and Sr (Dunbar et al., 1994; Glazner, 1988; Brooks, 1986; Chapin and Lindley, 1986). Sample JHKG1 and JHKG2 were found to have the highest abundances of Na and Ca and a lower relative abundance of K, when compared to all ten samples tested. These two samples represent the euohedral megacrystic variety of the Kowaliga Gneiss. Samples JHKG32, JHKG20, and JHKG5 represent highly sheared samples. These three samples have relatively lower amounts of Na and Ca and a higher relative abundance of K. Sample JHKG43 represents a slightly sheared sample of Kowaliga Gneiss with lower K amounts relative to the other samples tested; however, Na and Ca abundances are relatively consistent to the other samples. These data suggest that some degree of potassium metasomatism could have occurred within the samples of Kowaliga Gneiss that have experienced higher degrees of shearing, because  $K_2O:Na_2O$  ratios range from 1.5 to 3.6 and because all three samples are enriched in Rb and



**Figure 30.** Weight percent of Ca, Na, and K plotted for ten whole-rock analyses of samples of the Kowaliga Gneiss.



**Figure 31.** Weight percent of Mg, Ca, Mn, and Sr plotted for five whole-rock analyses of samples of the Kowaliga Gneiss. JHKGA is megacrystic; JHKG5, JHKG20, and JHK32 are sheared varieties; and JHK43 is slightly sheared.



**Figure 32.** Parts per million of Rubidium plotted for five whole-rock analyses of samples of the Kowaliga Gneiss. JHKGA is megacrystic; JHKG5, JHKG20, and JHK32 are sheared varieties; and JHK43 is slightly sheared.

depleted in Mg, Ca, Mn, and Sr. Rb enrichment in potassium metasomatized rocks is caused by the substitution of Rb within the potassium feldspar structure (Deer et al., 1992). It also suggests, however, that potassium metasomatism is not responsible for the origin of the euhedral megacrysts because  $K_2O:Na_2O$  ratios range from 1.0 to 1.2 with enriched Mg, Ca, Mn, and Sr abundances relative to the three sheared samples.

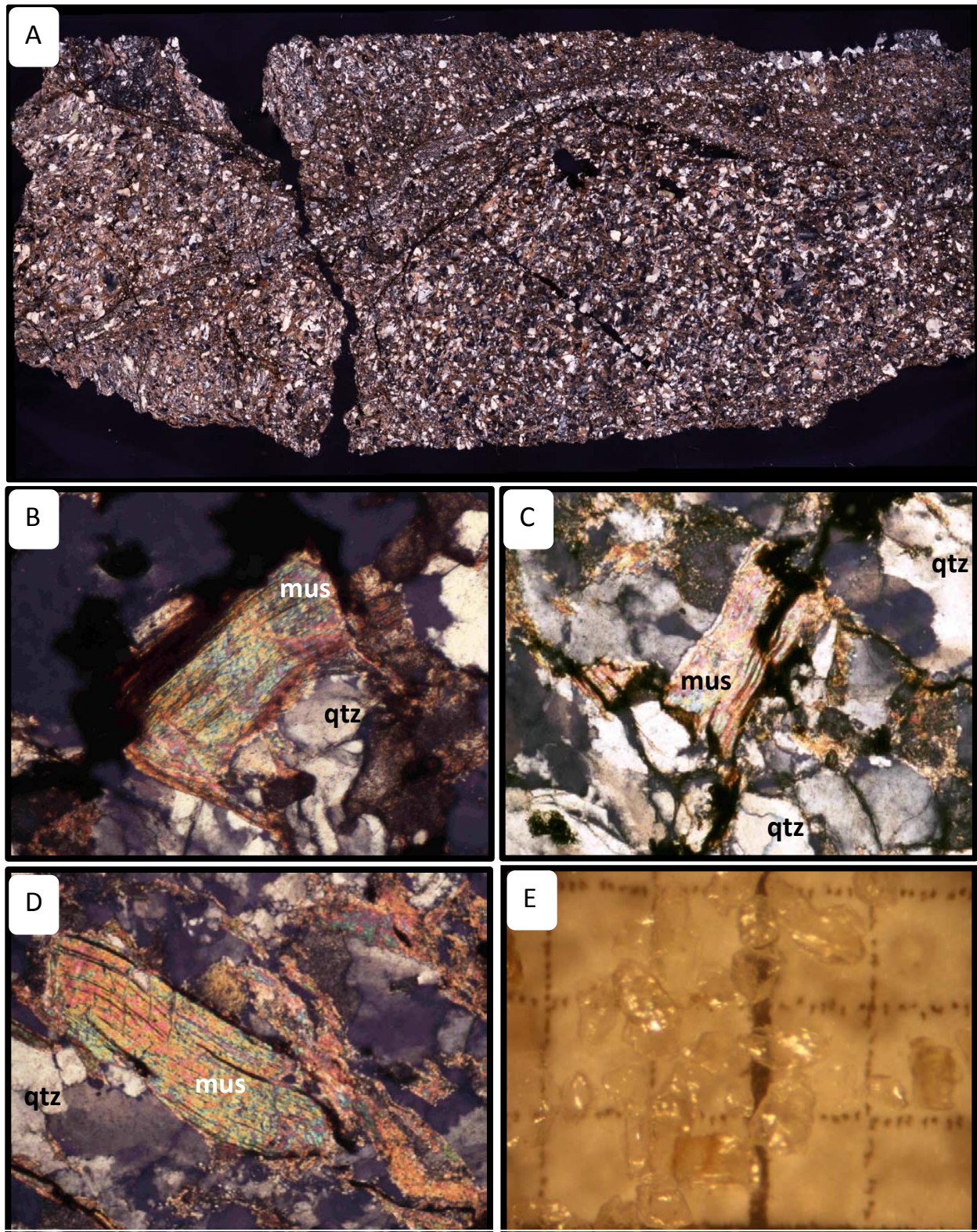
These observations argue strongly for a phenocrystic origin rather than porphyroblastic growth for the potassium feldspar megacrysts in the Kowaliga Gneiss. Augen generated within gneisses and mylonites are generally considered to be residual phenocrysts that have persisted through metamorphism and/or mylonitization as opposed to porphyroblasts generated within amphibolite-facies metapelites (Vernon and Clarke, 2008). The assumption of phenocrysts instead of porphyroblasts indicates that the Kowaliga megacrystic augen is the more characteristic phase of the Kowaliga intrusion, as first suggested by Bieler and Deiningner (1987), and that the more traditional appearance of the Kowaliga augen gneiss is the result of mechanical grain reduction and strain-induced recrystallization during mylonitization.



### **$^{40}\text{Ar}/^{39}\text{Ar}$ Analysis and Interpretations**

$^{40}\text{Ar}/^{39}\text{Ar}$  age dating was performed on muscovite grains separated from cataclastically deformed granite from the Our Town quadrangle (sample CV-1 location N32°51.840 W85°55.200) (Fig. 33A). The rationale for analyzing this sample was that at least some of the muscovite ages would reflect cooling or partial resetting associated with brittle fault movement along this zone. Thus, the muscovite ages could provide maximum age estimates for the timing of faulting. As noted previously, this cataclastic fault trends northeast-southwest across the northern section of the Our Town quadrangle but the degree of offset is unclear due to the limited amount of exposure. Small scale-folds in proximity of the fault suggest right-slip movement, but no clear sense of shear has been documented.

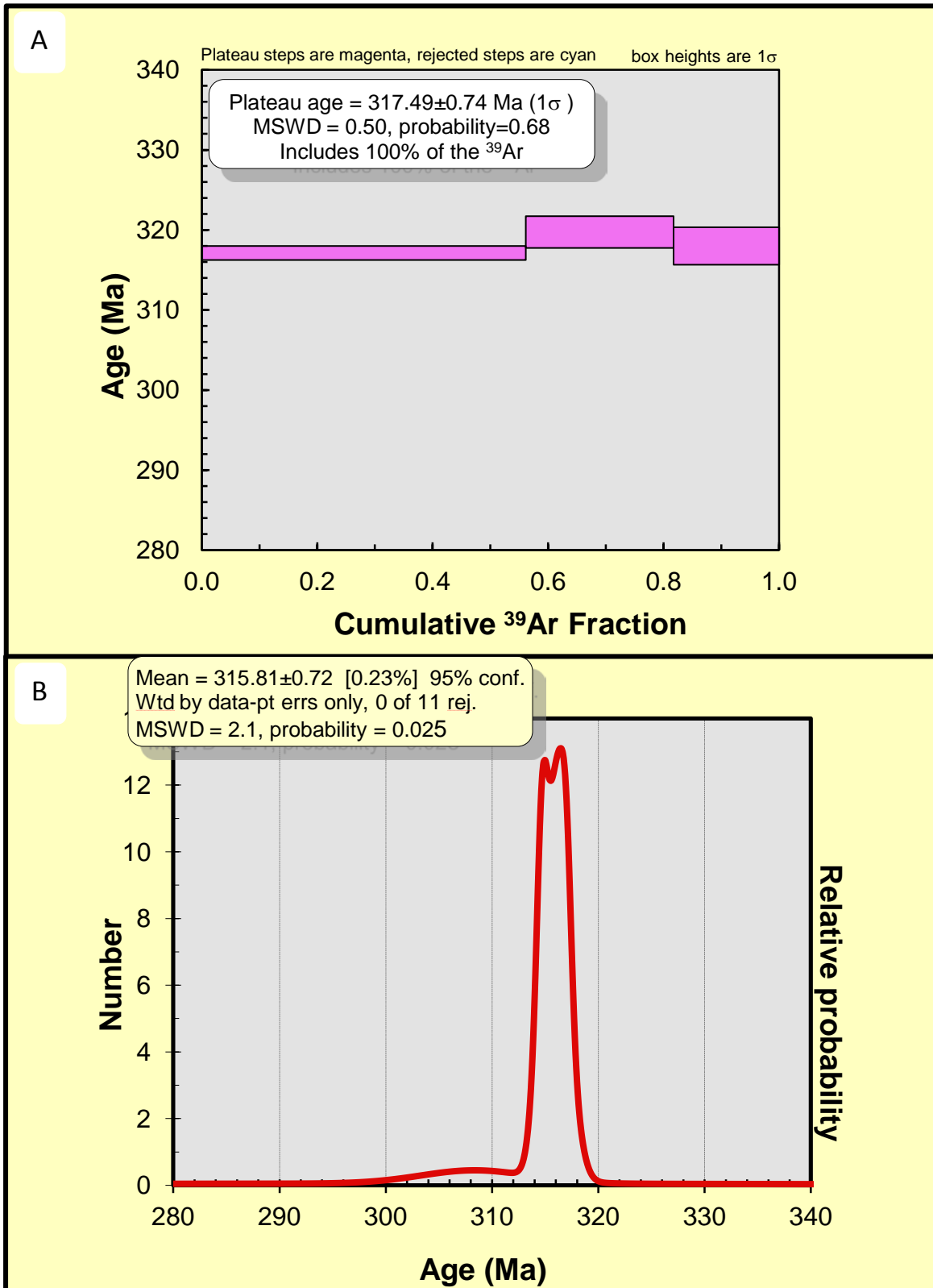
The samples collected for dating comprise quartz, feldspar (potassium feldspar and plagioclase), biotite, and muscovite. Quartz grains range up to 0.5 mm in diameter, they are highly angular, with strongly undulose extinction. Grain boundaries are irregular due to grain boundary migration recrystallization and ~80% of grains show varying degrees of subgrain rotation. Quartz recrystallization features are present in ~30% of the grains. The quartz microstructures are interpreted to have developed through brittle-plastic deformation at low metamorphic grade in event(s) preceding the latest cataclastic movement. Feldspar grains range up to 0.5mm in diameter and are highly weathered. The degree of weathering makes classification as potassium feldspar or plagioclase feldspar difficult, but some relict polysynthetic twinning (indicating plagioclase) is preserved. Feldspar grain alteration has



**Figure 33.** Cataclastic fault rock sample number CV1 used for  $^{40}\text{Ar}/^{39}\text{Ar}$  muscovite dating (N32 °51.840 W85°55.200). A. Full thin section slide view of the cataclastically deformed granite sample CV-1. B.to D. Enlarged view of the cataclastically deformed granite (2 mm field of view) E. Muscovites that were extracted and used for analysis.

produced sericite and saussurite concentrations along potassium grain margins. Biotite grains are up to 0.5 mm in length and are only slightly pleochroic. Grains show slight alteration to chlorite. Muscovite grains are up to 1 mm in length, and show evidence of deformation due to cataclasis (Figs. 33B to 33D). Dark anastomosing bands of finer grained material are interpreted to be hematite stained (dark-red-brown) sericite and/or saussurite. Methods for preparing the sample for isotopic analysis are as follows. The sample was crushed using a mortar and pestle and sieved. Size fractions from 60-80 mesh sieves, the preferred size for isotopic analysis of muscovite, were passed through the Frantz magnetic separator to further concentrate the muscovite. Approximately 75 to 100 muscovite grains were handpicked using a binocular microscope and were prepared for  $^{40}\text{Ar}/^{39}\text{Ar}$  analysis in the Auburn Noble gas Isotope Mass Analysis Laboratory (ANIMAL) (Fig. 33E). Ten grains were analyzed using Single-Crystal Total Fusion techniques. Further information concerning  $^{40}\text{Ar}/^{39}\text{Ar}$  methods and raw data are included in appendix 3.

Single-Crystal Total Fusion analyses yield a mid-Pennsylvanian mean age of  $315.81 \pm 0.72$  Ma, with 95% confidence. A probability density diagram (Fig. 34) contains a single strong peak that implies minimal influence by other thermal events. In detail, the MSWD of 2.1 and relatively low probability of fit (~3%) suggest variation in age beyond analytical precision. Such variation could arise from grain size control on  $^{40}\text{Ar}$  retention during slow cooling or minor, variable  $^{40}\text{Ar}$  loss during cataclasis. This result of 315 Ma is interpreted to reflect the time associated with regional cooling from an early Alleghanian metamorphic event recognized throughout the eastern Blue Ridge (Steltenpohl, 2005; Steltenpohl et al., 2013). This result can be explained in two ways: 1) either the argon isotopes in muscovite were not reset during the



**Figure 34.** Muscovite age data. A. Plateau age for a single crystal indicating  $317.4 \pm 0.7$  Ma. B. Probability density diagram for the ten muscovite grains from cataclastically deformed granite sample CV-1 analyzed in ANIMAL indicating  $315.8 \pm 0.7$  Ma with a MSWD of 2.1.

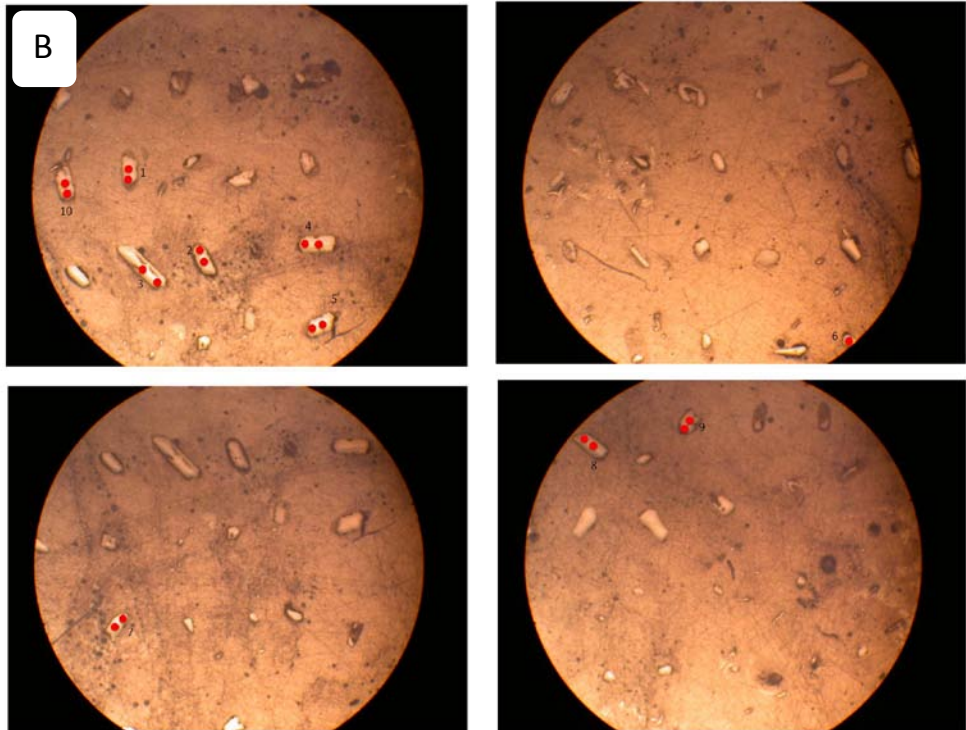
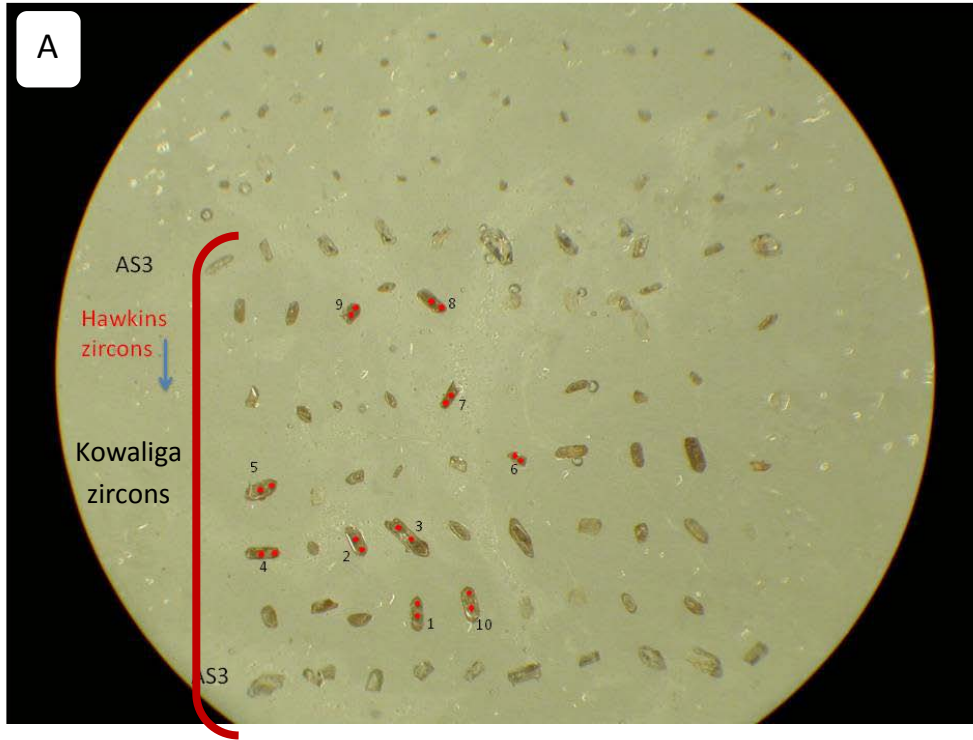
cataclastic event (perhaps due to occurrence at low temperatures in a brief event), or 2) the cataclastic fault zone is early Alleghanian and thermally re-equilibrated during cooling from the regional metamorphic event.

The latter scenario would seemingly require supra-brittle-ductile normal faulting in the middle Pennsylvanian, requiring that this part of the eastern Blue Ridge was at a high crustal level at this time. This seems reasonable considering that a nominal  $\sim 350^\circ\text{C}$  temperature of closure for muscovite corresponds roughly to the typical brittle-ductile transition levels in continental crust. Tops-down to the SSW movement along WNW-trending normal faults is well documented at precisely this time in the Black Warrior basin in west-central Alabama (Groshong et al., 2010). Future work on NW-trending cataclastic faults, similar to that of the present study in the Our Town quadrangle, could test their relationship to the extensional event commensurate with the faulting and evolution of the Black Warrior basin.

### **U/Pb Analysis and Interpretation**

Zircons were separated from a sample of the megacrystic variety of the Kowaliga Gneiss (JFKAZ1) for U-Pb analysis. The sample was selected because it contained well-preserved original igneous crystallization textures found only in the megacrystic varieties. The sample was fresh to slightly weathered and thus provides the best opportunity to date the time of igneous crystallization rather than subsequent metamorphic events that otherwise characterize eastern Blue Ridge granitoids. Samples were prepared in the rock preparatory lab at Auburn University. The sample was disc milled to approximately 25-50 microns. The disc mill was thoroughly cleaned with a wire brush, ethanol, and compressed air before the sample was processed. The crushed material was sieved and separated using methylene iodide heavy liquid (S.G. =3.335), and the zircons were picked from the heavy (sunk) material by hand.

Approximately 100 euhedral to subhedral zircons were extracted from the sample. From the zircons extracted, 10 polished zircon cores and rims were analyzed. The individual zircons are numbered 1 to 10 and their core and rim sample locations are marked in red in Figure 35. Analyses were performed using Secondary Ion Mass Spectrometry (SIMS) at the University of California at Los Angeles, and the data reported in Table 2 corresponds to the numbered zircons and core/rim analysis locations shown in Figure 35. Data obtained resulted in a mean square weighted deviation (MSWD) of 0.037. An MSWD of <2.5 is considered to define an isochron and a value of 0.037 indicates a single population of zircons (Brooks et al., 1972). U/Pb analysis yielded a Late Ordovician to Early Silurian concordia age of  $441 \pm 6.6$  Ma



**Figure 35.** Optical photographs of zircons from the Kowaliga Gneiss. A. Ten numbered zircons that were used for SIMS analysis (6 mm field of view). B. Location of core/rim analysis locations for the ten selected zircons (2 mm field of view).

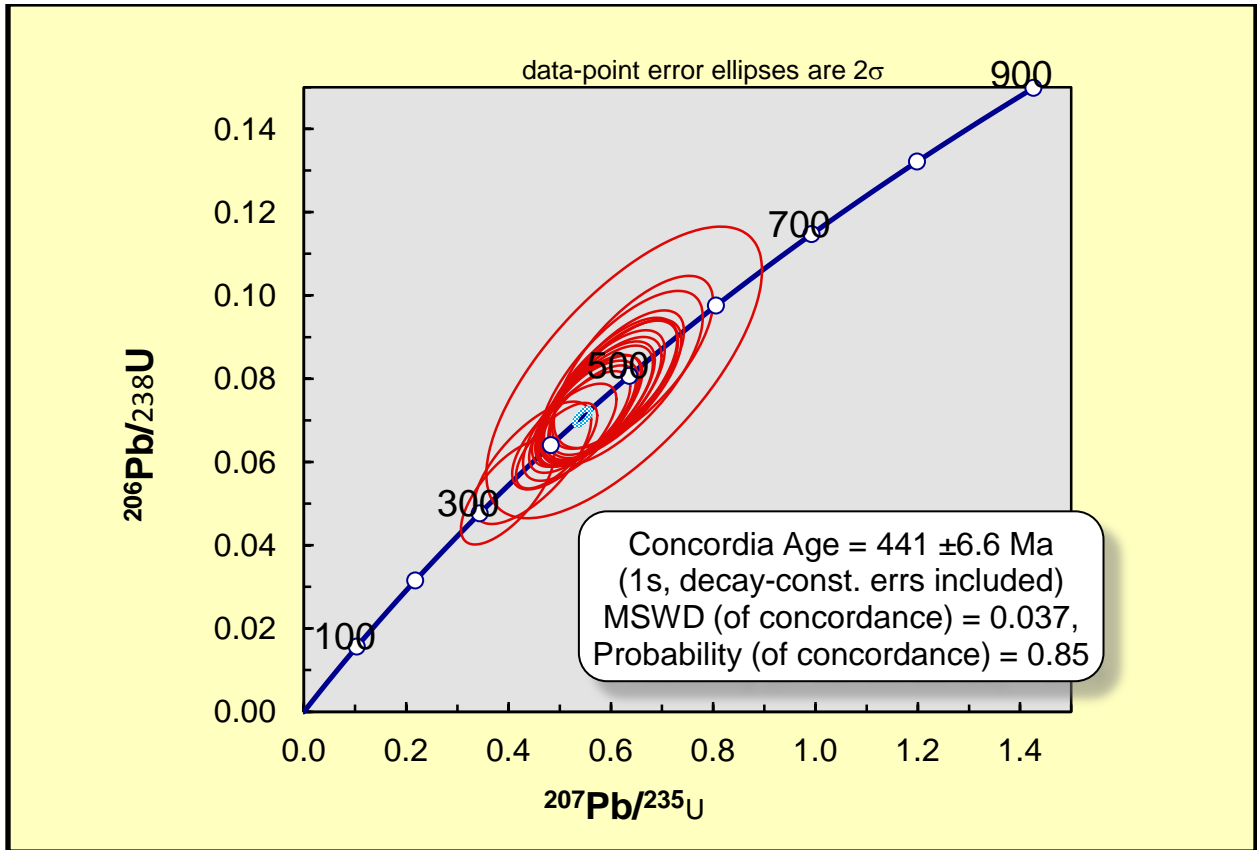
Sample	206Pb*/	206Pb*/	207Pb*/	207Pb*/	207Pb*/	207Pb*/	Age	Age	Age	Age	Age	Age
	238U	238U	235U	235U	206Pb*	206Pb*	(Ma)	(Ma)	(Ma)	(Ma)	(Ma)	(Ma)
		1 s.e.		1 s.e.		1 s.e.		1 s.e.		1 s.e.		1 s.e.
2012_12_10Dec\ Al_1_core.ais	0.0772	0.00684	0.6	0.0536	0.0563	0.000623	479	40.9	476.9	34	464.6	24.5
2012_12_10Dec\ Al_1_rim.ais	0.0815	0.0143	0.626	0.11	0.0557	0.000504	505	85.2	493.8	68.8	440.8	20.1
2012_12_10Dec\ Al_2_core.ais	0.0711	0.00494	0.554	0.0389	0.0565	0.000423	443	29.8	447.6	25.4	472.5	16.5
2012_12_10Dec\ Al_2_rim.ais	0.0722	0.00545	0.558	0.0422	0.0561	0.000254	449	32.8	450.5	27.5	457.5	10
2012_12_10Dec\ Al_3_core.ais	0.0527	0.00511	0.398	0.0371	0.0548	0.00153	331	31.3	340.2	27	402.8	62.7
2012_12_10Dec\ Al_3_rim.ais	0.0598	0.00599	0.447	0.0467	0.0542	0.00103	375	36.4	375.1	32.8	378	42.6
2012_12_10Dec\ Al_4_core.ais	0.0723	0.00549	0.552	0.0435	0.0553	0.0011	450	33	446	28.5	425.6	44.2
2012_12_10Dec\ Al_4_rim.ais	0.0699	0.0059	0.541	0.046	0.0562	0.000519	435	35.5	439.4	30.3	460.6	20.5
2012_12_10Dec\ Al_5_core.ais	0.084	0.00844	0.644	0.0637	0.0556	0.00076	520	50.2	504.9	39.4	437.7	30.4
2012_12_10Dec\ Al_5_rim.ais	0.0801	0.00857	0.62	0.0653	0.0561	0.00059	497	51.1	490	40.9	457.1	23.3

**Table 2.** Raw data for Kowaliga Gneiss zircon rims and cores collected from SIMS analyses. 1 s.e. is the standard error, which represents measurement uncertainty.



Sample	206Pb*/ 238U		207Pb*/ 235U		207Pb*/ 206Pb*		Age (Ma)	Age (Ma)	Age (Ma)	Age (Ma)	Age (Ma)	Age (Ma)
	0.0774	0.00705	0.597	0.0543	0.056	0.000333	481	42.2	475.6	34.5	451.2	13.2
	1 s.e.		1 s.e.		1 s.e.		1 s.e.		1 s.e.		1 s.e.	
2012_12_10Dec\ AI_6_core.ais	0.0774	0.00705	0.597	0.0543	0.056	0.000333	481	42.2	475.6	34.5	451.2	13.2
2012_12_10Dec\ AI_6_rim.ais	0.0758	0.00647	0.583	0.0499	0.0558	0.000282	471	38.7	466.6	32	445.7	11.2
2012_12_10Dec\ AI_7_core.ais	0.0776	0.00681	0.608	0.0531	0.0568	0.00121	482	40.7	482.2	33.5	483.1	46.9
2012_12_10Dec\ AI_7_rim.ais	0.0696	0.005	0.539	0.0403	0.0561	0.000731	434	30.1	437.8	26.6	457.7	28.9
2012_12_10Dec\ AI_8_core.ais	0.0748	0.00621	0.581	0.0482	0.0563	0.000464	465	37.2	465.2	31	464.7	18.3
2012_12_10Dec\ AI_8_rim.ais	0.0661	0.00519	0.509	0.0417	0.0559	0.00102	413	31.4	418	28	446.8	40.7
2012_12_10Dec\ AI_9_core.ais	0.0739	0.00614	0.569	0.0479	0.0559	0.00161	460	36.8	457.7	31	448.3	63.8
2012_12_10Dec\ AI_9_rim.ais	0.0735	0.00589	0.57	0.0459	0.0562	0.000217	457	35.4	457.8	29.7	460.8	8.55
2012_12_10Dec\ AI_10_core.ais	0.0779	0.00661	0.606	0.0512	0.0563	0.000234	484	39.5	480.8	32.4	466.2	9.21
2012_12_10Dec\ AI_10_rim.ais	0.0798	0.00679	0.614	0.0527	0.0558	0.000367	495	40.5	486.1	33.2	444.4	14.6
2012_12_10Dec\ AI_10_rim@1.ais	0.0639	0.0042	0.494	0.0325	0.056	0.000285	399	25.4	407.5	22.1	453.1	11.3

**Table 2.** Raw data for Kowaliga Gneiss zircon rims and cores collected from SIMS analyses. 1 s.e. is the standard error, which represents measurement uncertainty.



**Figure 36.** U/Pb isochron plot for zircons from Kowaliga Gneiss sample 2012\_12\_10Dec\Al. Chart was constructed and ages were determined using Isoplot (Ludwig, 2003).

with a probability of concordance of 85 percent (Fig. 36).

Traditionally the intrusive bodies within the Emuckfaw Group have been mapped either as smaller tabular bodies (Zana Granite) or as the larger, batholithic sized Kowaliga Gneiss (northwestern and southeastern bodies depicted in Figure 1). Recent U/Pb SHRIMP data obtained for the Zana suggested a crystallization age range of 480 to 410 Ma (Tull et al., 2013). Using the “zircon age extractor” function in Isoplot v. 3.75 (Ludwig, 2012) an age of 439 Ma can be inferred from the data. This date indicates a strong correlation with the crystallization age of the Kowaliga Gneiss that was determined to be  $441 \pm 6.6$  Ma. The pronounced similarities in crystallization age combined with strong geochemical trends visible in Harker plots of  $\text{Fe}_2\text{O}_3$ , CaO, MgO,  $\text{K}_2\text{O}$ ,  $\text{Al}_2\text{O}_3$  indicates little evidence to support the earlier differentiation of the Zana Granite and the Kowaliga Gneiss.

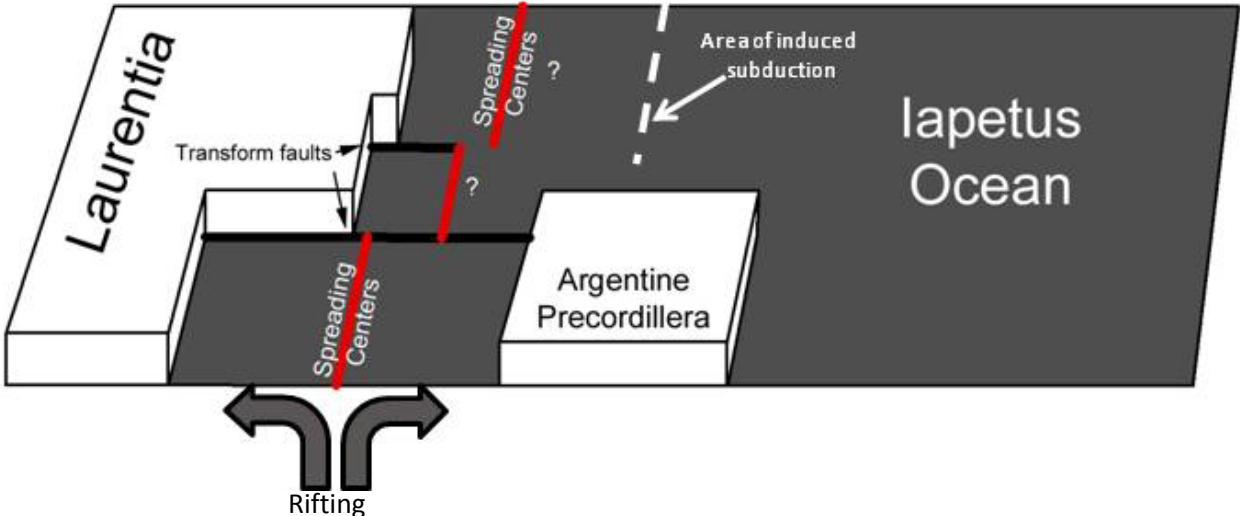
## Discussion

Multiple findings during the investigation of rocks and structures in the Our Town quadrangle have potentially significant implications for southern Appalachian tectonic evolution. These findings include the following: 1) a crystallization age for the Kowaliga Gneiss of  $441 \pm 6.6$  Ma; 2) the geochemical trace-element discrimination of Rb-Hf-Ta for the megacrystic Kowaliga Gneiss indicating possible intrusion within a volcanic-arc or a late to post-collisional edifice; and 3) the differentiation of the Emuckfaw Group lithologies based on the presence of metavolcanic units possibly associated with back-arc basin or arc volcanism. This allows for a tectonic interpretation that explains the depositional environment of the Emuckfaw Group and the related intrusions.

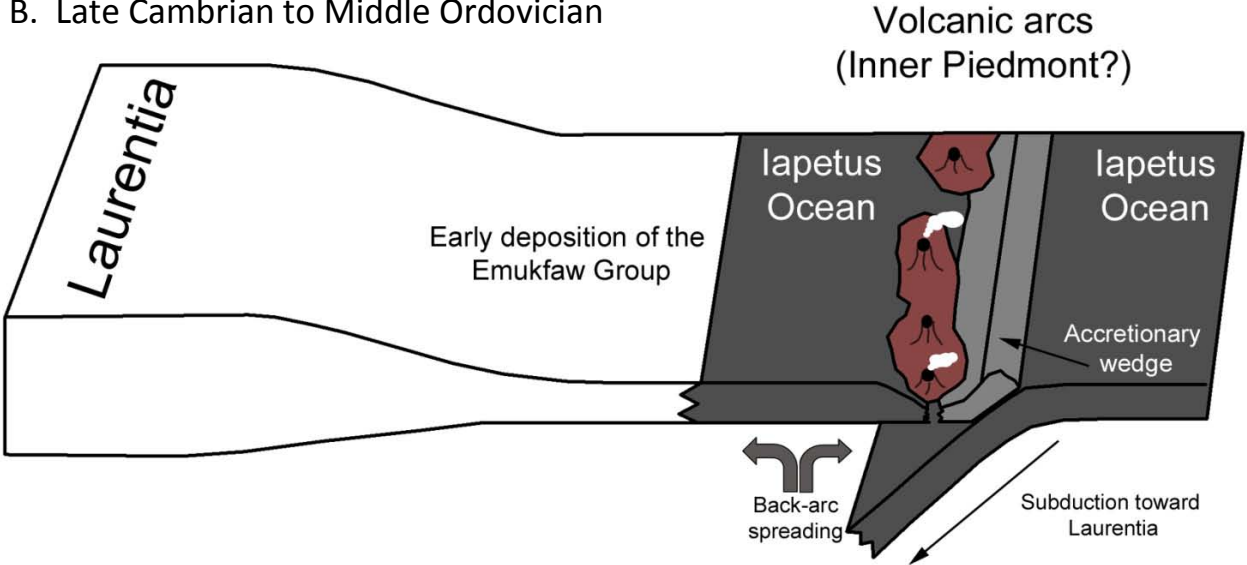
The crystallization age of  $441 \pm 6.6$  Ma for the Kowaliga Gneiss provides an age that is pre-Late Ordovician for the deposition of the Emuckfaw Group. The timing of deposition post-dates Cambrian to Early Ordovician rifting of the Argentine Precordillera away from the Laurentian margin (Thomas and Astini, 1996). As the Argentine Precordillera was sliding along the Alabama Promontory, rifting would cause crustal thinning and corresponding extensional faulting (Fig. 37A). Possible evidence for this crustal thinning is observed in the Our Town quadrangle in the form of metagabbros that might represent the mafic material intruded during rifting and basin formation. This period of extension could have prompted a minor westward dipping subduction zone resulting in a back-arc basin (Fig. 37B).

This newly induced subduction zone would result in the opening of a small back-arc

A. Cambrian to Early Ordovician



B. Late Cambrian to Middle Ordovician



**Figure 37.** Tectonic models for Cambrian to Middle Ordovician. A. Tectonic model showing the rifting of the Argentine Precordillera and region of induced subduction. B. Tectonic model of the developing volcanic arc and the depositional center for the Emuckfaw Group. Modified from Hatcher (2010).

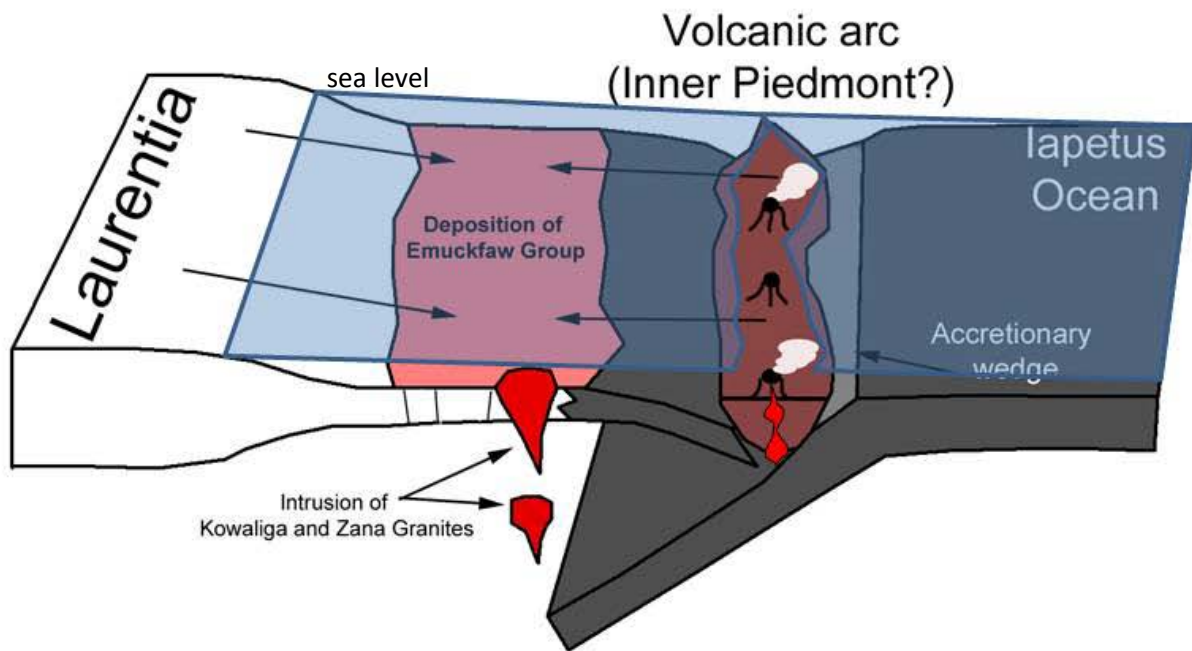
basin and would generate a linear volcanic arc extending parallel to the Laurentian margin (Fig. 37B). This newly formed back-arc basin would allow the Emuckfaw Group to be deposited stratigraphically above the earlier Laurentian slope-rise lithologies with sedimentary material having been sourced from both the margin of Laurentia and the volcanic arc. The influx of mafic source material from the volcanic arc is interpreted to account for the volcanogenic lithologies within the Emuckfaw Group including magnetite quartzites, garnetiferous amphibole-bearing quartzites, and amphibolites.

As the Emuckfaw Group was being deposited during Late Ordovician, westward dipping subduction produced melts that rose as plutons to crystallize into the Kowaliga Gneiss and Zana Granite. This suggests the same magmatic source for both intrusions, which is compatible with similar geochemical trends and crystallization ages observed for both intrusions.

Geochemical trace-element discrimination of Rb-Hf-Ta from the Kowaliga Gneiss (Fig. 26B) indicates two tectonic settings, volcanic-arc and late-to-post collisional. This is interpreted to indicate generation of the initial magmas in a volcanic arc setting. Due to the close proximity of the volcanic arc to Laurentia, the rising magmas were influenced by the Laurentian crust underlying the Emuckfaw Group contributing to the late-to-post collisional geochemical signatures (Fig. 26B).

The Emuckfaw Group and its intrusions were later metamorphosed to middle amphibolite grade and transported to their current location during later Acadian/Neocadian and Alleghanian orogenic phases. Within the Our Town quadrangle the regional northeast-striking southeast-dipping mylonitic foliation is attributed to the Alleghanian

Late Ordovician



**Figure 38.** Tectonic setting illustrating the depositional environment and possible source terranes for the Emuckfaw Group during Late Ordovician intrusion of the Kowaliga and Zana granites.

orogeny. This is supported by the  $^{40}\text{Ar}/^{39}\text{Ar}$  analysis that yields a date of  $315 \pm 0.72$  Ma. The probability density diagram in figure 34 has one central peak that corresponds to cooling associated with the Alleghanian orogeny and does not delineate any earlier cooling periods. This is due to either weak or absent effects of earlier heating/metamorphism or a complete overprinting by an early phase of the Alleghanian orogeny.

The Alexander City fault and the Abanda fault both have an oblique and normal-dextral sense of shear within the Our Town quadrangle. These two faults are believed to have a polyphase history originating as thrusts that were later reactivated as normal faults. The histories of these faults are discussed in more detail in Steltenpohl et al. (2013).

The most recent tectonic activity in the study area is expressed as aplite dike injections and normal faults that cut all lithologies and northeast-trending faults. The faults strike west-northwest and dip to the east-northeast. Analysis suggests northeast-southwest extension has stretched rocks of the area through the production of these normal faults.



## Conclusions

New discoveries brought about by this detailed geologic investigation of rocks and structures in the Our Town, Alabama quadrangle have potentially significant implications for southern Appalachian evolution.

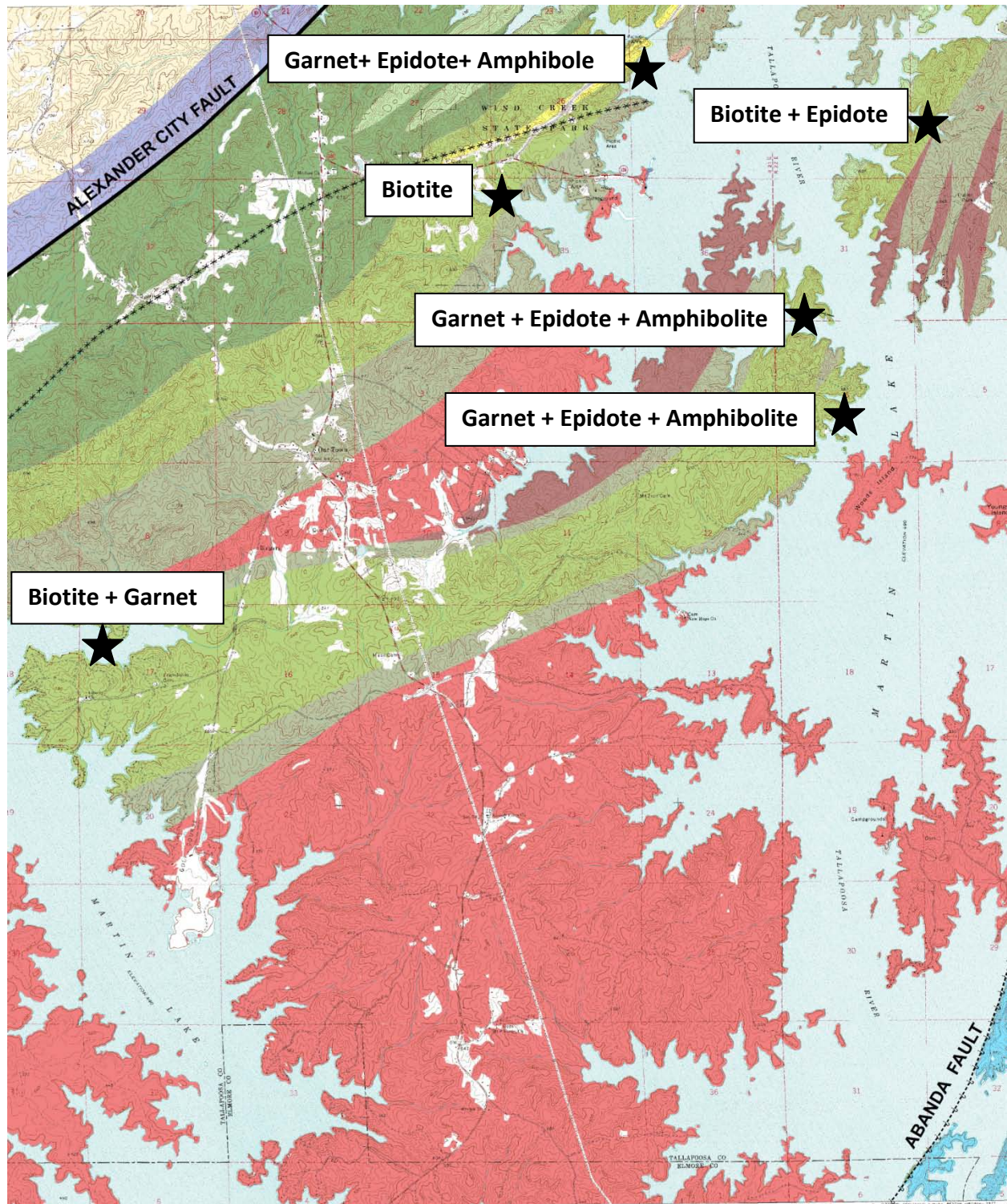
- The Emuckfaw Group contains metavolcanic units that include 3-4 cm thick amphibolites and 10-12 cm thick garnet-amphibole-bearing quartzites. The source of these mafic lithologies helps to shed light on the depositional and tectonic settings for the Emuckfaw Group, which involved volcanic input.
- Metamorphic mineral assemblages within the Emuckfaw Group indicate epidote/amphibolite to amphibolite-facies metamorphism.
- Retrograde mylonites and phyllonites of the Abanda fault indicate an oblique dextral-and-normal sense of movement similar to that recently reported for the Alexander City fault (Steltenpohl et al., 2013).
- Two sets of sub-vertical brittle normal faults occur throughout the eastern Blue Ridge in the Our Town quadrangle. Faults of the NW-SE-trending set cut the oblique dextral-normal phyllonites of the Abanda fault. Faults of the WSW-ENE set rarely are found to cut Abanda phyllonites and are similar to Mesozoic (?) faults known to cut the Alexander City and Towaliga mylonite zones (Steltenpohl et al., 2013).
- Whole-rock major and trace element analyses of the megacrystic and augen varieties of the Kowaliga Gneiss indicate a strong correlation with previously reported geochemical

data for the Zana Granite. Trace element discrimination of Rb-Hf-Ta for the megacrystic Kowaliga Gneiss plots in the late-to-post collisional and back-arc petrogenetic fields.

- Petrographic and geochemical analysis of megacrystic potassium feldspar within the Kowaliga Gneiss indicates that the megacrysts have a magmatic origin rather than a metamorphic one. The euhedral megacrysts in the Kowaliga Gneiss are interpreted as original magmatic features that experienced only minor effects of metamorphism.
- $^{40}\text{Ar}/^{39}\text{Ar}$  Analysis of muscovites extracted from a cataclastic zone within the study area yield a date of  $315.81 \pm 0.72$  Ma. It is interpreted that this date does not record the timing of movement along the cataclastic fault, but rather reflects cooling from regional metamorphism (early Alleghanian cooling). This would indicate this part of the eastern Blue Ridge was at a high crustal level during Middle Pennsylvanian.
- U-Pb SIMS dates on zircons from the megacrystic Kowaliga Gneiss yield an age of crystallization age of  $441 \pm 6.6$  Ma with no systematic or significant variations between the cores and rims. Previously reported tentative dates for the Zana Granite yield a crystallization age of 439 Ma (Tull et al., 2013). The strong similarities in geochemical signatures, crystallization ages, and field occurrences suggest that these intrusions, previously mapped as separate igneous suites, should be considered one intrusive event. Together with the identical age and field relations with the 441 Ma Farmville metagranite (Hawkins et al., 2013), this supports the hypothesis of Steltenpohl (2005) and Steltenpohl et al. (2011) that the footwall units to the Tallasse synform reside in a large tectonic window, the Dog River window, beneath the allochthonous Dadeville complex.

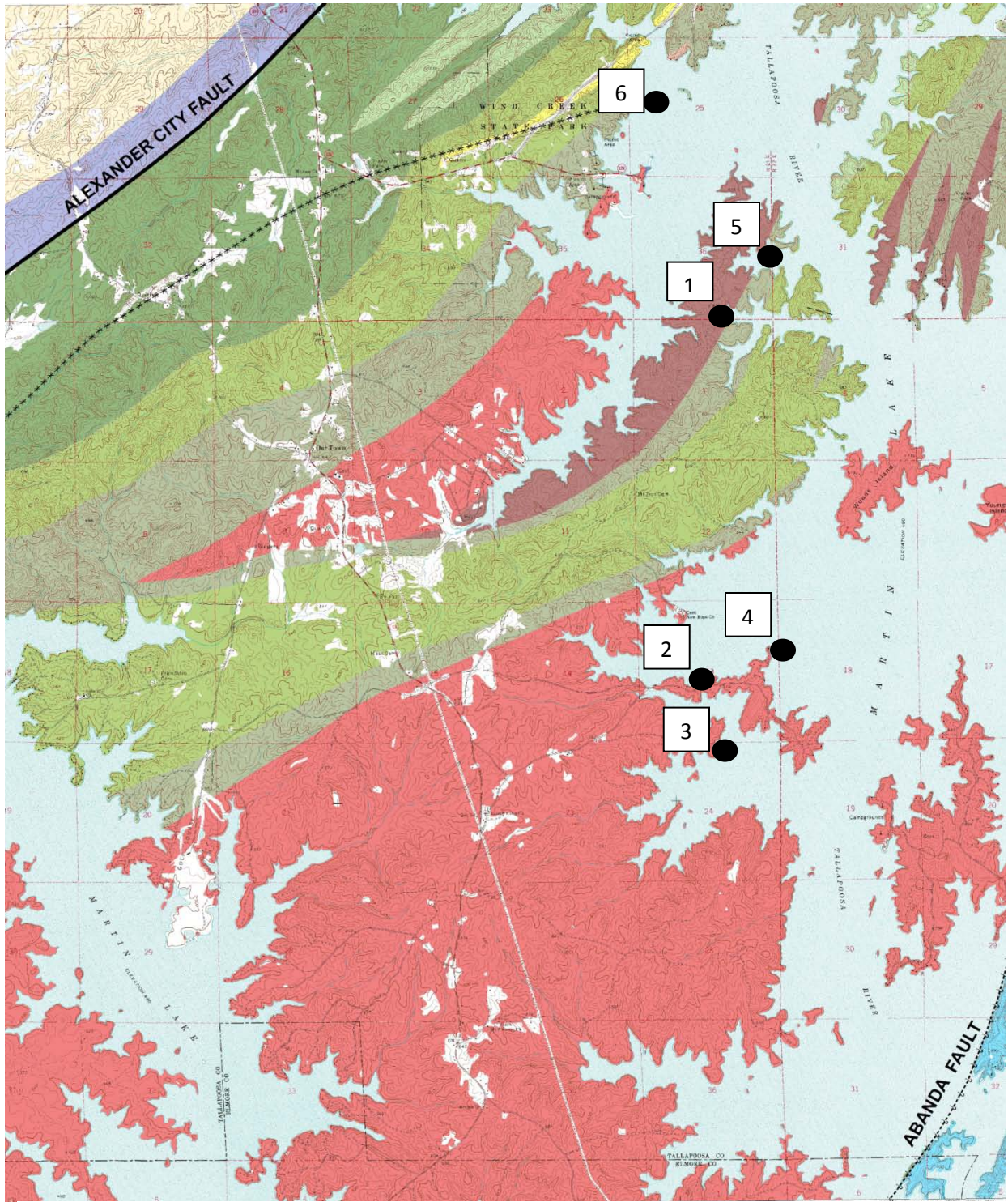
## **APPENDIX 1**

Location of metamorphic index minerals



**Appendix 1.** Geologic map of the Our Town quadrangle indicating locations of metamorphic index minerals.

**APPENDIX 2**  
Sample locations



**Appendix 2.** Geologic map of the Our Town quadrangle indicating the sample locations of rocks used in the geochemical analysis. Numbers correspond to the table in Appendix 3.

Samples	Latitude	Longitude	Description
1 JHKG A	N 32°50.337	W85°54.638	Megacrystic variety of the Kowaliga Gneiss.
2 JHKG 5	N32°48.420	W85°54.300	Sheared augen variety of the Kowaliga Gneiss
3 JHKG 20	N32°74.880	W85°54.599	Sheared augen variety of the Kowaliga Gneiss
4 JHKG 32	N32°47.999	W85°54.540	Sheared augen variety of the Kowaliga Gneiss
5 JHKG 43	N32°50.985	W85°54.273	Megacrystic variety in transition to a sheared augen variety of Kowaliga Gneiss
6 CV-1	N 32°51.840	W85°55.200	Cataclastically deformed granite

**Appendix 2.** GPS coordinates and description for the five samples used in the geochemical analysis.

**APPENDIX 3**  
<sup>40</sup>Ar/<sup>39</sup>Ar Data



Irradiation Package:	AU-16	
Monitor Age	28.02	(Ma, FCS)
Air <sup>40</sup> Ar/ <sup>36</sup> Ar:	293.0	+ 1.5
Mass Disc. (% per amu):	-0.0021151	± 0.00101523
( <sup>36</sup> / <sup>37</sup> )Ca:	0.00030	± 2.7E-06
( <sup>39</sup> / <sup>37</sup> )Ca:	0.000838	± 3.8E-05
( <sup>40</sup> / <sup>39</sup> )K:	0	± 4E-04
( <sup>38</sup> / <sup>39</sup> )Cl:	0.01	± 0.01

All analyses were completed within 10 months of irradiation.

#### Lab methods statement:

Samples were irradiated in the central core position of the McMaster nuclear reactor in Hamilton, Ontario, with cadmium shielding. Synthetic CaF<sub>2</sub> was included with the irradiation to determine calcium production factors, and Fish canyon sanidine (from an aliquot prepared at New Mexico Tech) was used to monitor production of <sup>39</sup>ArK, with an assigned age of 28.02 Ma (Renne et al., 1998). Monitors were placed in five of eight possible positions (four alternating radial positions and one central position) for each layer of the irradiation package. Vertical variations in J-value for the five layers of the irradiation package for these samples were found to be negligible, but radial variations were significant (up to ~ 2% across a given layer). Aliquots of air from an air pipette were measured daily to evaluate mass discrimination, and procedural blanks were measured following every five analyses of unknowns. Samples were analyzed in the Auburn Noble Isotope Mass Analysis Laboratory (ANIMAL) following gas extraction with a CO<sub>2</sub> laser using an automated extraction line, with data collection on an electron multiplier detector. Data presented are in moles unless otherwise indicated, and are corrected for backgrounds, mass discrimination, and decay of short-lived isotopes. 'P' refers to the laser power and 't' to seconds for laser heating; 'R' is the <sup>40</sup>Ar\*/<sup>39</sup>ArK ratio. Errors in measurement, individual calculated ages and plateau ages are 1 standard deviation; means are reported at the 95% confidence level. Plateau and mean calculations were made using Isoplot (Ludwig, K.R., 2003, *Isoplot v. 3.0, A geochronology toolkit for Microsoft Excel*, Special Publication #4, Berkeley Geochronology Center).

#### Single Crystal Total Fusion

	P	t	40	39	38	37	36	%Rad	R	Age (Ma)	%-sd
au16.4d.mus.93a.tx	1.6	15	1.761E-14 ± 1.29E-17	1.33E-15 ± 2.94E-18	4.37E-18 ± 1.06E-19	1.04E-18 + 7.14E-19	4.04E-19 ± 8.301E-20	99%	13.17441	315.11 ± 0.86	0.27%
au16.4d.mus.94a.tx	1.6	10	1.554E-14 ± 7.76E-18	1.17E-15 ± 2.84E-18	2.61E-18 ± 3.84E-20	3.43E-19 + 8.66E-19	1.44E-19 ± 7.916E-20	100%	13.25436	316.86 ± 0.92	0.29%
au16.4d.mus.95a.tx	0.0	0	1.644E-15 ± 2.41E-18	1.22E-16 ± 7.89E-19	4.11E-19 ± 2.53E-20	5.49E-19 + 6.23E-19	2.69E-19 ± 7.909E-20	95%	12.86785	308.36 ± 5.09	1.65%
au16.4d.mus.96a.tx	1.6	10	2.151E-14 ± 9.86E-18	1.62E-15 ± 2.78E-18	3.49E-18 ± 2.78E-20	1.25E-18 + 6.9E-19	3.55E-19 ± 7.627E-20	100%	13.22059	316.12 ± 0.66	0.21%
au16.4d.mus.97a.tx	1.6	10	1.464E-14 ± 1.35E-17	1.11E-15 ± 1.88E-18	2.32E-18 ± 2.17E-20	4.09E-19 + 6E-19	2.77E-19 ± 7.324E-20	99%	13.15674	314.72 ± 0.77	0.24%
au16.4d.mus.98a.tx	1.6	10	2.132E-14 ± 1.12E-17	1.6E-15 ± 1.7E-18	3.64E-18 ± 3.72E-20	1.52E-18 + 6.51E-19	2.83E-19 ± 6.825E-20	100%	13.26135	317.01 ± 0.48	0.15%
au16.4d.mus.1a.txt	1.5	10	1.587E-14 ± 1.39E-17	1.19E-15 ± 1.46E-18	2.87E-18 ± 3.32E-20	8.15E-19 + 6.25E-19	2.39E-19 ± 7.537E-20	100%	13.22375	316.19 ± 0.65	0.21%
au16.4d.mus.2aa.tx	1.8	10	2.102E-14 ± 1.28E-17	1.59E-15 ± 4.21E-18	3.78E-18 ± 2.34E-20	1.08E-18 + 5.83E-19	1.82E-19 ± 7.259E-20	100%	13.17172	315.05 ± 0.92	0.29%
au16.4d.mus.6a.txt	1.8	10	1.362E-14 ± 6.52E-18	1.02E-15 ± 2.98E-18	2.49E-18 ± 2.9E-20	5.5E-18 + 6.1E-19	1.54E-19 ± 7.532E-20	100%	13.26249	317.04 ± 1.07	0.34%
au16.4d.mus.4a.txt	1.8	10	4.008E-14 ± 1.53E-17	3.03E-15 ± 3.37E-18	7.53E-18 ± 8.76E-20	4.57E-18 + 9.44E-19	8.1E-19 ± 1.215E-19	99%	13.15649	314.7 ± 0.5	0.15%

#### Single Crystal Incremental Heating

au16.4d.mus.3a.txt	0.40	15	1.370E-14 ± 1.04E-17	1.02E-15 ± 2.02E-18	2.66E-18 ± 3.86E-20	-1.87E-19 ± 7.16E-19	6.66E-19 ± 7.357E-20	99%	13.26232	317.03 ± 0.9	0.27%
au16.4d.mus.3b.txt	0.45	15	6.289E-15 ± 7.45E-18	4.65E-16 ± 2.14E-18	1.46E-18 ± 5.61E-20	9.61E-19 ± 8.31E-19	2.31E-19 ± 8.201E-20	99%	13.38092	319.63 ± 2.0	0.62%
au16.4d.mus.3c.txt	0.50	15	4.445E-15 ± 6.1E-18	3.32E-16 ± 1.66E-18	7.33E-19 ± 2.61E-20	-1.05E-18 ± 7.51E-19	8.97E-20 ± 7.613E-20	99%	13.30129	317.89 ± 2.3	0.73%
au16.4d.mus.3d.txt	0.55	15	5.813E-17 ± 8.96E-19	3.88E-18 ± 2.14E-19	-8.44E-20 ± -2.41E-19	-1.41E-18 ± 7.72E-19	2.59E-20 ± 8.701E-20	87%	12.98335	310.91 ± 160.1	51.49%

#### Appendix 3. <sup>40</sup>Ar/<sup>39</sup>Ar Data

### List of References

- Barker, F., 1979, Trondhjemite: Definition, environment, and hypotheses of origin, *in* Barker, F., ed., Trondhjemites, dacites and related rocks: Elsevier, Amsterdam, p. 1-12.
- Baskin, Y., 1956, A study of authigenic feldspar: *Journal of Geology*, v. 64, p. 132-155.
- Bentley, R. D. and Neathery, T. L., 1970, Geology of the Brevard Fault Zone and Related Rocks of the Inner Piedmont of Alabama: Alabama Geological Society, 8th Annual Field Trip Guidebook, 119 p.
- Bieler, D.B., and Deininger, R.W., 1987, Geologic setting of the Kowaliga augen gneiss and the Zana granite, northern Alabama Piedmont, *in* Drummond, M.S., and Green, N.L., eds., Granites of Alabama: Alabama Geological Survey Special Publication, no. 2, p. 57-72.
- Blatt, H., Tracey, R.J., and Owens, B.E., 1996, Petrology: igneous, sedimentary, and metamorphic: New York, W.H. Freeman and Company, 529 p.
- Bowen, N.L., 1928, The Evolution of the Igneous Rocks: New York, Dover Publications, 334 p.
- Brantley, S.L., Evans, B., Hickman, S.H., and Crerar, D.A., 1990, Healing of microcracks in quartz: implications for fluid flow: *Geology*, v. 18, p. 136-139.
- Brooks, W.E., 1986, Distribution of anomalously high K<sub>2</sub>O volcanic rocks in Arizona: Metasomatism at the Picacho Peak detachment fault: *Geology*, v. 14, p. 339-342.
- Brooks, C., Hart, S.R., and Wendt, I., 1972, Realistic use of two-error regression treatments as applied to rubidium-strontium data: *Review of Geophysics and Space Physics*, v. 10, p. 551-577.
- Chapin, C.E., and Lindley, J.I., 1986, Potassium metasomatism of igneous and sedimentary rocks in the detachment terranes and other sedimentary basins: Economic implications: *Arizona Geological Society Digest*, v. 16, p. 118-126.
- Coleman, D.S., Bartley, J.M., Glazner, A.F., and Law, R.D., 2005, Incremental assembly and emplacement of Mesozoic plutons in the Sierra Nevada and White and Inyo Ranges, California *in* Rethinking the Assembly and Evolution of Plutons: Field Tests and Perspectives: *Geology Society of American Field Trip Guide*, p. 55.

- Deer, W.A., Howie, R.A., and Zussman, J., 1992, *An Introduction to the Rock-Forming Minerals*: England, Pearson Education Limited, 696 p.
- Drummond, M.S., Allison, D.T., and Weslowski, D.J., 1994, Igneous petrogenesis and tectonic setting of the Elkahatchee Quartz Diorite, Alabama Appalachians: Implications for Penobscotian magmatism in the eastern Blue Ridge: *American Journal of Science*, v. 294, p. 173-236.
- Drummond, M.S., Neilson, M.J., Allison, D.T., and Tull, J.F., 1997, Igneous petrogenesis and tectonic setting of granitic rocks from the eastern Blue Ridge and Inner Piedmont, Alabama Appalachians, *in* Sinha, A.K., Whalen, J.B., and Hogan, J.P., eds., *The Nature of Magmatism in the Appalachian Orogen*: Boulder, Colorado, Geological Society of America Memoir 191, p. 147-164.
- Dunbar, N.W., Chapin, C.E., Ennis, D.J., and Campbell, A.R., 1994, Trace element and mineralogical alteration associated with moderate and advanced degrees of K-metasomatism in a rift basin at Socorro, New Mexico: *New Mexico Geological Society Guidebook*, v. 45, p. 225-231.
- Ernst, W.G., 1973, Interpretative synthesis of metamorphism in the Alps: *Geological Society of America Bulletin*, v. 84, p. 2053-2078.
- Gault, H.R., 1945, Petrography, structures and petrofabrics of the Pinckneyville Quartz Diorite, Alabama: *Geological Society of America Bulletin*, v. 56, p. 181-246.
- Glazner, A.F., 1988, Stratigraphy, structure, and potassic alteration of Miocene volcanic rocks in the Sleeping Beauty area, central Mojave Desert, California: *Bulletin of the Geological Society of America*, v. 100, p. 414-435.
- Groshong, R.H., Jr., Hawkins, W.B., Jr., Pashin, J.C., and Harry, D.L., 2010, Extensional structures of the Alabama Promontory and Black Warrior foreland basin: Styles and relationships to the Appalachian fold-thrust belt: *Geological Society of America Memoir* 206, p. 579-605.
- Guthrie, G.M., and Dean, L., 1989, Geology of the New Site 7.5-Minute Quadrangle, East-Central Ashland-Wedowee Belt, Alabama Appalachians: *Geological Society of America Abstracts with Programs* v. 21, no. 3, p. 19.
- Harris, N.B.W., Pearce, J.A., and Tindle, A.G., 1986, Geochemical characteristics of collision-zone magmatism, *in* Coward, M.P., and Reis, A.C., eds., *Collision tectonics: Special Publication Geological Society*, v. 19, p. 67-81.

- Hatcher, R.D., Jr., 2010, The Appalachian orogen: A brief summary, *in* Tollo, R.P., Bartholomew, M.J., Hibbard, J.P., and Karabinos, P.M., eds., *From Rodina to Pangea: The Lithotectonic Record of the Appalachian Region: Geological Society of America Memoir 206*, p. 1-19.
- Hawkins, J.F., and Steltenpohl, M.G., 2011, Geologic map of the 1:24,000 Our Town, Alabama, U.S.G.S. Topographic Quadrangle: Alabama Geological Survey Open-File Special Map.
- Hawkins, J.F., Steltenpohl, M.G., Zou, H., Mueller, P.A., and Schwartz, J.J., 2013, New constraints on Ordovician magmatism in the southernmost exposures of the eastern Blue Ridge in Alabama: *Geological Society of America Abstracts with Programs*, v. 45, p. 62.
- Holdaway, M.J., 1971, Stability of andalusite and the aluminosilicate phase diagram: *American Journal of Science*, v. 271, p. 97-131.
- Johnson, B.R., Glazner, A.F., and Coleman, D.S., 2006, Significance of K-feldspar megacryst size and distribution the Tuolumne Intrusive Suite, California: *Geological Society of America Abstracts with Programs*, v. 38, p. 93.
- Ludwig, K.R., 2003, *User's Manual for ISOPLOT 3.00: A geochronological toolkit for Microsoft Excel: Berkeley Geochronology Center Special Publication no. 4*. 70 p.
- Ludwig, K.R., 2012, *Isoplot 3.75: A geochronological toolkit for Microsoft Excel: Berkeley Geochronology Center Special Publication no. 5*, 75 p.
- Marshak, S., and Mitra, G., 1988, *Basic Methods of Structural Geology: Englewood Cliffs, New Jersey, Prentice-Hall Publishers*, 448 p.
- Moore, J.G., and Sisson, T.W., 2007, Igneous phenocrystic origin of K-feldspar megacrysts in granitic rocks from the Sierra Nevada batholith: *American Geophysical Union*, v. 88, no. V43G-07., p. 43.
- Neathery, T. L., and Reynolds, J. W., 1973, Stratigraphy and metamorphism of the Wedowee Group, a reconnaissance: *American Journal of Science*, v. 273, p. 723-741.
- Neuendorf, K.E., Mehl, J.P., Jr., and Jackson, J.A., 2005, *Glossary of Geology: Virginia, American Geological Institute*, 779 p.
- Oliver, N.H.S., 2001, Linking of regional and hydrothermal systems in the mid-crust by shearing and faulting: *Deformation Process in the Earth's Crust: Tectonophysics*, v. 335, p. 147-161.
- Passier, C. W., and Trouw, R. J., 2005, *Micro-tectonics: Germany, Springer*, 366 p.

- Pazel, J., 2012, Structural emplacement and stratigraphic setting of eastern Blue Ridge plutonic complexes and associated lithologies, Alabama Appalachians [M.S. thesis]: Tallahassee, Florida State University, 78 p.
- Pearce, J.A., Harris, N.B.W., and Tindle, A.G., 1984, Trace element discrimination diagrams for the tectonic interpretation of granitic rocks: *Journal of Petroleum Geology*, v. 25, p. 956-983.
- Quinn, A.W., 1944, Magmatic contrasts in the Winnepesaukee region, New Hampshire: *Bulletin of the Geological Society of America*, v. 55, p. 473-496.
- Raymond, D.E., Osborne, W.E., Copeland, C.W., and Neathery, T.L., 1988, Alabama 1255 Stratigraphy: Geological Survey of Alabama, Tuscaloosa, 97 p.
- Rollinson, H., 1993, *Using geochemical data: evaluation, presentation, interpretation*: England, Pearson Education Limited, 352 p.
- Steltenpohl, M.G., 2005, An introduction to the terranes of the southernmost Appalachians of Alabama and Georgia, *in* Steltenpohl, M.G., *Southernmost Appalachian terranes, Alabama and Georgia: Field trip Guidebook for the Geological Society of America Southeastern Section 2005 Annual Meeting*, p.1-18.
- Steltenpohl, M.G., Higgins, M.W., and Crawford, R.F., 2011, The Dog river window, Alabama and Georgia: a first-order structure in the southern Appalachian orogen: *Geological Society of America Abstracts with Programs*, v. 43, no. 2, p. 15.
- Steltenpohl, M.G., Schwartz, J.J., Miller, B.V., 2013, Late-to-post Appalachian strain partitioning and extension in the Blue Ridge of Alabama and Georgia: *Geosphere*, in press.
- Sterling, J.W., 2006, Geology of the southernmost exposures of the Brevard zone in the Red Hill Quadrangle, Alabama [M.S. thesis]: Auburn, Auburn University, 118 p.
- Stoddard, P.V., 1983, A petrographic and geochemical analysis of the Zana Granite and Kowaliga Augen Gneiss: Northern Piedmont, Alabama [M.S. thesis]: Memphis, Memphis State University, 74 p.
- Swanson, S.E., 1977, Relation of nucleation and crystal-growth rate to the development of granitic textures: *American Mineralogist*, v. 62, p. 966-978.
- Tobisch, O.T., Barton, M.D., Vernon, R.H., and Patterson, S.R., 1991, Fluid-enhancement deformation: transformation of granitoids to banded mylonites, western Sierra Nevada, California, and southeastern Australia: *Journal of Structural Geology*, v. 13, p. 1137-1156.
- Thomas, W.A., and Astini, R.A., 1996, The Argentine Precordillera: A traveler from the Ouachita

Embayment of North America Laurentia: *Science*, v. 273, p. 752-757.

Tull, J.F., Barineau, C.I., and Holm-Denoma, C.S., 2013, Characteristics, Extent, and Tectonic Significance of the Middle Ordovician Back-Arc Basin in the Southern Appalachian Blue Ridge, *in* Barineau, C.I., and Tull, J.F., The Talladega Slate Belt and the eastern Blue Ridge: Laurentian plate passive margin to back-arc basin tectonics in the southern Appalachian orogen: Field Trip Guidebook for the Alabama Geological Society, p. 12-26.

Vernon, R.H., 1968, Microstructures of high-grade metamorphic rocks at Broken Hill, Australia: *Journal of Petrology*, v. 9, p. 1-22

Vernon, R. H., 1986, K-feldspar megacrysts in granites - phenocrysts, not porphyroblasts: *Earth-Science Reviews*, v. 23, p. 1-63.

Vernon, R. H., 1999, Quartz and feldspar microstructures in metamorphic rocks: *Canadian Mineralogist*, v. 37, p. 513-524.

Vernon, R.H., 2004, *A Practical Guide to Rock Microstructure*: Cambridge University Press, Cambridge, 594 p.

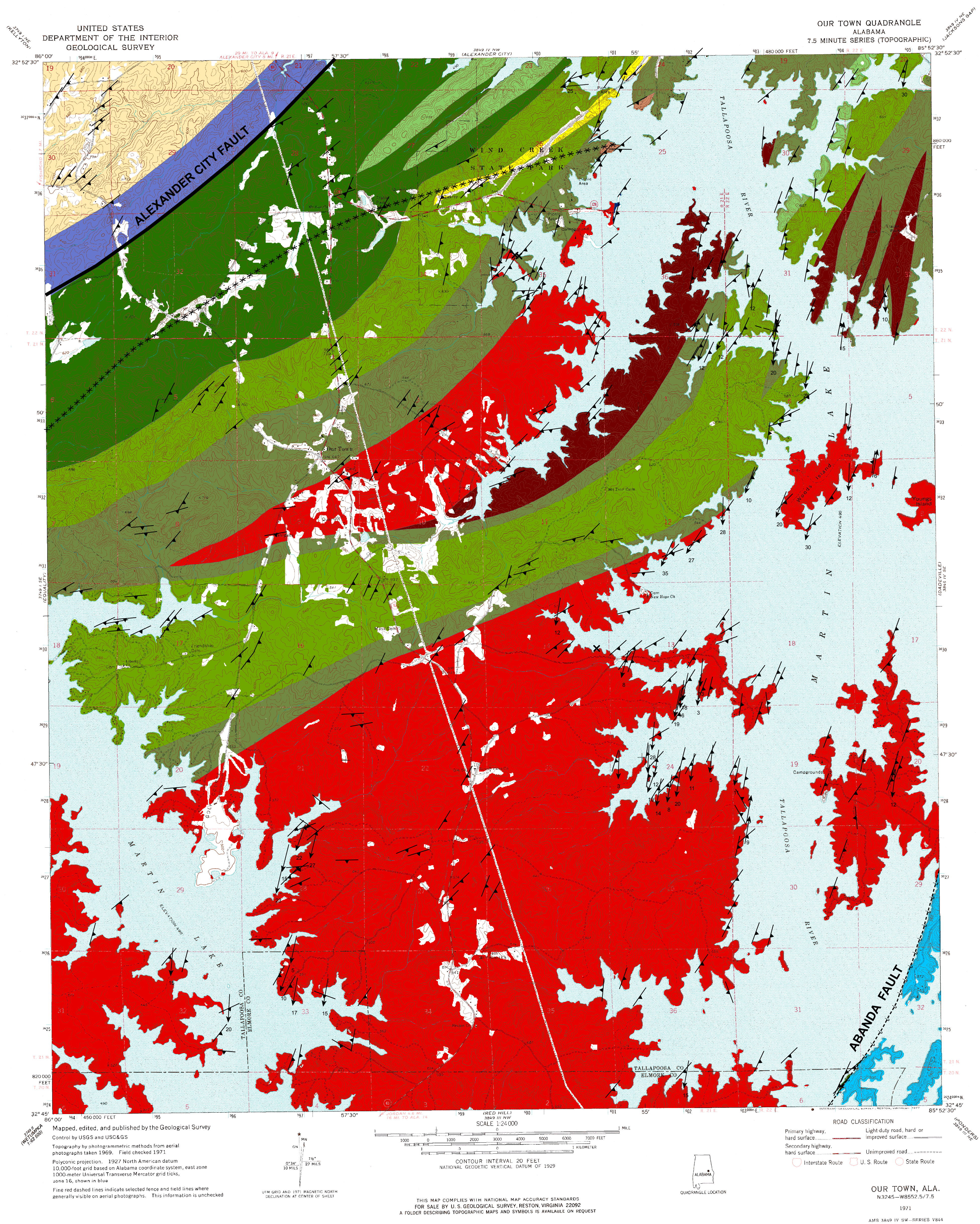
Vernon, R. H., and Patterson, S.R., 2008, How late are K-feldspar megacrysts in granites?: *Science Direct*, v. 104, p. 327-336.

Vernon, R.H., and Clarke, G.L., 2008, *Principles of Metamorphic Petrology*: Cambridge, Cambridge University Press, 446 p.

**Plate 1**  
Geologic Map of the Our Town  
Quadrangle Alabama

# Geologic Map of the Our Town Quadrangle Alabama

John Hawkins and Mark Steltenpohl



## Lithologies

(\* superscripts are not used to suggest stratigraphic order)

egn	<b>Elkahatchee Quartz Diorite Gneiss</b> Mesocratic to melanocratic, fine- to coarse-grained, massive to strongly foliated, locally sheared quartz diorite gneiss.
we	<b>Wedowee Group</b> Schist and phyllonite with alternating, centimeter and finer scale, dark and light colored banding (garnet and biotite-rich vs. quartz-rich). Minor quartzite and amphibolite layers occur in this package of rocks.
em	<b>Emuckfaw Group</b> Tan to buff muscovite schist containing 2-5 cm layers of quartzite. Schist weathers to a deep red and the quartzite has a reddish stain.
em <sup>1</sup>	<b>Emuckfaw Group<sup>1</sup></b> Tan to buff muscovite schist interbedded with more silty, biotite-rich layers, thin (2-5 cm) rare amphibolites, and thin (10-15 cm) quartzites that locally contain amphiboles and garnets. Schist weathers to a dark red, biotite-rich layers are light to dark brown, and quartzites have a reddish stain.
em <sup>2</sup>	<b>Emuckfaw Group<sup>2</sup></b> Tan to buff muscovite schist with interbedded layers of highly competent fine grained biotite-rich quartzites. Schist weathers to a dark red and biotite-rich layers are light to dark brown.
em <sup>3</sup>	<b>Emuckfaw Group<sup>3</sup></b> Layers up to 1.5 m of tan to buff muscovite schist interbedded with more silty, biotite-rich layers and tabular bodies of interbedded muscovite rich, biotite poor, highly foliated granites, ranging up to 2 m thick. Schist weathers to a dark red and the granites are light tan.
qzt	<b>Emuckfaw Quartzite</b> Layers up to 15 cm containing amphiboles and granets up to 3 mm in diameter. Color ranges from light grey to black. Quartzite weathers a white and rust color oxidation surface.
ptm	<b>Protomylonite</b> Coarse to fine-grained metagranite with angular quartz exposed on weathered surfaces. Weathers to a pale pink in color.
kgn	<b>Kowaliga Gneiss</b> Biotite rich granite to granodiorite with sheared potassium feldspar grains up to 2 cm in diameter, highly foliated, and sheared by discrete shear zones. Brown to bronze in color and weathers to a deep red.
kgn <sup>1</sup>	<b>Kowaliga Augen Gneiss</b> Intermediate granite varying to alkali feldspar granite containing euhedral potassium feldspar megacrysts up to 10 cm long, with biotite defining foliation, anastomosing shearing of potassium feldspar grains seen locally in this lithology. Surface exterior is stained black, augen are pink in a white and black matrix, augen weather to white with matrix weathering to a light grey.
maf	<b>Meta-gabbro</b> Fibrous to bladed calc-clinoamphiboles with an interstitial matrix of potassium feldspars, massive to highly foliated with asbestos form amphiboles occurring along small scale shears, locally epidote rich. Color ranges from pale to dark green.
jgt	<b>Jacksons Gap Group</b> Medium to fine-grained, tan to buff colored, massive to thinly layered quartzite and metaconglomerate and layers of graphitic quartz schist, locally containing small garnets (5 mm).

## Legend

x	Aplite and Pegmatite Dikes
↖ ↗	Strike and Dip
↘ ↙	Biotite Lineation
---	Normal Fault
*****	Brittle Fault
==	Right Slip Fault
- - - - -	Oblique Dextral-Normal Fault

Mapping supported by a USGS-EDMAP grant to Mark Steltenpohl (2010-2011)